## INFORMATION TO USERS

This reproduction was made from a copy of a manuscript sent to us for publication and microfilming. While the most advanced technology has been used to photograph and reproduce this manuscript, the quality of the reproduction is heavily dependent upon the quality of the material submitted. Pages in any manuscript may have indistinct print. In all cases the best available copy has been filmed.

The following explanation of techniques is provided to help clarify notations which may appear on this reproduction.

1. Manuscripts may not always be complete. When it is not possible to obtain missing pages, a note appears to indicate this.

2. When copyrighted materials are removed from the manuscript, a note appears to indicate this.

3. Oversize materials (maps, drawings, and charts) are photographed by sectioning the original, beginning at the upper left hand corner and continuing from left to right in equal sections with small overlaps. Each oversize page is also filmed as one exposure and is available, for an additional charge, as a standard 35mm slide or in black and white paper format.*

4. Most photographs reproduce acceptably on positive microfilm or microfiche but lack clarity on xerographic copies made from the microfilm. For an additional charge, all photographs are available in black and white standard 35mm slide format.*

***For more information about black and white slides or enlarged paper reproductions, please contact the Dissertations Customer Services Department.**

**Dobson, Roy Lee Martin**

A CAPILLARY COLUMN GAS CHROMATOGRAPHY, RESONANCE ENHANCED MULTIPHOTON IONIZATION, TIME-OF-FLIGHT MASS SPECTROMETRY, LASER-INDUCED FLUORESCENCE, FLAME IONIZATION DETERMINATION SYSTEM FOR THE DETECTION OF POLYNUCLEAR AROMATIC COMPOUNDS IN COMPLEX MIXTURES

*Iowa State University* PH.D. 1986

# A capillary column gas chromatography, resonance enhanced multiphoton ionization, time-of-flight mass spectrometry, laser-induced fluorescence, flame ionization detection system for the determination of polynuclear aromatic compounds in complex mixtures

by

Roy Lee Martin Dobson

A Dissertation Submitted to the
Graduate Faculty in Partial Fulfillment of the
Requirements for the Degree of
DOCTOR OF PHILOSOPHY

Department: Chemistry
Major: Analytical Chemistry

Approved:

Signature was redacted for privacy.
In Charge of Major Work

Signature was redacted for privacy.
For the Major Department

Signature was redacted for privacy.
For the Graduate College

Iowa State University
Ames, Iowa

1986

TABLE OF CONTENTS

# LIST OF FIGURES

# LIST OF TABLES

# I. INTRODUCTION

Of the thousands of chemical compounds that have been deemed mutagenic or carcinogenic, it is generally agreed that the polynuclear aromatic compounds (PAC) are among the most potent. A greater than average incidence of cancer among chimney sweeps and other workers acutely exposed to substances containing high levels of PAC provides reason for concern (1). Within the PAC chemical class, polynuclear aromatic hydrocarbons (PAH) have been studied most extensively. A number of PAH and their metabolites have been shown to exhibit a high degree of carcinogenicity and/or mutagenicity in bioassay tests (2-5). With the recent emphasis on the development of alternative energy sources, such as production of solvent refined coal, shale oil, or the use of high sulfur coal and crude oil, there has been a growing interest in the more polar PAC classes. These include nitrogen (PANH), sulfur (PASH), and oxygen (PAOH) containing heterocyclic compounds. Many compounds within each of these classes have also been shown to exhibit strong carcinogenic and/or mutagenic tendencies (6-9).

There are many sources of PAC in the environment, both natural and anthropogenic. Natural sources include, for example, fossil fuels (10), combustion products of forest fires, and even in animal pigments (11). Anthropogenic PAC sources are many and varied. PAC have been found in exhausts from internal combustion engines (12), in residue from fuel-rich flames (13), in coal conversion processes (14), and in the environment of the coke production industry (15). Studies even show that PAC concentrations of up to 164 parts per billion may be found in smoked and charcoal-broiled meats (16).

The possible fates of these PAC in the environment are as numerous as their sources. They may, for example, collect in soils and sediments (17,18), in fresh water supplies (19) or enter an ecosystem food chain (20). The high chemical stability of most of these PAC compounds the problem, as their environmental concentrations will continue to increase with time (11). It is, therefore, becoming more and more important to control the level of anthropogenic PAC released into the environment.

Before PAC levels can be judiciously regulated, they must be monitored by appropriate analytical methodology. The many different sources and variety of matrix compositions of PAC-contaminated materials present a serious problem to the analytical chemist. To further complicate the situation, it has been shown that there is a wide range of potency, even among geometric isomers (3,21,22) and various substitutional derivatives (3,6,23), which often have virtually identical physical, chemical and spectroscopic properties. Figures 1A and 1B provide several examples of PAC isomers and derivatives characterized by considerably different carcinogenic and mutagenic potencies, respectively. On top of all of this, there is evidence that carcinogenicity of certain compounds is enhanced in mixtures through synergistic effects (24). Thus, it is not always sufficient to just detect certain "target" compounds. Usually, environmental mixtures containing PAC should be characterized as completely as possible.

The complex problem described above imposes several stringent requirements on analytical methodologies for environmental PAC monitoring. Not only must the technique be capable of detecting trace levels of both polar and nonpolar PAC in complex environmental matrices, it must also

# CARCINOGENICITIES OF PAH GEOMETRIC ISOMERS

## 5-Ring PAH

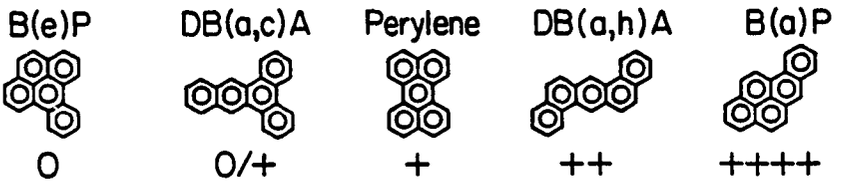


## Fluoranthenes

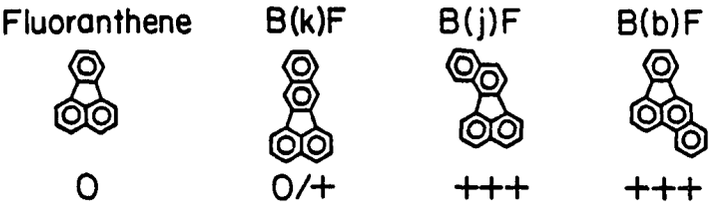


## Methylbenz(a)anthracenes

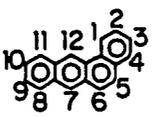


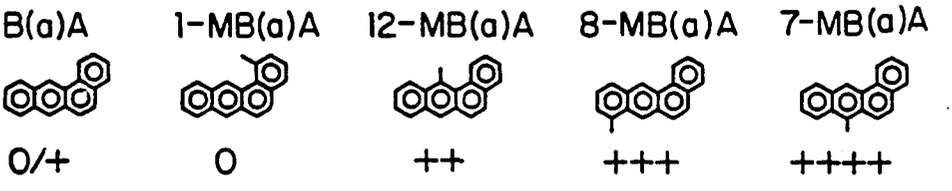


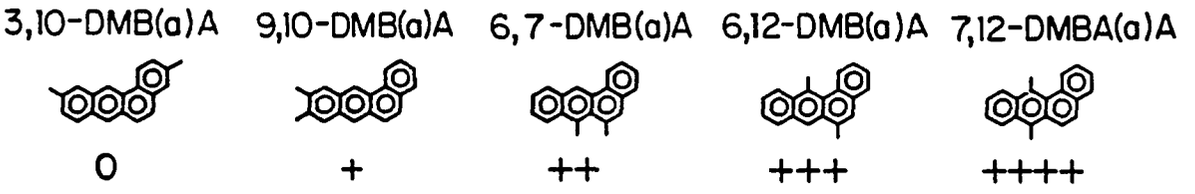


Figure 1A. Range of carcinogenic potency among PAH geometric isomers (0=noncarcinogenic, ++++=highly carcinogenic, as described in reference 3.)

# MUTAGENICITIES OF PAC SUBSTITUTIONAL ISOMERS

## Nitro- and Amino-Substituted PAC

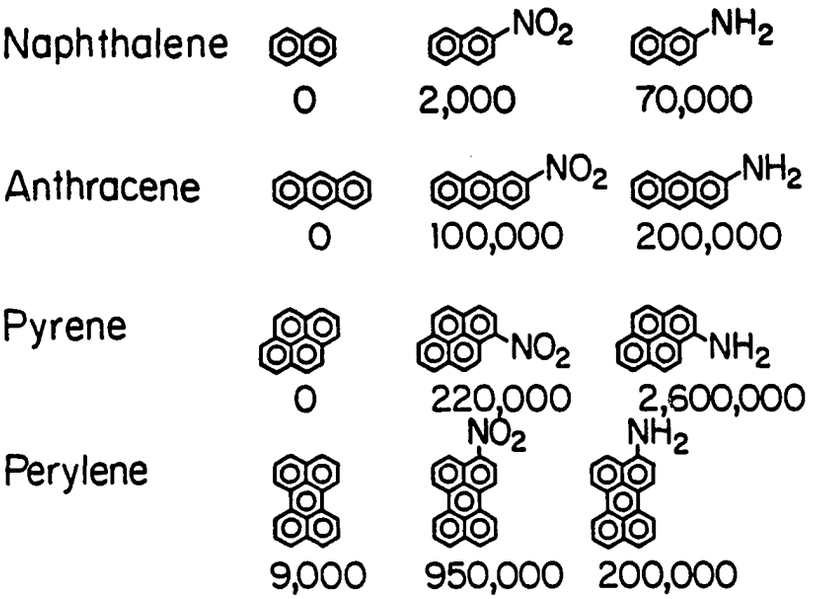


## N-Heterocyclic Compounds

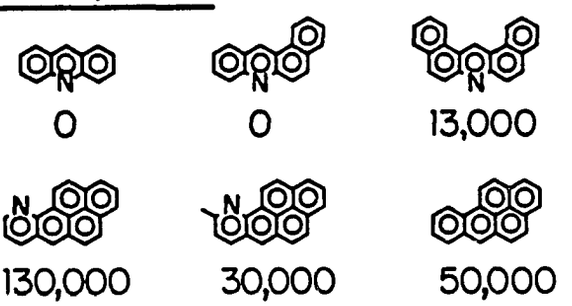


Figure 1B. Range of mutagenic potency among PAC substitutional isomers. Mutagenic values have units of revertants per mg of test chemical (6)

provide adequate selectivity so as to distinguish between compounds differing only slightly in structure. Other requirements include acceptable accuracy and sample throughput, and the capability of detecting nonvolatile, as well as volatile species.

In this dissertation, an instrument will be described which, when implemented to the full extent of its capabilities, may provide a solution to the complex analytical problem described here. In the configuration to be described, the entire technique is termed capillary column/gas chromatography, rotationally cooled/resonance enhanced multiphoton ionization, time-of-flight/mass spectrometry, rotationally-cooled/laser-induced fluorescence, with parallel flame ionization detection, or CC/GC-RC/REMPI-TOF/MS-RC/LIF-FID. While Hirschfeld (25) would certainly consider this hyphenated instrumental approach to be part of the "rising tide of alphabet soup" that threatens to drown us, it is this extensive multidimensionality that may provide the means to solve this extremely vital and complex analytical problem.

The focus of this dissertation will be on the instrumental design and include some preliminary data demonstrating the sensitivity and selectivity of this technique for the analysis of complex mixtures. Before discussing the underlying principles of the various aspects of this technique, conventional approaches to this analytical problem, as well as recent developments in other state-of-the-art high resolution methodologies, will be discussed briefly and assessed.

# II. LITERATURE REVIEW

## A. Traditional Approaches

Traditional approaches to analytical problems involving the characterization and quantitation of trace PAC in environmental samples have all utilized some form of chromatography. Most commonly, final separations and component identifications have been made using the highest resolution chromatographic technique, namely capillary column/gas chromatography (CC/GC), although some work has been conducted utilizing various forms of high performance liquid chromatography (HPLC) (26-30), thin layer chromatography (TLC) (31-33) and, most recently, capillary column/supercritical fluid chromatography (CC/SFC) is growing in popularity (34-36). Although widely varying degrees of chromatographic resolution are available for each of the above techniques, ultimate resolution and sensitivity is determined by the characteristics of the chromatographic detector. Here, the discussion of detectors will be limited to those utilized for CC/GC.

Prior to final CC/GC separation and detection, all complex environmental samples must undergo a clean-up procedure that normally involves an extraction and/or preconcentration step (37). This step is usually followed by an elaborate liquid chromatographic prefractionation process, in which the sample is separated into compound classes (38-42) and subsequently reconcentrated prior to CC/GC separation. The extent of prefractionation required is largely dependent on the complexity of the sample and the specificity of the CC/GC detector. Often, environmental samples contain thousands of compounds and, even with an extensive prefractionation process, many components within a given compound class

may be impossible to resolve chromatographically (30,43-45). In order to minimize laborious prefractionation for a given sample, as well as provide aid in qualitative identification, a number of selective CC/GC detectors have been used.

1. Fixed response CC/GC detectors

This section describes, very briefly, a number of fixed response CC/GC detectors commonly used in environmental analysis. By definition, a fixed response detector has a constant relative response factor for a given compound, as opposed to variable response, or tunable, detectors as discussed in the next section.

The flame ionization detector (FID) is the most popular CC/GC detector. It responds well to all organic compounds and, therefore, offers almost no selectivity when used as a "stand alone" detector. The electron capture detector (ECD) is very sensitive for compounds containing functional groups possessing a high electron affinity and has, therefore, been useful in the determination of ultratrace levels of halogenated compounds in environmental samples, particularly polychlorinated biphenyls (PCB) (46,47) and polyhalogenated dioxins (48). Although the ECD is selective for a large class of compounds, it is not considered to be a highly specific detector. The thermionic, or nitrogen-phosphorous detector (NPD) is also a "class-selective" detector. Although it has recently been found to be useful for the determination of the nitrogen-containing PAC distribution in petroleum (49) and diesel particulate extracts (50), by itself the NPD is far from specific. Still another "class-selective" detector is the photoionization detector (PID), which utilizes a 10.2-eV(121 nm) hydrogen lamp to induce one-photon ionization

of the CC/GC analyte molecules. In general, the PID has a higher sensitivity for unsaturated hydrocarbons, especially aromatic compounds, than for saturated hydrocarbons (51). Unfortunately, it responds to all of these compounds, in varying degrees, making characterization of the analyte difficult, unless the PID is used in tandem with another detector, such as an FID (52) or ECD (53).

All of the above fixed response detectors allow quantitation of the analyte, at various sensitivities, after qualitative identification has first been established. If they are used as "stand alone" detectors, a truly positive identification of sample components would be impossible. Commonly, these detectors are used in series or in parallel, after splitting, to provide more than one dimension of analytical information. Each available dimension provides additional clues which may narrow the number of possible identities of a particular component. This multidimensionality is often not sufficient to provide definitive identification of all, or even most, chromatographic effluents in complex mixtures, especially when one considers the high probability of having coeluting species (43).

2. Tunable CC/GC detectors

Tunable CC/GC detectors are much more versatile than the fixed response variety discussed above. The term "tunable" indicates that the detector parameters may be adjusted, by some means, to access a range of possible relative response factors. This tunability feature greatly enhances the versatility because a single detector may provide multicompositional information. A tunable detector may operate with fixed parameters that are preselected for a given chromatographic run, in which

case certain compound types may be targeted for selective detection. Alternatively, some tunable detectors may be rapidly scanned, in a cyclic fashion, providing access to a three-dimensional chromatogram. Examples of both classes of detectors will be discussed in this section.

The ultraviolet (UV) absorption detector is a good example of a tunable CC/GC detector. The wavelength is chosen to target a certain compound class prior to any given run by selecting the proper bandpass filter or tuning a simple monochromator. Novotny et al. demonstrated that gas chromatograms of complex separations could be simplified to varying degrees, depending upon the wavelength chosen, by using a UV absorption detector (54).

Tunable detectors that monitor emission from selected atomic lines or molecular bands have found a number of applications in gas chromatography. Detectors of this type subject the analyte effluent to an energetic atomization/excitation process that results in atomic and/or molecular band emission. Characteristic emission from a particular class of species is then selectively monitored, by way of a monochromator or an appropriate interference filter, with a photomultiplier detector. Such detectors, which show promise for specialized applications, are the inductively coupled plasma (ICP) (55), the microwave induced plasma (MIP) (56), and the atmospheric pressure active nitrogen (APAN) detector (57). However, the most popular system is the flame photometric detector (FPD) (58,59). The FPD utilizes a hydrogen combustion flame to atomize and excite the analyte thermally. There are a number of environmental analytical applications that have utilized the FPD as a CC/GC detector, including the detection of PASH in coal liquids and shale oils (9), the speciation of

organotin compounds (60), and the determination of chlorinated organics, including pesticides (61).

The rapid scanning tunable detectors are by far the most useful systems for determining the identity of a CC/GC effluent. Typically, the scanning rate is such that at least one entire "spectrum" of information may be collected during the elution time of a CC/GC chromatographic peak. This spectrum then serves as a "fingerprint" which, when matched to a standard spectrum within a data base, serves to identify the corresponding compound. Such detectors are, therefore, capable of providing a full three-dimensional chromatogram, provided the proper computerized data acquisition system is employed. Although rapid scanning mass spectrometers are included in this catagory, they will be discussed separately in the next section.

The ion mobility spectrometer (IMS) has been utilized as a relatively simple rapid scanning CC/GC detector (62-65). The IMS detector first ionizes the analyte, either by photoionization (64) or utilizing $^{63}Ni$ foil (62,63). Once formed, ions achieve characteristic velocities as they travel in an electric field through an inert gas at atmospheric pressure and become separated in space. Ions are then resolved according to their arrival time at a collector plate. Analyte ions thus provide a characteristic ion mobility spectrum (66,67) that may be compared to those of standard compounds within the IMS data base. As a relatively new technique, however, the ion mobility data base is very limited. Also, while IMS may serve as a simplified substitute for low-resolution mass spectrometry in a number of applications, it certainly does not possess comparable resolution.

The Fourier transform infrared (FT/IR) spectrometer has been growing in popularity as a rapid scanning detector for CC/GC (68-74). The Fourier transform process has made it possible to obtain full infrared absorption spectra of compounds "on-the-fly", enabling FT/IR to be applied as a detector for gas chromatography. The IR spectrum of each compound then serves as a fingerprint which may be compared with standard spectra within the system data base for qualitative identification. Although FT/IR is less sensitive than many other detection schemes, such as mass spectrometry, its use in conjunction with other techniques makes it a valuable tool for identification of unknowns (72). Despite the present limited data base of FT/IR (69), CC/GC-FT/IR has recently found applications in the identification of components of complex environmental samples (72,73).

3. Capillary column GC-MS in PAC analyses

Based on the large number of application papers recently published, CC/GC-MS is currently the method of choice for the determination of PAC in complex environmental samples (18,38-42,75-84). The combination of the high chromatographic resolution of CC/GC and the rapid scanning capabilities of an appropriate mass spectrometer provides a highly selective tool for the qualitative determination of components of complex samples. At least one mass spectrum is obtained for each resolved chromatographic peak, which serves as a "fingerprint" to be compared with standard mass spectra within the data base library.

In general, when components are included in the data base library, when they are well-resolved chromatographically and are present in sufficient concentration to provide clear mass spectra, major and minor

constituents are easily identified (65,85). Unfortunately, most complex environmental samples are not so well-behaved. Although the lack of availability of reference PAC, and their characteristic mass spectral data certainly imposes a limitation on the range of CC/GC-MS as an identification tool (83,84), this same limitation must also be imposed on any other competing analytical technique. Also, whereas a goal of most new analytical techniques is to improve detection limits, the high sensitivity of mass spectrometry detection systems is well-established, hence, this author does not consider it a limitation of CC/GC-MS. This section will, therefore, focus on the shortcomings imposed primarily by insufficient chromatographic resolving power, and, hence, the inability of traditional mass spectrometric techniques to distinguish between similar components of unseparated mixtures.

Prior to CC/GC-MS analysis, environmental samples must undergo a clean-up procedure and a chemical class separation, utilizing liquid chromatography fractionation. For the analysis of "messy" samples, such as coal liquids, shale oil, and particulates from fossil fuel combustion, it is quite probable that all potential analytical methodologies will require some form of sample clean-up. In addition, chemical class separations are often required, in the case of CC/GC-MS, primarily because of the inability of the GC to resolve chromatographically the thousands of components that may be present. By dividing the compounds into chemical classes, the resultant chromatograms are greatly simplified, reducing the frequency of occurrence of coeluting species. A number of very useful prefractionation schemes have been devised for this purpose and utilized in comprehensive PAC determinations in environmental samples (38-42).

Probability calculations show that a 200-component mixture will, on the average, contain 40 compounds appearing as coeluting multiplets, even if two-second GC-MS resolution is assumed during the course of 60-minute runs (43). This problem is amplified, in the case of environmental samples, due to the presence of structural isomers. Thus, even after extensive prefractionation, there remain a number of coeluting species in each fraction (38,39,42) that cannot be properly determined due to the insufficient selectivity of the mass spectrometer. Examples of such coeluting isomers are chrysene and triphenylene, several methylphenanthrenes, the methylbenz(a)anthracenes, the benzofluoranthenes, and the dibenzanthracenes (18,30,44,45). Thus, not only does the use of conventional CC/GC-MS require an extensive, time consuming, sample preparation process, but even after prefractionation there are still a large number of instances where the technique cannot distinguish between particular compounds.

Recently, efforts have been made to alter the ionization mode of the mass spectrometer to allow selective determination of a few "target" PAC isomers. Hilpert et al., utilizing negative ion chemical ionization mass spectrometry (NICIMS) as a GC detector, showed that, under optimized conditions, the molecular anion ($M^-$) of benzo(a)pyrene was three orders of magnitude more abundant than that of its isomer, benzo(e)pyrene, when methane was used as the reagent gas (86). Simonsick et al. showed that charge-exchange, chemical ionization mass spectrometry ((CE/CI)-MS), with argon-methane mixtures as the reagent gas, gave slightly different mass spectra for isomeric PAH and that the differences were predictable based on the ionization potential of the molecule (87). Typically, the ratio of

the $(M+H)^+$ to the $(M)^+$ ion signal intensity was used to differentiate isomeric structures of PAH. Whereas both CI approaches may be useful for some specific applications, they are certainly not a general solution to this analytical problem, as ion source conditions must be optimized to target particular compounds.

The incorporation of other CC/GC detectors in parallel with a mass spectrometer may provide complementary information useful in determining the identity of chromatographic effluents. The addition of a fixed reponse detector, such as an ECD (48) or a NPD (50,82), may assist in the characterization of chromatographically resolved components or be useful in quantitation, but this multiplex of information still cannot distinguish between coeluting isomers. Alternatively, the incorporation of a second type of rapid-scanning, variable-response detector may ultimately solve this problem for some applications. For example, FT/IR has recently been incorporated in parallel with MS as a CC/GC detector (88,89). In these studies, the tandem detection system was able to distinguish between alkylated isomers of benzene. Although this new approach shows some promise, it is unlikely that it will be able to distinguish between the larger PAC isomers.

So far typical examples of a variety of conventional detector types for CC/GC have been discussed. There are a number of appropriate applications for each of these detectors and, when utilized in parallel or series with other detectors, the multidimensional information available is very useful in the characterization of complex environmental samples. However, unless chromatography is improved to a point where all isomers of interest are clearly resolved, which is very unlikely (90), none of these

techniques can distinguish between most PAC isomer types on a routine basis. Certainly CC/GC-MS will continue to be the workhorse in the analysis of complex samples, however, there remains a definite need for alternative analytical methodologies that are capable of selective detection of PAC isomers. Hopefully, these new methodologies will also minimize the time-consuming sample preparation process.

## B. Laser-Based Methodologies for Selective PAC Determinations

Selective detection of molecules may be achieved spectroscopically by utilizing differences in the ultraviolet/visible absorption characteristics of respective species. Several approaches have been used to detect the presence of molecules that have absorbed light, including absorption, fluorescence, photoacoustic, thermal lensing, and resonance enhanced multiphoton ionization spectroscopies. In all cases, however, the characteristic molecular absorption spectra are indicative of the specificity with which each species may be detected in a mixture. While broad, ambient-temperature, molecular absorption spectra may be sufficiently different to allow selective detection in many cases, often the absorption profiles of two isomers are too similar to allow clear distinction. This problem becomes even more difficult in complex mixtures. The deterrents to spectroscopic selectivity will be discussed in Appendix B.

Several approaches that have recently been developed to increase the specificity of spectroscopic PAC detection will now be discussed. Generally, these approaches involve prior chromatographic "mixture simplification" and/or low temperature "spectral simplification". In some

cases, multidimensional detection schemes are also used for further specificity. All of these methods involve the use of laser-based analytical schemes. The advantages of utilizing lasers in spectroscopic studies have been well noted previously (91,92). In brief summary, there are four principal advantages in utilizing lasers in place of conventional excitation sources, listed as follows:

a) Narrow sprectral bandwidth-Monochromaticity;

b) Wide tunability range (dye lasers)-Versatility;

c) High peak power (pulsed lasers)-Power;

d) Highly collimated beams-Convenience.

Laser spectral bandwidths are extremely narrow, typically less than 0.01 nm for visible lasers. This monochromaticity allows high resolution interrogation of very fine spectral features in absorption profiles. Various dye lasers may be tuned over a range from 330 nm to above 750 nm and, with the use of frequency doubling crystals, may access ranges down to 245 nm (93). Such lasers are thus quite versatile, in terms of potential applications, in that they may be tuned "continuously" from the ultraviolet to the near infrared. High peak power is required in many multiphoton experiments and is advantageous in most fluorescence studies. Many pulsed dye laser systems, owing to their high pulse energy and very narrow temporal width, are capable of peak powers in excess of 8 MW. All lasers intrinsically provide highly collimated light beams. This collimation feature allows simple excitation source manipulation by way of prisms, mirrors, and lenses. Lasers may be, for instance, conveniently focused into the small volumes required for good HPLC (94) or GC (95) detection.

1. Ambient-temperature GC/laser ionization detection

At ambient temperatures, large PAC have broad, almost featureless, absorption profiles, in the gas phase. In complex PAC mixtures, it is then impossible to specifically detect the presence of particular compounds of interest. However, the spectral features of two or three compounds, in a simple mixture, often differ sufficiently to allow characterization. Thus, if a complicated mixture could be divided into simple mixture subsets and sequentially examined, each subset may be spectroscopically characterized. A gas chromatograph can provide this "mixture simplification" function by dividing a sample into a continuous series of simple mixtures. Some components may be well-resolved chromatographically providing, in effect, a one-component mixture, in which case spectral selectivity is only important in terms of identifying a single eluent. Coeluting compounds are essentially transient simple mixtures of only a few compounds with which ambient temperature spectral selectivity may be sufficient for characterization.

Klimcak and Wessel successfully demonstrated the feasibility of the general analytical scheme described above, utilizing laser induced, resonance enhanced multiphoton ionization (REMPI) and a very sensitive proportional counter cell for the detection of GC effluents (95). In their study, quantitative spectral differentiation was demonstrated for the coeluting PAH isomers, anthracene and phenanthrene. Each compound was detected independently of the other by proper choice of the laser excitation wavelength, as determined by their respective two-photon ionization spectra.

Rhodes and co-workers have recently demonstrated the quantitative

analytical utility of a laser-based multiphoton ionization detector for CC/GC (96). A KrF excimer laser was used to excite two-photon ionization of PAH effluents. The ion detector was a time-of-flight mass spectrometer (TOF/MS), which provided mass selective capabilities. In their study, both low detection limits and a linear dynamic range of greater than four decades were demonstrated. Although a tunable dye laser was not employed in their study, spectral selectivity was demonstrated, in a very specific case, by comparing the ionization signal for two coeluting PAH isomers, chrysene and triphenylene, at two different laser wavelengths. In this case, the excitation wavelengths were characteristic of the KrF and XeCl excimer gases that were used, in turn, in the excimer laser, providing 248.5 nm and 308.0 nm excitation sources, respectively. The results showed that both isomers were ionized by the 248.5 nm excitation source, while only chrysene was detected with the 308.0 nm radiation. Without being able to continuously tune the wavelength of the excitation source, however, spectral selectivity was impossible in all but coincidental instances, such as the example cited in this study. It then follows that the incorporation of a tunable dye laser into such a detection system would allow much greater flexibility in designing experiments for selective determination of a variety of coeluting species.

2. Low-temperature, solid-state fluorescence spectroscopies

Spectral simplification is an alternative to mixture simplification, as discussed above, for the selective characterization of complex PAC mixtures. The vibronic bandwidths found in the characteristic absorption spectra of large molecules at room temperature are typically several hundred $cm^{-1}$, while spectral resolution on the order of 10 $cm^{-1}$ is often

required to resolve mixtures of many substitutional and/or geometric PAC isomers. These broad and complex spectra must first be greatly simplified if spectral selectivity is to be achieved. To this end, several low temperature spectroscopic techniques have been developed recently that provide the necessary spectral simplification for many applications. The approaches to be discussed here utilize laser-induced fluorescence (LIF) of analyte isolated in low-temperature matrices. These techniques are laser-excited Shpol'skii spectrometry (LESS), fluorescence line narrowing spectrometry (FLNS), and matrix-isolation fluorescence spectrometry (MIFS). In all of these, a laser serves as a very narrow bandwidth excitation source, which is required to take full advantage of the great spectral simplification provided by these low temperature matrices.

When PAC are solvated in appropriate n-alkane solvents and rapidly cooled to cryogenic temperatures, individual solute molecules become isolated and trapped in a frozen crystalline matrix. In a great many cases, the sample molecules are compelled to conform to a discrete number of possible sites, or orientations with respect to the host matrix, as compared to the almost infinite number of possible solute orientations within a room-temperature solution. This so-called "Shpol'skii effect", first observed by Shpol'skii and co-workers (97), results in quasilinear, 1-10 $cm^{-1}$ FWHM (full width at half-maximum intensity), absorption and fluorescence vibranic bands, which typically occur in multiplets. The number of quasilinear bands within each multiplet is simply equal to the number of sites within a particular matrix (98). Thus, inhomogeneous spectral broadening is greatly reduced, by proper choice of solvent, and homogeneous thermal broadening is all but eliminated, in most cases, by

use of cryogenic temperatures.

A number of analytical applications have been reported which utilize conventional broad band, ultraviolet (99-105) or x-ray (106,107), sources to excite PAC fluorescence in Shpol'skii matrices. In this case, however, because all PAC molecules, occupying several different sites, are simultaneously excited with these conventional sources, the resulting fluorescence spectra become unnecessarily complicated, increasing the likelihood of spectral interferences in complex PAC mixtures. Yang et al. have overcome this difficulty by employing narrow line laser excitation that enabled them to selectively excite molecules occupying a particular site (108-111). This analytical technique is known as laser-excited Shpol'skii spectrometry (LESS). Site-selective excitation results in the simplification of corresponding emission spectra, to a point where the selective determination of particular PAH compounds, such as benzo(a)pyrene, benzo(e)pyrene, pyrene, and perylene, in coal liquids and shale oil is possible, with minimal sample preparation (108,111).

Although the analytical utility of LESS has been proven for a number of applications, there are still definite limitations to its range of applicability. Many compounds, particularly polar PAC, are not highly soluble in n-alkane solvents. Also, even though the Shpol'skii effect has been observed for hundreds of compounds, it is far from being a universal phenomena (112,113). Further, as is the case with all of these low-temperature, solid-state techniques, LESS is not applicable to nonfluorescent compounds, nor may it easily be utilized as an on-line, real-time analytical tool.

Fluorescence line narrowing spectrometry (FLNS), a relatively new

analytical technique, was originally applied by Small and co-workers (114-117), to the determination of PAC in amorphous glass matrices at cryogenic temperatures. A complete explanation of the FLNS technique has been recently given (118,119). In this approach, the analyte is dissolved in one of a number of glass solvents (e.g., water, DMSO, or glycerol), or solvent mixtures, and cooled to approximately 4 K. This results in the formation of an amorphous glass matrix. By definition, glasses have no natural order. Thus, solute molecules may be trapped in an essentially infinite number of energetically different sites upon freezing. This gives rise to considerable inhomogeneous line broadening in the absorption profile of the solute. Typical vibronic bandwidths are on the order of 300 $cm^{-1}$ (120), which is comparable to those of room-temperature spectra. However, because homogeneous, or thermal, band broadening is minimal at these low temperatures, quasilinear fluorescence emission spectra may be obtained by utilizing a laser, as a narrow spectral bandwidth source, to excite a very narrow distribution of absorbers. Thus, because only those species which absorb can fluoresce, quasilinear fluorescence results, with linewidths determined largely by the bandwidth of the excitation source.

LESS, in principle, is much more selective than FLNS, due to the virtual elimination of inhomogeneous broadening, which allows great selectivity in the excitation process. However, the FLNS technique is much more versatile than LESS, due in large part to the wide range of glass matrices that are available. In FLNS, the solvent is chosen to serve as a "universal host", based on its solvating properties. In LESS, however, the applicability to a particular problem is limited by the solubility of the analyte in only one type of solvent, the n-paraffins.

Thus, FLNS excels in the detection of polar PAC. Applications in the determination of amino-PAH (115), PANH (121), and PAH metabolites (118,122) are representative of the versatility of FLNS.

Another recently-developed, low-temperature, solid-state analytical technique for the high resolution determination of PAC is matrix isolation fluorescence spectrometry (MIFS). In MIFS, a sample is vaporized in a Knudsen cell, mixed with a large excess of diluent, or matrix gas, and deposited on a "cold finger" cryostat, which is typically maintained at less than 20 K (123-126). A number of diluent gases have been utilized in MIFS, including argon, xenon, nitrogen, n-heptane, and perfluorohexane. Once a sample is prepared and trapped on the cold finger, the spectroscopy is very similar to that employed by FLNS or, depending on the matrix type, by LESS. Early reports, in which conventional broad band excitation sources were employed, presented fluorescence spectra for PAC with vibronic bandwidths on the order of 90 $cm^{-1}$ (123,127,128). However, by utilizing narrow line laser excitation, a discrete number of energetically similar sites may be excited and a correspondingly narrow band fluorescence spectrum detected. Reported fluorescence bandwidths for MIFS are typically 15 to 35 $cm^{-1}$ FWHM, when laser excitation was used (129). Although, the spectral resolution is not quite as good as that reported for LESS or FLNS, a number of successful applications in the selective determination of PAC have been reported (129-132).

MIFS offers two primary advantages over other low-temperature, solid-state techniques. First, this method of sample preparation provides the best physical isolation of analyte molecules from each other, to a point where aggregate formation is eliminated and long range energy transfer

processes are negligible. Perhaps the greatest advantage of the matrix isolation approach is that analyte solubility is not a prerequisite. Almost any material which is a gas or liquid at room temperature can be used as the diluent matrix material (129,133). Thus, the diluent may be chosen to minimize analyte-matrix interactions, which often result in the loss of sharp line fluorescence structure (134-136). This factor is particularly important in the determination of polar PAC, many of which are prone to interactions with matrix materials (137). In such cases, a more inert matrix is normally preferred (129).

There are some obvious inconveniences and limitations of the MIFS technique, relative to LESS and FLNS. Sample preparation procedures are elaborate, tedious, and often difficult to reproduce. This results in the need to employ an internal reference approach for quantitaion. Also, MIFS is only applicable to those compounds which can be efficiently vaporized without thermal decomposition.

All three of the cryogenic solid-state analytical techniques discussed above provide considerable spectral simplification, which greatly improves selectivity in the characterization of PAC in complex environmental samples. Of these three approaches, LESS is preferred, both in terms of spectral resolution and sensitivity. However, as LESS is not applicable to many compounds, both FLNS and MIFS are useful alternatives in a number of cases.

Even with the high specificity offered by these cryogenic spectroscopic techniques, there are still a number of shortcomings. It is obvious that all of the above techniques are applicable only to compounds that have appreciable quantum yields for fluorescence. Thus, several

environmentally significant nonfluorescing, or "dark", compounds, such as many halogenated aromatics, are not amenable to this sort of analysis. Also, it is unlikely that any one solvent or matrix will be found to be satisfactory for all PAC types in any of these techniques. Further, in very complicated environmental mixtures, spectral resolution, alone, is likely insufficient to distinguish all substitutional isomers that may be present. Therefore, complementary dimensions of selectivity may be required for complete characterization. However, because of the solid-state form of the analyte, dictated by these low-temperature techniques, it seems unlikely that other detection schemes can be conveniently combined with them. The utilization of an alternative, gas-phase, low-temperature technique, to be discussed in the next section, eliminates many of the inconveniences and potential shortcomings that are intrinsic to these solid-state approaches.

3. Rotationally-cooled, jet spectroscopies

Rotationally-cooled, jet spectroscopy is a low-temperature, gas-phase technique that provides great spectral simplification. A description of the principles of the rotational cooling process is available in Appendix B and elsewhere (138-142). In this approach, the molecule of interest is "seeded" in a rare gas carrier and expanded, through a small orifice or nozzle, into a high vacuum. The expansion, often referred to as a supersonic jet expansion, translationally cools the gas mixture. A subsequent series of two-body collisions, between the translationally cold carrier atoms and the seed molecules, results in the relaxation of molecular internal degrees of freedom. Thus, the seed molecules become cooled translationally, vibrationally, and rotationally. Even though

temperatures of less than 1 K have been achieved by such methods, the molecules do not condense because they are isolated from one another by the diluent carrier gas. Molecules prepared in this way are considered to be "spectroscopically perfect", in that they are totally isolated from matrix effects while existing at cryogenic temperatures. Thus, inhomogeneous and homogeneous spectral broadening are both greatly reduced. Also, because this approach deals with gas phase molecules, ionization as well as fluorescence detection schemes may be utilized.

Rotationally-cooled, jet techniques have been used widely for fundamental spectroscopic studies. Typically, a pure compound is seeded in a carrier and the jet is used to allow resolution of spectral features of a single compound. High-resolution, rotationally-cooled, laser-induced fluorescence (RC/LIF) and rotationally-cooled, resonance-enhanced multiphoton ionization (RC/REMPI) spectra have been reported for a wide variety of compounds in these fundamental studies. Of particular interest here are the sharp line spectra of PAC including fluorene (143,144), anthracene and its derivatives (145,146), tetracene (147-151), pentacene (152,153), triptycene (154), and ovalene (152,155). The spectral bandwidths reported are typically on the order of 1 $cm^{-1}$ for these PAC, suggesting the potential of high resolution analytical applications. In the studies referenced above, only pure compounds were investigated, hence two primary considerations related to chemical analysis, sensitivity and quantitation, were not considered.

As mentioned above, the spectral resolution provided by the rotational cooling technique is more than adequate to be analytically useful. Small and coworkers showed the analytical feasibility of RC/LIF

by distinguishing between methyl substitutional isomers of naphthalene in simple mixtures (156). They also first suggested a simple gas chromatographic sample introduction scheme to provide quantitative transfer of analyte to a RC/LIF detector (114,156) and later demonstrated the analytical utility of this so-called RC/LIF-GC detector for the direct determination of some naphthalene derivatives in crude oil (157,158). This work proved that RC/LIF could be quantitative and sensitive, as well as highly selective.

More recently, other groups have also explored the analytical utility of RC/LIF (159-161) and RC/REMPI (162-166) in the selective detection of trace levels of a variety of aromatic isomers. Both LIF (159) and REMPI (162,164) have been shown to provide detection limits of less than 10 ppb. REMPI offers two advantages, over LIF, however, in its ability to detect so-called "dark", nonfluorescing, as well as fluorescing species and in that the produced ions are amenable to mass analysis by time-of-flight mass spectrometry (162,164,167,168). This author, however, views LIF and REMPI as complementary, rather than alternative, modes for the detection of rotationally-cooled molecules.

Regardless of which of the above detection modes is used, there are still two general requirements that an analyte must meet when rotationally-cooled, jet spectroscopy is employed. Obviously, as with other spectroscopic techniques, the analyte must absorb in a wavelength range accessible to the excitation source (typically a laser) employed. Also, the analyte must be volatile enough to produce a partial vapor pressure of greater than $10^{-7}$ torr (159) at jet operation temperatures. Evan et al. have conducted fundamental studies of a variety of porphyrins

with their jet system, which may be operated at temperatures approaching 520 $^{o}$C (169-171). Operation of the jet at high temperatures, however, is not a general solution to this requirement, as many compounds are not chemically stable under these conditions. Thus, at this point, rotationally-cooled, jet spectroscopy must be limited to the investigation of compounds that are not thermally labile at typical jet operation temperatures. This does not preclude such an application in the future, however, as supercritical fluid chromatography (SFC) is emerging as a potentially useful separation technique for nonvolatile and/or thermally labile compounds (34-36,172). For rotational cooling, the SFC outlet might be interfaced to a jet system and the supercritical fluid, which is simply a pressurized gas heated above its critical temperature, would serve both as a solvent and as the carrier gas in the rotational cooling process. While such a sampling system would greatly expand the range of applicability of rotationally-cooled, jet spectroscopy, no such system has been successfully tested.

The rotational cooling technique obviously differs from other state-of-the-art cryogenic approaches in a number of ways. Significant advantages over these solid-state methods are realized due to four primary differences, listed as follows:

a. Very Low Temperatures-As the jet is capable of cooling the analyte to lower temperatures than are possible with the cryostats used in solid-state methodology, homogeneous broadening is reduced to a greater extent;

b. No Matrix-In the jet, analyte molecules are totally isolated, not only from one another but from the carrier

gas as well, at the point of interrogation. Thus, both multiple site problems and inhomogeneous broadening are nonexistent. This aspect, combined with (a), leads to a projection of up to a 100-fold selectivity improvement over solid state methods (156). Also, the absence of a matrix precludes any analyte-matrix interaction. Therefore, rotationally-cooled, jet spectroscopy may eventually prove to be the method of choice for the determination of many polar PAC and other compounds that experience band broadening in the solid state (137,156).

c. Gas Phase-As a gas-phase technique, rotationally-cooled, jet spectroscopy is amenable to ion detection schemes and is, therefore, not limited to the detection of fluorescing species. Mass analysis of the ions formed should provide an additional dimension of selectivity. Also, such a gas-phase detector has potential in applications involving on-line analysis of flowing gaseous streams, such as combustor stack emissions (161) or chromatographic effluents (157). Such on-line capabilities do not exist for solid-state spectroscopies.

d. Instantaneous Freezing-Use of the jet requires no prefreezing step. Cooling occurs almost instantaneously at the time of analysis. This feature is also a requirement for dynamic gaseous stream analysis, which solid-state techniques do not meet.

A potential selectivity problem, which has not been addressed in the

context of chemical analysis, is the effect of the vibrational quasicontinuum (VQ) that exists, even in the jet, for all large molecules (152). This VQ likely results from random intramolecular radiative coupling between upper level vibronic states (173) and gives rise to a congested level structure in the molecular absorption spectrum. This structure typically begins above 1000 $cm^{-1}$ on the high energy side of the first excited singlet state. Thus, the congested level structure does not obstruct the lower-energy, sharp vibronic bands that may be utilized for selective excitation of similar isomers in simple mixtures. However, in very complicated mixtures containing a wide range of compounds, as is found in typical environmental samples, the rotationally-cooled narrow band structure of one isomeric compound group will likely overlap with the congested level structure of other types of species in the mixture. In this case, therefore, true selectivity can not be achieved in the excitation step alone. If the compounds of interest are fluorescent, the emission may be dispersed for selective detection, otherwise an ion detection scheme involving mass spectrometry as an added dimension of selectivity would be required. If these measures do not provide sufficient selectivity, the use of a prior chromatographic separation may also be necessary.

Rotationally-cooled, jet spectroscopy is still in its infancy as an analytical methodology. It has shown great potential in a number of applications and, in principle, has appeared to be far superior to the alternative solid-state cryogenic techniques. However, much preliminary work must still be done in several areas, including the development of appropriate sampling systems for particular applications, and the

development of alternative quantitation methods. To this point, no one has utilized this technique for extensive characterization of PAC in environmental samples.

4. Capillary column/gas chromatography, rotationally-cooled/resonance enhanced multiphoton ionizaton, time-of-flight/mass spectrometry, rotationally-cooled/laser-induced fluorescence, with parallel flame ionization detection

Throughout this chapter, both traditional and state-of-the-art analytical approaches to solving difficult PAC characterization problems have been discussed and assessed briefly. Each approach offers its own particular advantages, however, most detection methods offer little hope in completely solving the problem if used as "stand alone" techniques. even the promising selective laser-based methodologies will not likely provide coverage comprehensive enough to solve every analytical problem. However, combining a number of these state-of-the-art detection schemes into one multidimensional system offers the potential of a very flexible and powerful analytical instrument. It is largely the design and functionality of such an instrument to which this dissertation work is addressed.

The multidimensional technique, which may totally solve this PAC characterization problem is termed, as mentioned in Chapter I, capillary column/gas chromatography, rotationally-cooled/resonance enhanced multiphoton ionization, time-of-flight/mass spectrometry, rotationally-cooled/laser-induced fluorescence, with parallel flame ionization detection (CC/GC-RC/REMPI-TOF/MS-RC/LIF-FID). This acronym also conveniently summarizes the present capabilities of the instrument to be

described in this dissertation. This multi-hyphenated instrumental technique is quite flexible in that, depending on the particular application, it may be advantageous to employ only a portion of its capabilities. On the other hand, it is a very powerful analytical instrument that, when utilized to the full extent of its capabilities, should provide sufficient selectivity to solve even the most difficult of PAC characterization problems.

Although the specific components of this new analytical instrument will be described fully in subsequent chapters, it is informative to first consider the general capabilities of each aspect on the system. A CC/GC serves as the mixture simplification dimension that, in effect, provides a series of "simple mixtures" to the laser-based detector. The CC/GC effluent is introduced into the ion source of a TOF/MS, where it is interrogated by a tunable pulsed laser beam. This may result in both LIF and REMPI of the absorbing species. Ions so formed are extracted and mass analyzed, while provisions are included for the simultaneous collection and detection of fluorescence radiation. Therefore, while complementary fluorescence information is available, the REMPI aspect expands the range of potential applications to include the determination of nonfluorescing compounds, while allowing molecular weight determination by TOF/MS.

The CC/GC-TOF/MS interface may be modified routinely to operate in either a rotational cooling or ambient temperature mode by installing or removing a nozzle, respectively. The ambient temperature approach is somewhat more universal than the supersonic jet alternative and is, therefore, preferred when high spectral resolution is not required. Even without the use of rotational cooling, a number of coeluting isomers may

be determined selectively through the appropriate choice of excitation wavelength. The use of the rotational cooling approach would be necessary only for characterizing coeluting species of the same molecular weight and similar ambient-temperature, gas-phase absorption spectra. This optional feature will prove to be very useful, as a number of PAC substitutional isomers fall into this catagory.

The laser-based portion of the experimental system is primarily effective only in the detection of absorbing species and, therefore, provides little information as to the overall complexity of a sample. To this end, the chromatographic effluent is split and a portion directed into an FID. The FID serves as a universal, fixed response chromatographic detector to provide information on all species present, including aliphatics. Other types of fixed response detectors, such as the ECD or the NPD, could be utilized in place of or in tandem with the FID to provide further information as to the overall sample composition. The FID was chosen for use in these preliminary studies primarily for convenience and because of its universality.

# III. PRINCIPLES OF NONCONVENTIONAL INSTRUMENTAL ASPECTS

In the previous chapter, the CC/GC-RC/REMPI-TOF/MS-RC/LIF-FID analytical system was briefly described. Before elaborating on the various components of this multidimensional instrument, it is important to consider the general underlying principles involved in the nontraditional aspects of the detector. This chapter will provide a qualitative description of the dynamic process of laser-analyte interaction and the principles of time-of-flight mass spectrometry. A discussion of deterrents to spectroscopic selectivity and qualitative principles of rotational cooling of large polyatomic molecules in a free jet expansion is provided in Appendix B.

## A. Gas-Phase, Laser-Analyte Interaction

When intense, monochromatic laser light interacts with a molecule, a variety of processes may occur, depending on the spectral characteristics of the molecule and the wavelength and power density of the laser beam. Such interactions have been discussed at length elsewhere (174-178), therefore, qualitative consideration will be given only to those aspects relevant to the work at hand.

Simplified schematic energy-level diagrams for two different molecules are shown in Figure 2. Both molecules have ionization energies (IP) so that ionization may occur through the successive absorption of two photons. This stepwise photoionization process is termed multiphoton (MPI). For molecule-A, the first step involves excitation of the molecule to a virtual (nonresonant) state, the lifetime

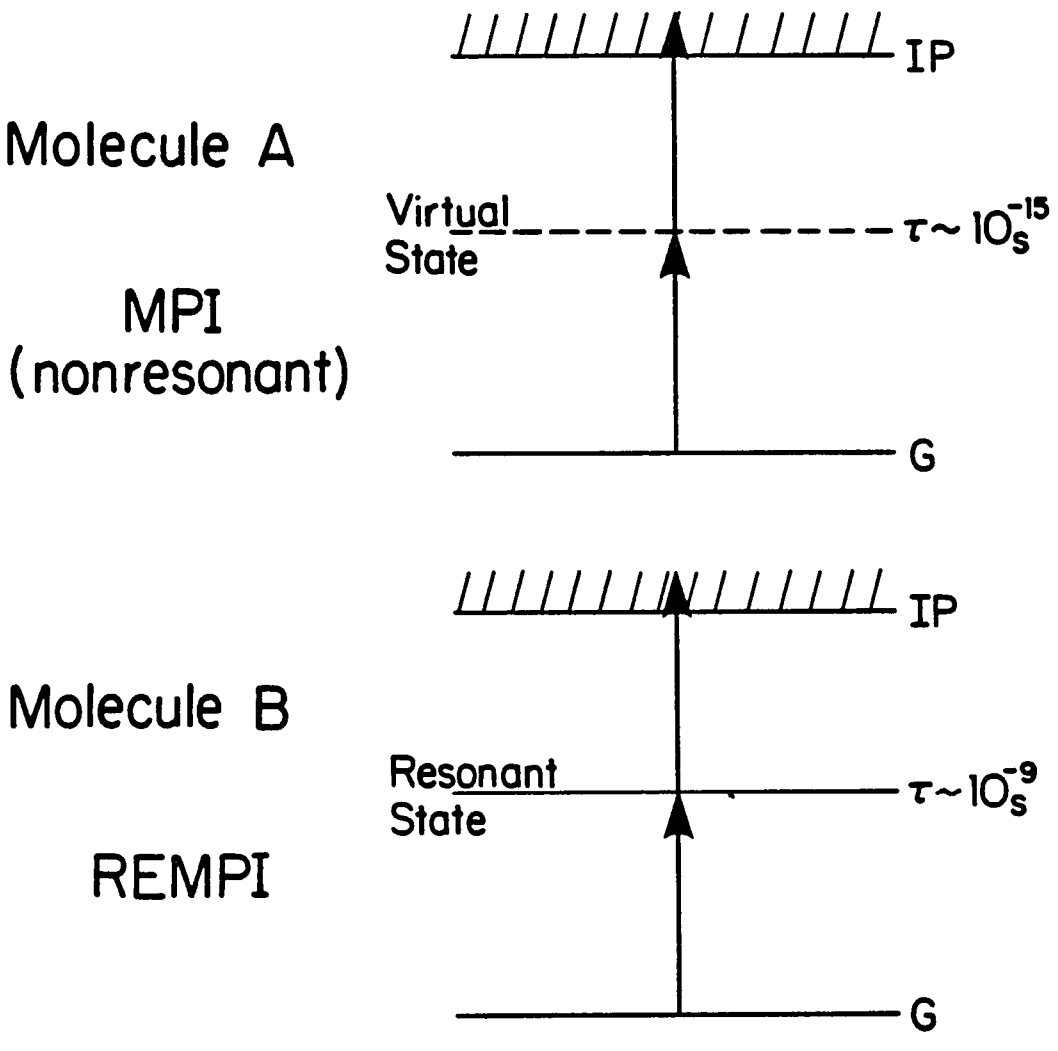


Figure 2. Simplified energy level diagrams for molecules undergoing photoionization by nonresonant MPI (top) and REMPI (bottom) processes

of which is on the order of $10^{-15}$ seconds (175). If ionization is to occur, a second photon must then be absorbed before the molecule relaxes back into a ground vibronic state. On this time scale, the two photons must be absorbed almost simultaneously, hence requiring an extremely intense light source. It is for this reason that tightly focused laser beams are typically employed in such experiments. Obviously, the MPI process alone provides only limited selectivity because all molecules with sufficiently low IP would be ionized with similar efficiencies.

Spectral selectivity may be achieved through a two-stage process that utilizes a real intermediate (resonant) vibronic molecular state as a "stepping stone" toward ionization. This process is illustrated for molecule-B, in which case the laser wavelength has been chosen to provide the precise energy necessary for excitation to a resonant state, the lifetime of which is typically on the order of $10^{-9}$ seconds (175). This relatively long, intermediate-state lifetime somewhat relaxes the laser power density requirements and results in an increase of up to several orders of magnitude in the overall ionization efficiency. This process, termed resonance enhanced multiphoton ionization (REMPI), provides a great enhancement of molecular ion yield, to a point where the nonresonant MPI process may be negligible by comparison. Thus, by tuning the laser wavelength to selectively populate resonant states in molecules of interest, selective excitation/ionization may be achieved. Selectivity limitations of this process at ambient temperatures, are discussed in Appendix B.

The Jablonski diagram in Figure 3, although perhaps still somewhat oversimplified, provides an overview of those dynamic processes associated with laser-analyte interactions that are relevant to the present detection

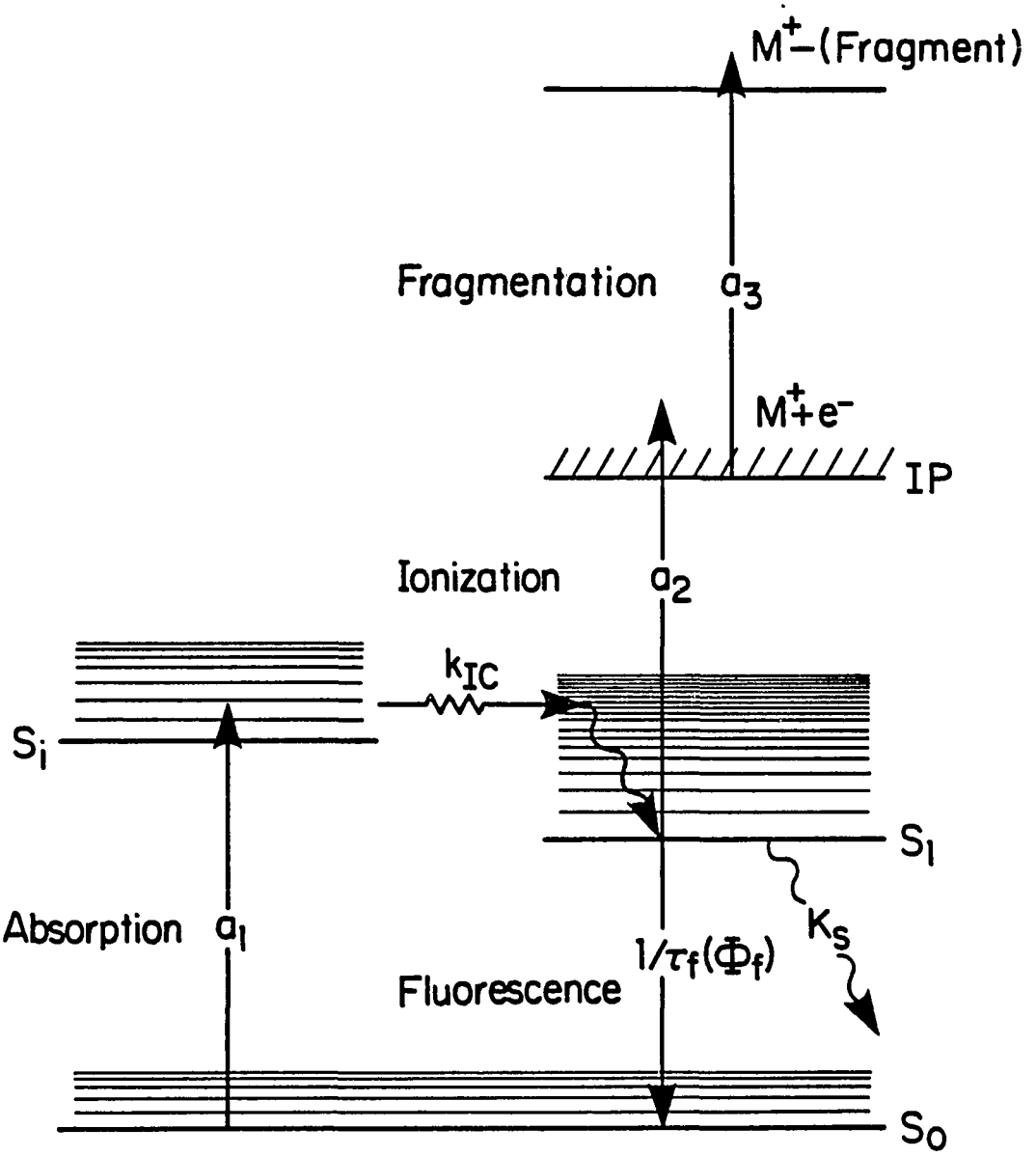


Figure 3. Jablonski diagram (simplified) representing possible energy transfer pathways of laser-analyte interaction. Absorption cross sections: $a_1$, $a_2$, $a_3$; Fluorescence decay lifetime: $\tau_f$; Fluorescence quantum yield: $\Phi_f$; Intramolecular conversion rate constant: $k_{IC}$; and Total nonradiative $S_1$ relaxation rate: $K_S$, are characteristic of the analyte

scheme. Typically, a molecule is excited to an upper vibronic state through the absorption of a resonant photon. This state then undergoes "immediate" intramolecular conversion to the congested upper level vibronic bands of the lowest excited electronic singlet (Kasha's Rule), followed by relaxation to the zero-point vibrational level (179,180). The molecule may then absorb more photons to become ionized and perhaps undergo subsequent fragmentation. Alternatively, the molecule may relax to a ground vibronic state either through the spontaneous release of a photon (fluorescence) or by a nonradiative decay pathway. The nonresonant MPI contribution is taken to be negligible, as the laser beam power densities employed in this study are sufficiently low. Also, intermolecular deactivation of excited species is essentially nonexistant because the laser-analyte interaction occurs at "collision-free" pressures of $10^{-4}$ torr or less.

The probability that a molecule will follow a particular energy transfer pathway is dependent on both the intensity of the laser light and the spectroscopic properties of the molecule. For instance, at high laser intensities, ionization and fragmentation processes tend to dominate, while at lower laser intensities spontaneous emission and nonradiative decay are more likely to prevail.

The spectroscopic properties of molecules form the primary basis for the selectivity available from this laser-analyte interaction process. The first excitation step is dependent on the absorption cross section, $a_1$, of the $S_o$ to $S_i$ transition (Figure 3). Both the ionization and fluorescence pathways are dependent on the efficiency of this first step and, therefore, are restricted according to the characteristic absorption

spectrum of the species of interest. It is important to note that the laser-analyte interaction is very dynamic, in that ionization, spontaneous emission, and nonradiative decay are all competing processes. Thus, after the excited molecules settle into the $S_1$ level, the relative probabilities for each of these processes for a given laser intensity is dictated by $a_2$ (photoionization cross section of $S_1$), $t_f$ (fluorescence lifetime) and $\Phi_f$ (fluorescence quantum yield), and the nonradiative decay probability, respectively (177). Further, an obvious requirement for ionization is that the IP must be low enough to allow one photon ionization form $S_1$.

As the above molecular spectroscopic constants differ from species to species, knowledge of their relative values could be quite helpful in qualitative characterization studies. The precise values for such constants have been determined for only a few PAC, therefore, their utility, as applied to analytical characterization experiments, is limited at present. However, through the simultaneous monitoring of all laser-analyte interaction products, characteristic detector responses may be determined for each species, at a selected laser wavelength and intensity. These responses are actually the manifestation of the characteristic molecular spectroscopic constants and may equally be utilized in analytical qualitative identification studies.

The gas sample cell, shown in highly schematic form in Figure 4, illustrates a general arrangement that allows simultaneous monitoring of all analytically useful signals generated by the laser-analyte interaction. This excitation/ionization process occurs between two properly biased parallel plates, so that electrons resulting from

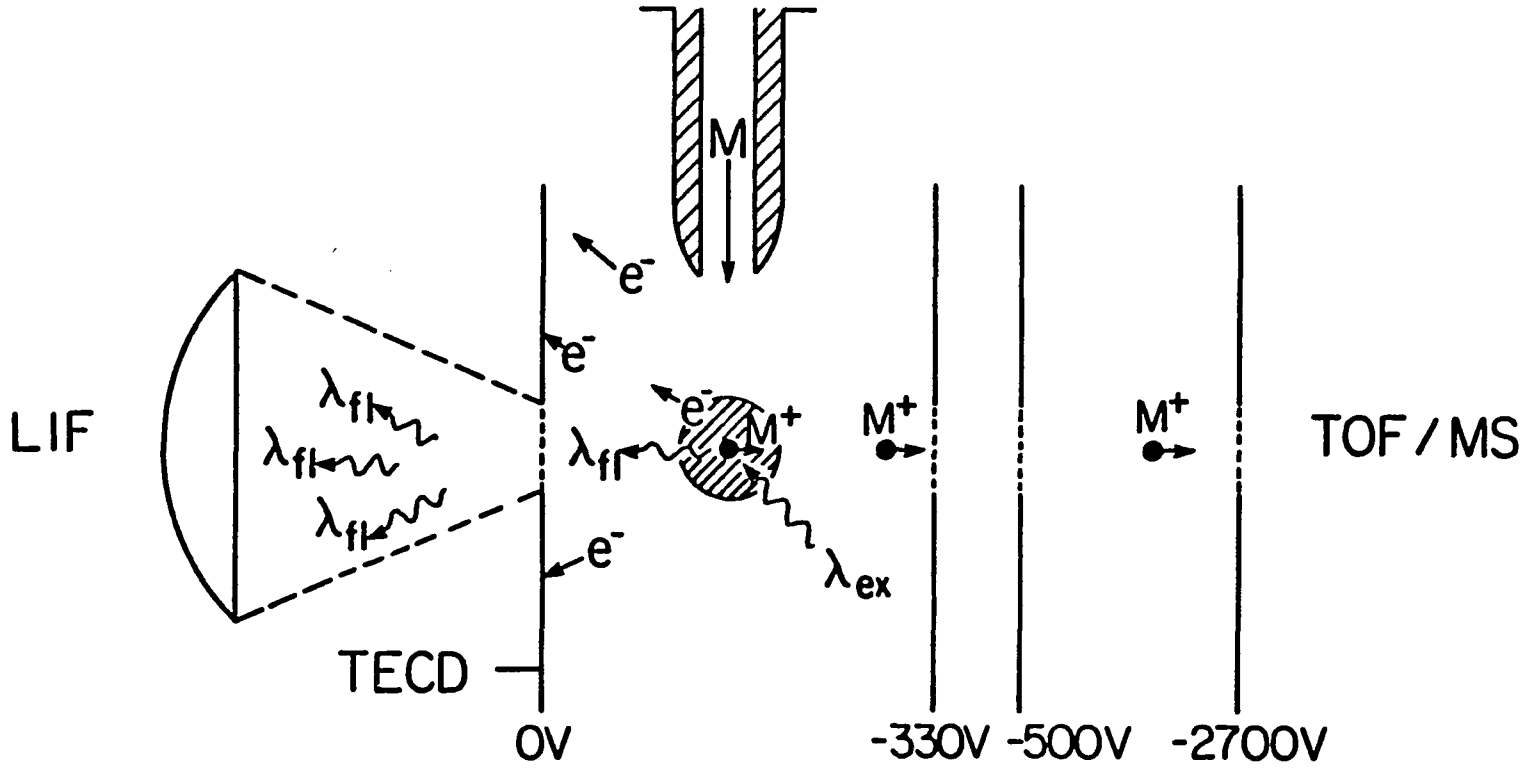


Figure 4. Schematic diagram of a dynamic gas sample cell for monitoring all analytically useful products of laser($\lambda_{ex}$)-analyte(M) interaction at low pressure. Interaction products: cations($M^+$), electrons($e^-$), and photons($\lambda_{fl}$)

molecular ionization are efficiently captured and monitored, utilizing a total electron current detector (TECD), and cations are extracted into a time-of-flight mass spectrometer (TOF/MS). A fraction of the photons are also collected, employing an appropriately positioned quartz lens, thus providing access to laser-induced fluorescence (LIF) information as well.

The details of each detection scheme will be provided in the following chapter. The next section presents a discussion of TOF/MS principles and the advantages of this approach over other mass analysis detection schemes for pulsed laser ionization experiments.

## B. TOF/MS: Principles and Advantages for MPI Detection

The incorporation of a mass analysis dimension into the detection scheme for gas phase photoionized molecules is often quite straight forward and results in a very powerful analytical technique. Several types of mass spectrometers have been employed as detectors in such experiments. Examples of these are quadrupole (176,181-183), magnetic sector (184-186), time-of-flight (96,162,168,187), and Fourier transform mass spectrometers (FT/MS) (188,189). Of these, the time-of-flight mass spectrometer (TOF/MS) is currently the detector of choice for pulsed laser MPI experiments. To better understand why TOF/MS is preferred, it is important to first consider the basic principles of this approach. As excellent reviews of general TOF/MS theory are available elsewhere (190,191), this section will only briefly describe these principles and how they relate to the application at hand.

1. Basic TOF/MS principles

Figure 5 depicts the essential components of a TOF/MS system. It is composed of two primary sections, the ionization-acceleration region and the field-free drift tube. These sections are defined by two planar grids and an ion detector. A gaseous sample is allowed to enter the first region where it is ionized, and perhaps fragmented, by an energetic pulsed beam that passes between and precisely parallel to the two grids. Traditionally, a narrow electron beam is utilized, however, the same principles apply to the laser ionization approach. Once formed, the ions are accelerated in the direction of the drift tube by applying a negative voltage pulse, $E_a$, to the acceleration grid. This pulse serves to provide each ion with the same kinetic energy (KE). More precisely:

$$KE=qdE_a=1/2MV^2, \qquad (1)$$

where q is the charge of the ion, d is the distance over which the electric field is applied, M is the mass of the ion, and V is the velocity magnitude of the accelerated ion.

The ions enter the field-free drift tube simultaneously, however, depending on their respective masses, they will each have a characteristic velocity, defined by rearranging equation 1:

$$V_i=(2q_idE_a/M_i)^{1/2}, \qquad (2)$$

where i labels an ion of a particular mass. Thus, as ions pass through the drift tube, they become physically separated according to mass. From the reference frame of the detector, the ions are separated in time, with the lighter (faster) ions arriving first. Thus, relative flight times of the various ionized species are actually measured in order to assign proper mass-to-charge ratios, hence the term "time-of-flight". For a

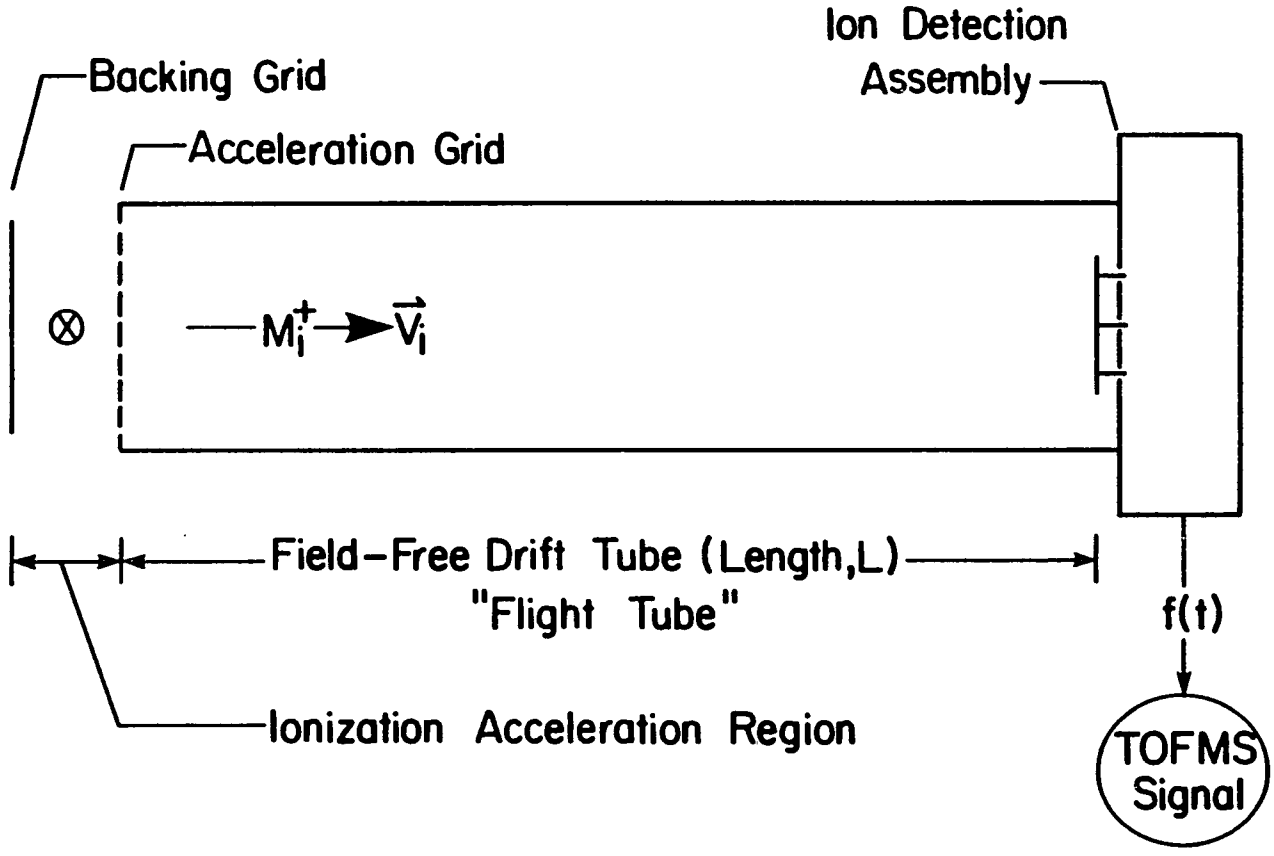


Figure 5. Essential components of a TOF/MS system. A pulsed ionizing beam passes through the ionization/acceleration region precisely parallel to the planar grids

drift tube of length L, (typically 40 to 200 cm) the flight time, $t_i$, may be predicted according to the following equation:

$$t_i = L(M_i/2q_i dE_a)^{1/2}. \quad (3)$$

If the assumption is made that all ions are singly charged, it is apparent that the flight time is directly proportional to the square root of the mass. This relationship results in an intrinsic limitation of this method, that is, resolution degrades with increasing mass. To illustrate this quantitatively, Table 1 lists the calculated flight times for a number of singly charged cations under a typical set of TOF/MS conditions. Note that low mass ions experience a greater separation in time from adjacent mass "peaks" than is the case for heavier ions. For example, $H^+$ and $D^+$ are separated by 0.5 microseconds, whereas $^{200}Hg^+$ and $^{201}Hg^+$ are separated by only 0.05 microseconds.

It is apparent that in order to achieve adequate resolution for the study of large compounds, several experimental parameters must be optimized. First, the detector must be fast enough to differentiate these events in time, on the order of nanoseconds or better. This represents no real problem for state-of-the-art electron multiplier detectors and associated processing electronics, such as boxcar averagers and high speed transient digitizers, as discussed in the next chapter.

More fundamentally, TOF mass resolution is primarily limited by the temporal width of the isobaric ion "packets" from the reference frame of the detector. This width is largely determined by the quality of the original ion pulse formed. The three key factors involved in establishing this are:

i) Cross-section of the ionizing beam.

Table 1. Calculated[a] flight times

| Cation | Mass (u) | Flight Time (μs) |
|---|---|---|
| $H^+$ | 1 | 1.50 |
| $D^+$ | 2 | 2.00 |
| $He^+$ | 4 | 4.00 |
| $H_2O^+$ | 18 | 6.10 |
| $N_2^+$ | 28 | 7.60 |
| $O_2^+$ | 32 | 8.60 |
| $(Naphthalene)^+$ | 128 | 17.20 |
| $^{200}Hg^+$ | 200 | 21.50 |
| $^{201}Hg^+$ | 201 | 21.55 |

[a]Calculations based on a 1.0 m flight tube utilizing an acceleration potential of -1.9 kV.

ii) Initial thermal velocity distribution of the analyte.

iii) Sharpness of the leading edge of the voltage pulse.

The first factor indicates that "distance equals time" in a TOF/MS system. If the initial spatial distribution of ions formed is too large, resolution must suffer. However, by decreasing the size of the ionizing beam, less analyte is interrogated, limiting sensitivity. Thus, there exists the inevitable trade-off of resolution versus sensitivity. Typically, the ionizing beam diameter is on the order of 1 mm.

Item ii) emphasizes that an ion moves through the drift tube at a velocity that is actually the sum of a velocity component due to the KE imparted by the pulsed acceleration grid plus its initial thermal velocity. This initial thermal velocity distribution results in the spreading of each isobaric packet as it traverses the drift tube. The velocity distribution for a gaseous analyte is relatively narrow compared to that for ions produced in surface desorption experiments, for example, when a high power density pulsed beam is utilized to "blast" material from the surface of a sample. However, the ambient-temperature, gas-phase, velocity distribution does represent an ultimate limitation to mass resolution. It is anticipated that by making use of a supersonic jet expansion to introduce the sample, this limitation will be greatly relaxed. Not only does the jet provide rotational and vibrational cooling, it also results in substantial Doppler (translational) cooling, as discussed in Appendix B. Hopefully, this will all but eliminate thermal ion peak spreading. Lubman and coworkers have recently demonstrated improved mass resolution, by utilizing such a sample introduction technique, in a TOF/MS system (187).

Item iii) is normally dependent on the quality of the electronics being used. Obviously, if the ions are accelerated instantaneously by applying a perfect square wave voltage pulse to the acceleration grid, minimal peak spreading will result. A pulsed laser beam is not affected by a static electric field and therefore, unlike the case of electron impact ionization, affords the luxury of applying the acceleration voltage constantly. Thus, the uniformity of ion acceleration is limited only by the temporal width of the pulsed laser beam and not by the electronics, as explained in the next chapter.

Properly designed TOF/MS systems are capable of achieving unit mass resolution beyond 400 u and mass ranges of up to several thousand mass units have been reported (192).

## 2. TOF/MS advantages for MPI detection

Obviously, the TOF/MS is an extremely efficient detector. In principle, every ion that is extracted from the source may be detected and mass analyzed. This is in contrast to magnetic sector and quadrupole mass filter instruments that must be electronically scanned in order to obtain a full mass spectrum. Such mass spectrometers only transmit a narrow m/q window to the detector at any one time and, therefore, waste most of the ions. These scanning instruments are adequate for selective ion monitoring (SIM) experiments, but their low efficiency results in relatively poor signal-to-noise ratios (S/N) when large mass ranges are of interest. This consideration is very important for the case of pulsed MPI experiments, in which the repetition rate and duty cycle of the ion formation process are quite low.

Another shortcoming of scanning mass spectrometers is their

susceptibility to problems arising from pulse-to-pulse variations in ion signal. As such systems are "blind" to all but one m/q signal at a time, there is no way to compensate for signal fluctuations that may occur during the course of a scan. Two general categories of pulse-to-pulse variations in MPI experiments are laser-related and sample-related processes. The laser-related category includes uncontrollable shot-to-shot laser pulse energy fluctuations, the magnitudes of which are characteristic of the stability of the laser, and controllable variations, intentionally imparted on the system by scanning the excitation wavelength of the laser.

Sample-related variations result from rapid changes in analyte concentration within the ion source of the mass spectrometer. Most, if not all, modes of sample introduction are unable to provide a perfectly constant and uniform concentration of analyte to the ion source. This problem is particularly acute for the case of a CC/GC sample introduction system, in which a particular effluent may pass completely through the ion source in less than one second. Thus, with a 10 Hz laser system, it would be impossible to obtain even a marginal mass spectrum on this time scale when a scanning instrument is utilized.

The relatively high efficiency of TOF/MS overcomes the above problems, as an entire mass spectrum may be collected for each and every laser shot. Thus, relative peak heights are invariant to small fluctuations in laser power and the detector responds immediately to pulse-to-pulse changes in mass spectra due to variations in laser wavelength or fluctuations in analyte concentration. Such response characteristics make the TOF/MS an attractive alternative to the

traditional scanning instruments, particularly for pulsed MPI experiments in which chromatographic sample introduction systems are employed. Further, such "real time" characteristics are highly desirable for applications requiring on-line monitoring of dynamic processes.

A further advantage of the TOF/MS is its simple design and operating principles, which allows the cost to remain lower than other mass spectrometers of similar analytical capabilities. Also, this simplicity results in a more durable instrument (193). It is important to note that recent studies have demonstrated that FT/MS is, also, a satisfactory detector for MPI (188,189). In fact, it has the potential for mass resolution superior to that offered by TOF/MS. However, such systems have become available only recently and their cost is prohibitive, as of yet, when compared to that of simple TOF/MS systems.

# IV. INSTRUMENTAL FACILITIES

A general block diagram of the essential components of the instrument is shown in Figure 6. As shown in the diagram, this instrument allows simultaneous access to LIF, TECD, SIM, and TOF/MS analytical signals. The specific components employed in the present study are summarized in Table 2. A more detailed description of the overall system is given below.

## A. Excitation/Ionization System

A Quantel model YG481 Nd:YAG (neodynium: yttrium aluminum garnate) laser was used to pump a Quantel model TDLIII tunable dye laser (92,194). A 532 nm (green) pump beam was created by passing the 1.064 μm fundamental output of the Nd:YAG laser through a KDP (potassium dihydrogen phosphate) crystal (93). As the conversion efficiency was approximately 40 % (by power), the green output was first separated from the Nd:YAG fundamental by a dichroic mirror before being steered into the dye laser. When operated at an input voltage of 1.8 kV (typical maximum voltage) and a repetition rate of 10 Hz, the 532 nm pump beam had an average power of 4 W, a temporal pulse width of 10-15 ns, and thus a peak power of approximately 30 MW.

The 532 nm pump beam was passed through a series of beamsplitters that were positioned at an incident angle of $45^{o}$. Thus, as shown schematically in Figure 7, a portion of the green laser beam was used to pump transversely each of the four flow-through dye cells within the dye laser. The Quantel model TDLIII contains one oscillator dye cell and a series of three amplifier dye cells. The oscillator cavity, in which the precise laser wavelength is defined, is shown in greater detail in

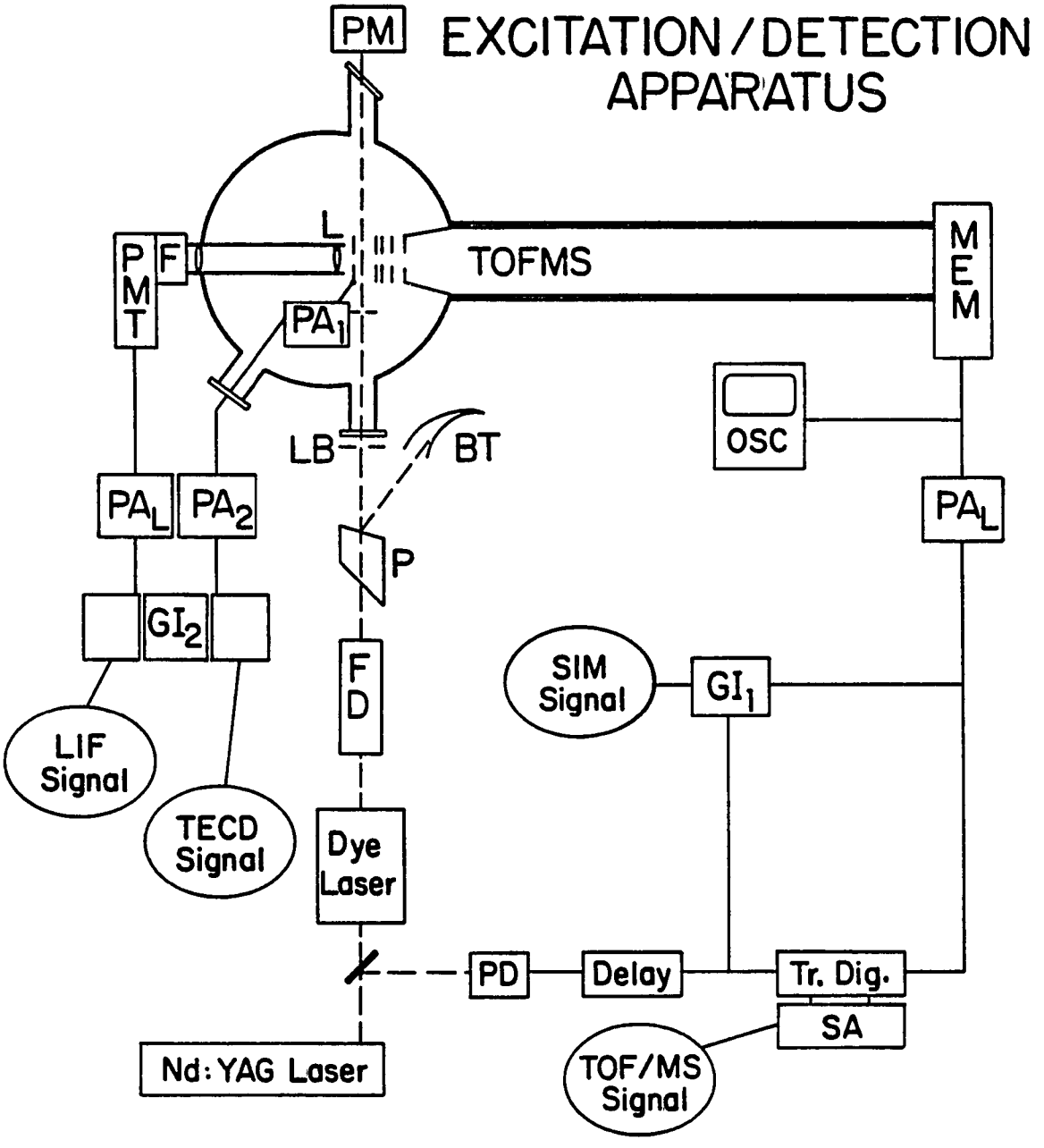


Figure 6. Laser-based excitation/detection system of the CC/GC-REMPI-TOF/MS-LIF-FID analytical instrument. Specific components are summarized in Table 2

Table 2. Components of laser-based excitation/detection apparatus

| Component | Symbol[a] | Model No. | Manufacturer |
|---|---|---|---|
| A. Laser System | | | |
| Nd:YAG Laser | | YG481 | Quantel International, Santa Clara, CA |
| Dye Laser | | TDLIII | Quantel International, Santa Clara, CA |
| Dye Laser Scan Controller | | ASC-2 | Quantel International, Santa Clara, CA |
| Frequency Conversion Apparatus | FD | FCA-1 | Quantel International, Santa Clara, CA |
| Volume Absorber, | PM | 38-0101 | Scientech, Boulder, CO |
| Power Meter | | 36-1002 | Scientech, Boulder, CO |
| B. Detection System | | | |
| TOF/MS(MEM) | | MA-2000[b] | CVC Products, Inc., Rochester, NY |
| Oscilloscope | OSC | 475A | Tektronix, Inc. Beaverton, OR |
| Preamplifier | $PA_L$ | 6102 | LeCroy Research Syst., Spring Valley, NY |
| Source Preamplifier | $PA_1$ | --- | Ames Laboratory Constructed |
| Active Filter Preamplifier | $PA_2$ | --- | Ames Laboratory Constructed |

[a]Refer to Figure 6.

[b]The basic components of this instrument were adapted for photoionization studies. For details, refer to Table 5 and Figures 11 and 14.

Table 2. Continued

| Component | Symbol[a] | Model No. | Manufacturer |
|---|---|---|---|
| Transient Digitizer/ Signal Analyzer | Tr. Dig. SA | 3500SA200 | LeCroy Research Syst., Spring Valley, NY |
| Gated Integrator/ Boxcar Averager | $GI_1$ | 162/165/ 165 | EG&G Princeton Applied Research, Princeton, NJ |
| Gated Integrator/ Boxcar Averager | $GI_2$ | SR280/250/ 250/225/200 | Stanford Research Syst., Inc., Palo Alto, CA |
| Fast Photodiode Circuit | PD | --- | Ames Laboratory Constructed |
| Pulse Delay Generator | Delay | --- | Ames Laboratory Constructed |
| Photomultiplier Tube | PMT | R955 | Hamamatsu, Co., Middlesex, NJ |
| C. Misc. Components | | | |
| Colored Glass Filters | F | | Schott Optical Glass, Inc., Duryea, PA |
| Pellin Broca Prism | P | | |
| Fused Silica Lenses | L | | Melles Griot, Irvine, CA |
| Light Baffles | LB | --- | Ames Laboratory Constructed |
| Laser Beam Trap | BT | --- | |

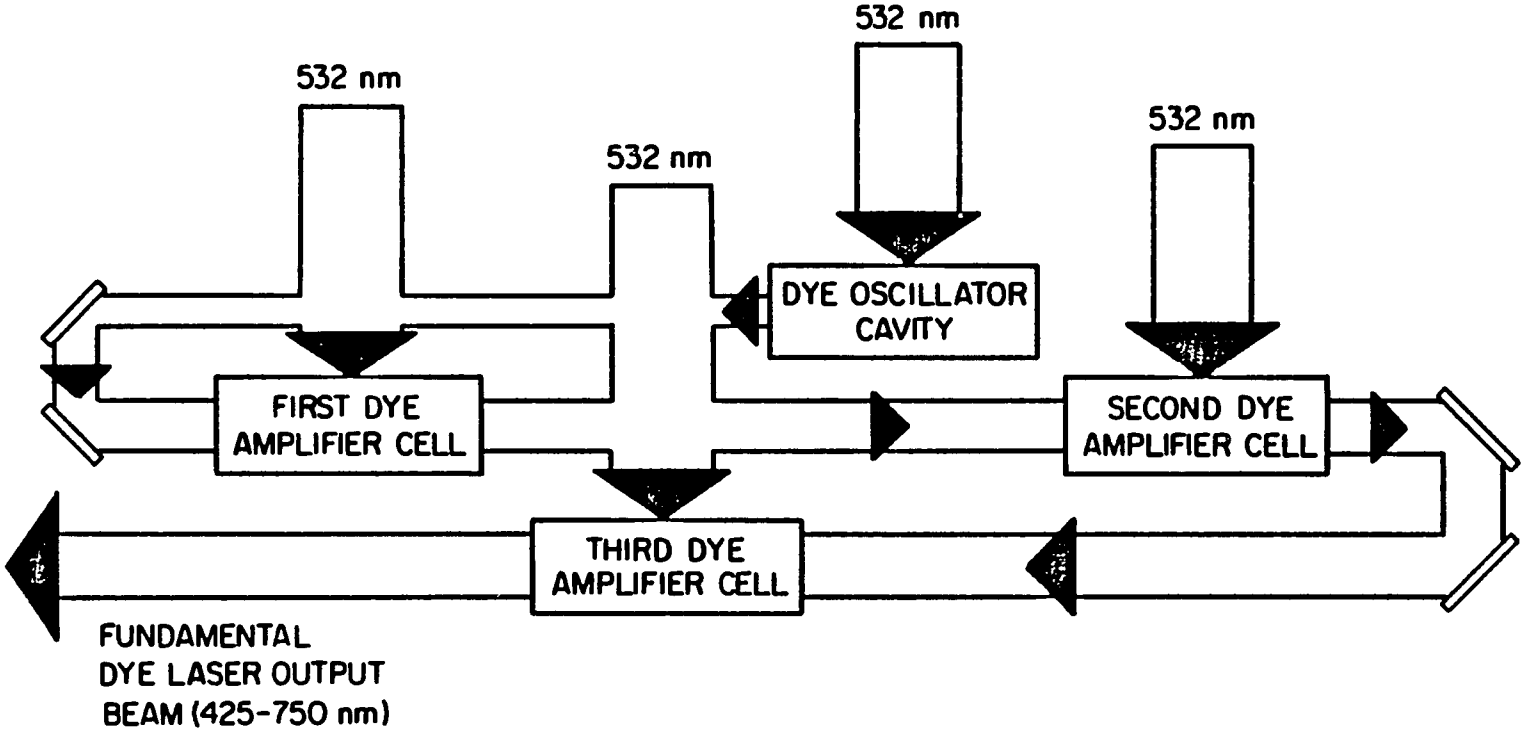


Figure 7. Schematic diagram of the pumping scheme of the tunable dye laser

Figure 8. The tuning rear cavity mirror and the output mirror define the oscillator cavity. A fixed, holographic grating disperses the broadband molecular fluorescence originating from the excited dye in the oscillator flow cell. By rotating the rear cavity mirror, a very narrow band of this fluorescence is selected to be directed back on its original optical path to induce monochromatic stimulated emission (lasing) of the excited dye molecules within the oscillator cell. The resultant "monochromatic" laser beam is then directed through a series of amplifier cells (see Figure 7), providing a large increase in the laser power. The narrow bandwidth package (Figure 8) is a unidirectional prism beam expander assembly that increases the spectral resolution of the oscillator monochromator system. This results in the narrowing of the dye laser spectral bandwidth. The characteristic output beam diameters and spectral bandwidths of the dye laser were 5 mm and less than 0.12 $cm^{-1}$ at 600 nm, respectively. The dye laser was either operated at fixed wavelengths, by manually setting the position of the tuning mirror, or linearly scanned in wavelength utilizing the Quantel model ASC-2 dye laser scan controller.

The laser dyes utilized in the present investigations are listed in Table 3, along with other associated data. Each dye or dye mixture was chosen according to its characteristic lasing wavelength range and power conversion efficiency. These dyes, cumulatively, allow dye laser tuning throughout the 565-700 nm range and are relatively efficient when pumped by a frequency-doubled (532 nm) Nd:YAG laser. The rhodamines, for instance, are capable of power conversion efficiencies in excess of 35 % at their respective peak lasing wavelength (195). Under optimum conditions, a tunable dye laser beam with average powers of greater than

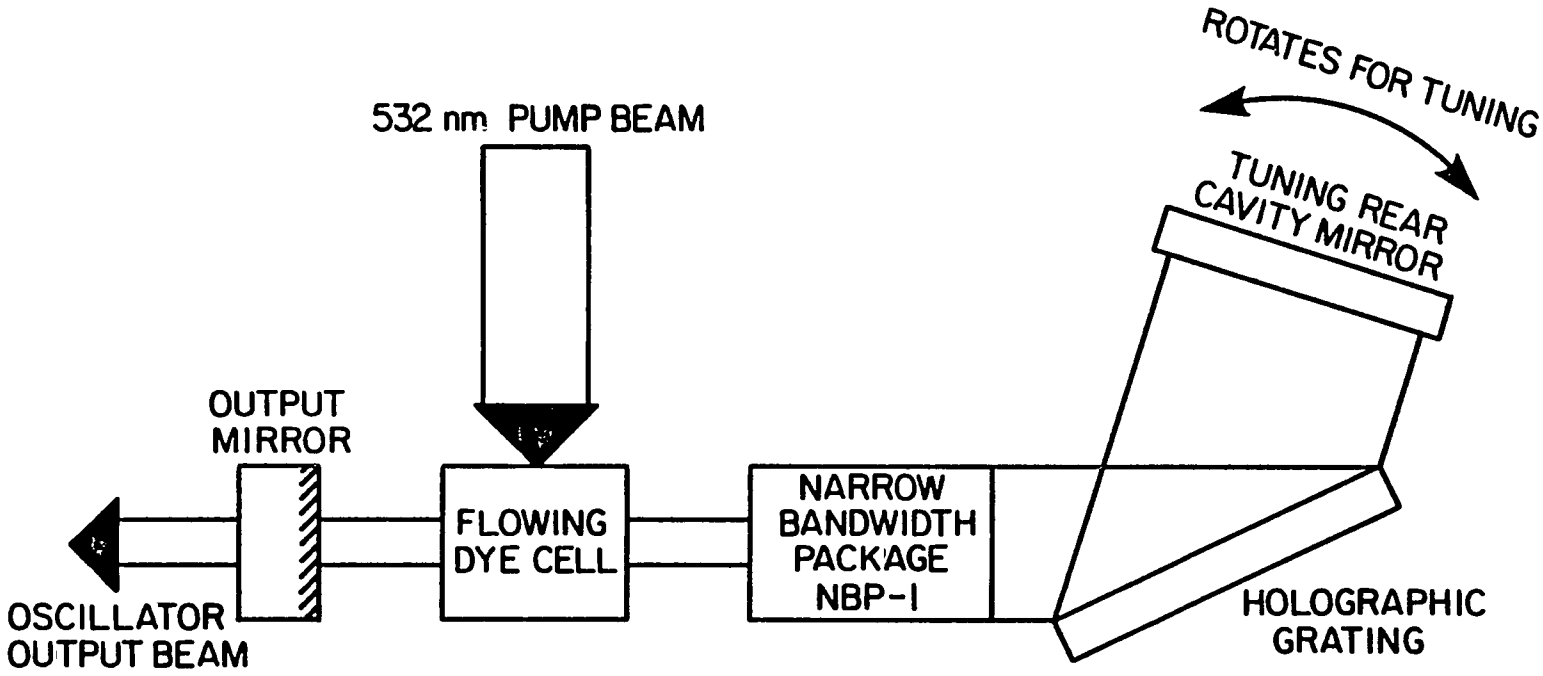


Figure 8. Oscillator cavity: dye laser tuning process

Table 3. Experimental conditions of laser dyes

| Dye[a] | Concentration (mg/L)[b] | | Wavelength Range[c] (nm) |
|---|---|---|---|
| | Oscillator | Amplifier | |
| Rhodamine 590 Chloride | 169.2 | 33.8 | 565-605 |
| Rhodamine 610 Chloride | 176.1 | 67.0 | 592-625 |
| Rhodamine 640 Perchlorate | 577.4 | 122.0 | 620-660 |
| Oxazine 720 Perchlorate/ | 361.9 | 110.4 | |
| Rhodamine 640 Perchlorate | 115.5 | 24.4 | 660-700 |

[a]Exciton Chemical Co., Inc., Dayton, OH 45431.

[b]Dye solvent: Absolute methanol, AR grade, obtained from Mallinckrodt, Inc., Paris, KY 40361.

[c]Assumes 532 nm Nd:YAG pump laser; Quantel International, Santa Clara, CA 95050.

1 W at 10 Hz was produced. However, it is important to note that dye laser conversion efficiency is wavelength-dependent (196) and typical experiments were run at much lower powers.

The output of the tunable dye laser was collimated down to a beam diameter of approximately 2 mm by means of a homemade dual lens telescope. Because all of the PAC studied absorb in the ultraviolet (UV) portion of the spectrum, this condensed beam was subsequently passed through a Quantel model FCA-1 frequency conversion apparatus (FD in Figure 6). The FCA-1 was used in the frequency doubling mode by employing KDP crystals (93), thus providing a tunable UV laser beam capable of covering a 282-350 nm range. Conversion efficiency was approximately 5-10 % of input power. The fundamental (visible) beam was then separated from the second harmonic (UV) beam, through the use of a Pellin Broca prism, after which it was trapped by a beam dump.

The UV laser beam was carefully aligned through the center of the multidimensional detector, as is roughly indicated in Figure 6. The beam entered the high vacuum chamber through a fused silica window and emerged on the opposite side by way of a quartz window placed at Brewster's angle, with respect to the axis of the laser beam, in order to minimize back reflections. The exiting beam was then trapped by a surface absorbing disc calorimeter that served to provide a constant measure of average UV laser power. Although the selected laser power level varied from experiment to experiment, all investigations were conducted with UV pulse energies in the 0.05-3.0 mJ range.

Four optical baffles were strategically positioned (see Figure 6) within the high vacuum chamber to serve as references for alignment and to

minimize stray laser light caused by reflections and/or scattering within the detector. The internal diameter of these baffles was approximately 6 mm, with each machined down to create a knife-edged aperture in order to reduce the possibility of reflections originating from the baffles themselves. Stray laser light presented no problem for the REMPI detection schemes, but it did create a background signal problem in the LIF optical detection system. These empirically positioned baffles greatly reduced this problem.

## B. Sampling Systems

In most of the studies to be presented here, a capillary column gas chromatograph (CC/GC) was an integral part of the sample introduction system. Obviously, the dimension of chromatographic retention time provided an additional degree of selectivity. However, there are a number of other advantages to utilizing a CC/GC in the sampling system of the present instrument. These advantages are discussed below, followed by a detailed description of the entire sampling system.

### 1. Advantages of CC/GC sample introduction

Before an analytical instrument can be employed for routine analyses, characteristic detector responses must be established for the compounds of interest by utilizing high purity reference compounds. The CC/GC provides a simple means of reproducibly introducing minuscule amounts of these reference compounds. Typically, a microliter of a volatile solvent, that contains a small amount of the reference compound may be injected. In this case, nanogram-level samples pass through the column, according to

their characteristic retention times, and pass into the detector as a "plug". Thus, detector responses may be determined for each compound on-the-fly, while allowing only a very small amount of the compound to enter the detection system. This is particularly important when a large number of compounds must be characterized, because any residual analyte present in the detection system may result in background signals that might severely limit sensitivity.

By preparing reference mixtures of several chromatographically resolvable compounds, a number of characteristic detector responses may be determined, in series, for a single injection of sample. Thus, more reference compounds may be characterized for each chromatographic run if a high resolution CC/GC is employed in the sampling system. Further, as the chromatographic effluent may be easily split to allow the use of parallel detection schemes, a portion of the effluent may be channeled into a universal chromatographic detector, such as a FID, so as to provide information regarding those components not excited by the laser-based detection system. Also, because of the relatively low flow rates of CC/GC, it is preferred over packed column GC for this application, as the required GC-high vacuum interface may be much simpler.

For the analysis of complex environmental samples that contain a number of PAC, the "mixture simplification" aspect of CC/GC, as suggested in Chapter II, greatly relaxes the spectral selectivity requirements for the laser-based detector. Another important advantage of utilizing a chromatographic sampling system is that quantitation becomes quite straightforward when reference compounds and real samples may both be reproducibly introduced (157).

2. The CC/GC sampling system

The layout of the complete sampling system is shown in Figures 9 and 10, and the specific components utilized in the present studies are summarized in Table 4. For discussion purposes, this system can be logically broken down into the chromatographic section, the transfer line, and the GC-high vacuum interface. The chromatographic section is discussed first.

A Tracor model 560 temperature-programable gas chromatograph, equipped with a capillary inlet system and a FID detector was utilized in these studies. As emphasis was not placed on high resolution chromatography, a modest 15 m x 0.32 mm DB-5 bonded stationary-phase, fused-silica capillary column was used. Although capillary columns with greater than 200,000 effective theoretical plates (197) are readily available, the approximately 40,000 plates of this particular column were adequate for the studies at hand. A relatively short column length was chosen in order to minimize chromatographic retention times. Also, such bonded phase columns are very durable and may be used at temperatures of up to 350 $^{o}$C without appreciable column degradation. This is an important factor for the analysis of mixtures that contain high boiling point compounds. The DB-5 bonded stationary phase has properties that are equivalent to the more familiar SE 54 [(94 %)Dimethyl-(5 %)diphenyl-(1 %) vinyl-polysiloxane] apolar liquid phase (197) that is commonly used in PAC characterization studies (78).

A vitreous-silica outlet splitter was installed at the capillary column exit, within the GC oven. The split effluent was, therefore, transferred to both the FID and the GC-high vacuum interface via

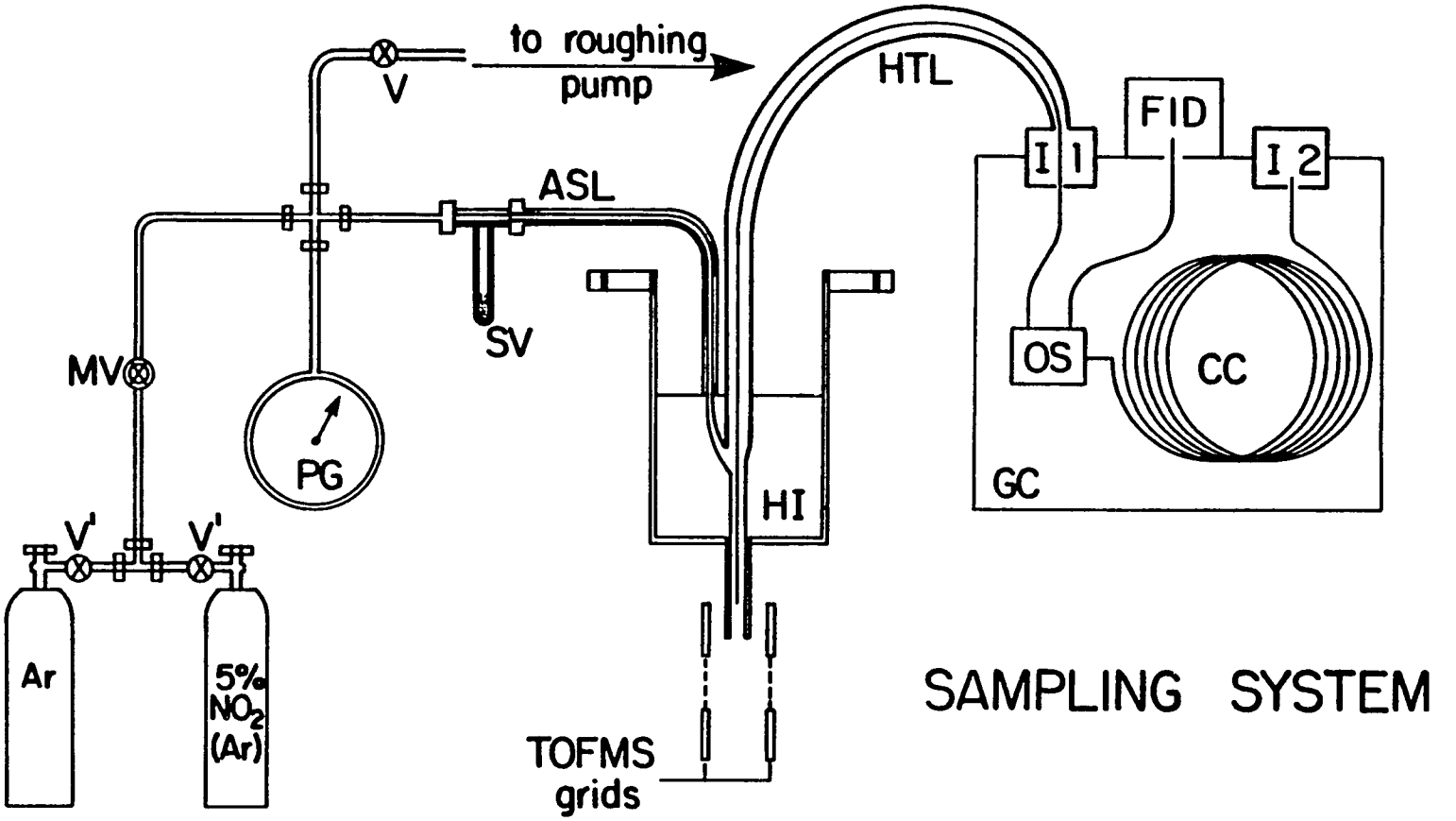


Figure 9. Complete sampling system layout. Specific components are summarized in Table 4

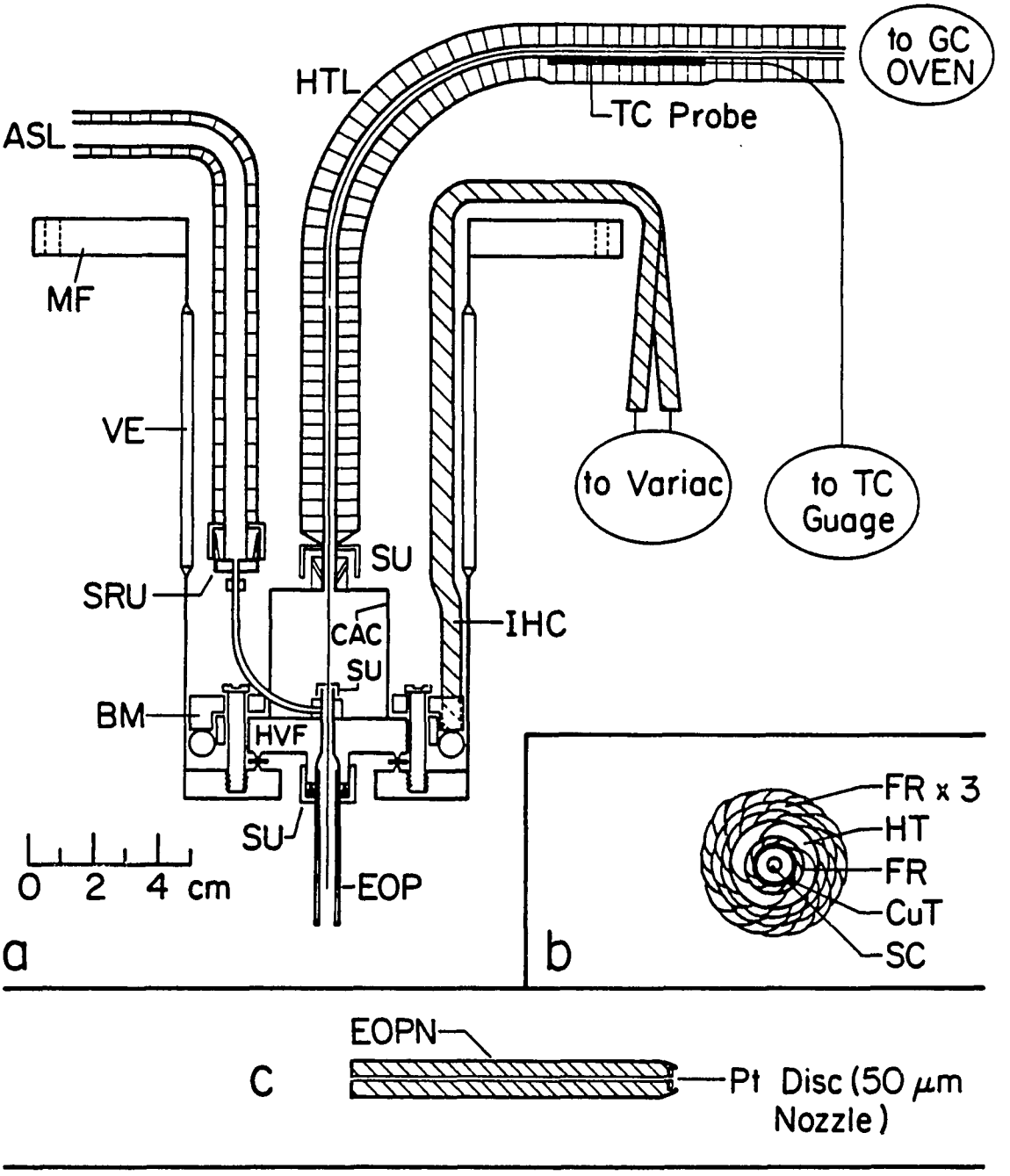


Figure 10. Transfer line and GC-high vacuum interface. Specific components are identified in Table 4. a) Overall assembly (to scale); b) cross section of heated transfer line; c) Extended oven probe nozzle

Table 4. Sampling system components[a]

| Component | Symbol | Model No. | Manufacturer |
|---|---|---|---|
| Gas Chromatograph | GC | 560 | Tracor Instruments, |
| Flame Ionization Detector | FID | | Austin, TX |
| Sample Inlet 1 | I1 | | |
| Sample Inlet 2 | I2 | | |
| Capillary Column | CC | DB-5 | J&W Scientific, Inc., Rancho Cordova, CA |
| Vitreous Silica Outlet Splitter | OS | VSOS | SGE, Austin, TX |
| Heated Transfer Line | HTL[b] | ----- | Ames Laboratory |
| Splitter Capillary | SC | | Constructed |
| Copper Tubing | CUT | | |
| Fiberglass Ribbon | FR | | |
| Heating Tape | HT | | |
| Thermocouple Probe and Guage | TC | 4001KC | Omega Engineering, Inc., Stamford, CT |
| Heated Interface | HI[b] | ----- | Ames Laboratory |
| Mating Flange | MF | | Constructed |
| High Vacuum Flange | HVF | | |
| Cut-away Cylinder | CAC | | |
| Brass Mantle | BM | | |
| Immersion Heater | IHC | | |
| Extended Oven Probe | EOP | | |
| Extended Oven Probe Nozzle | EOPN | | |
| Vacuum Envelope | VE | 807A0296-3 | Ceramaseal, Inc., New Lebanon, NY |
| Swagelok Union | SU | | Crawford Fitting, Co., |
| Swagelok Reducing Union | SRU | | Solon, OH |
| Alternative Sampling Line (Heated) | ASL | ----- | Ames Laboratory Constructed |
| Sample Vial | SV | | |

[a]Refer to Figures 9 and 10.

[b]Details in Figure 10.

deactivated vitreous-silica tubing of 1 m and 2 m lengths, respectively. The characteristics of the splitter were such that approximately 70 % of the chromatographic effluent was introduced into the laser-based detection system, while the remainder flowed into the FID. Inlet number-2 of the Tracor GC served as the sample injection port for the split mode injections employed in the present studies. Inlet number-1 was slightly altered to serve as the outlet port for the 2-m capillary tubing through which a portion of the CC/GC effluent flowed.

3. Transfer line and GC-high vacuum interface

The transfer line and GC-high vacuum interface portion of the sampling system was designed and fabricated in-house to meet experimental requirements. The detailed assembly is displayed, roughly to scale, in Figure 10a. The entire effluent transfer system had to be maintained at or above chromatographic temperatures in order to prevent condensation of the analyte. All components were, therefore, capable of tolerating in excess of 350 $^{o}$C. The 2-m vitreous-silica splitter capillary was fed out of inlet number-1 and threaded through 0.32 x 100 cm copper tubing that was securely anchored, at its respective ends, to the GC-high vacuum interface assembly and the septum nut of the GC by 0.32 cm Swagelok nuts and ferrules. As shown in Figure 10b, the copper tubing was first wrapped by a layer of fiberglass ribbon, after which a 1.3 x 183 cm flexible electric heating tape was coiled around its entire length. This transfer line was then wrapped with three additional layers of fiberglass ribbon to minimize radiant heat losses. A thermocouple probe, interwoven next to the copper tubing, was connected to a digital temperature gauge to serve as a temperature monitor for the transfer line. A Variac voltage

controller was empirically set to maintain the transfer line above chromatographic temperatures, typically 340 $^{o}$C. The copper tubing not only served as a guide for the 2-m capillary tubing, but also protected the later from breakage due to stress at times when it was necessary to move the line. Also, because of the excellent heat conducting properties of copper, the tubing was able to provide uniform heating of the capillary tubing, precluding any problems that may have resulted from the presence of hot or cold spots in the line.

The capillary tubing emerged from the top of a cut-away stainless steel cylinder positioned so that it was directly in line with a 0.16 cm Swagelok fitting that was mounted in the center of the top of a 7 cm vacuum flange. The cut-away portion of the cylinder was necessary in order to allow access to the 0.16 cm Swagelok fitting through which the capillary was threaded. The end of the capillary then emerged through the center of a 0.64 cm Swagelok fitting that was mounted on the opposite side of the flange, and positioned approximately 3.8 cm below the flange. A vacuum seal was then made between the capillary tubing and the 0.16 cm Swagelok fitting by means of a Vespel/graphite capillary reducing ferrule. A 0.64 x 5.1 cm copper rod, machined to an internal diameter of 1 mm, was positioned over the capillary outlet and secured to the flange using a Swagelok nut and a brass ferrule. This so-called extended oven probe served to keep the end of the capillary tubing hot. A 0.16 cm stainless steel line, mounted in the base of the 0.16 cm Swagelok vacuum feedthrough, provided access to sampling systems other than CC/GC. For the majority of experiments, however, it was simply capped off near the flange.

The entire 7 cm vacuum flange assembly was mounted inside the vacuum envelope oven. A knife-edge vacuum seal was made between the flange and the base of the oven by means of a copper gasket. A brass mantle, in intimate thermal contact with both the flange and an immersion heater coil positioned inside the circumference of the base of the oven, allowed even heating of the system and served as a heat sink that greatly reduced the possibility of sudden temperature changes within the oven. Again, a Variac voltage controller was empirically set to maintain the oven at an appropriate temperature.

The base of the oven was mounted to the bottom of a kovar/alumina vacuum envelope, the top of which was sealed to a 19 cm(o.d.) stainless steel flange. The entire vacuum interface assembly was then mounted on the top vacuum port of the high vacuum chamber (Appendix C), with the vacuum seal being made utilizing a rubber o-ring gasket. The alumina sleeve thermally isolated the hot oven base from the high vacuum chamber, thereby preventing excess heating of the chamber. Also, the hollow shell of the vacuum envelope oven was packed with glass wool in order to minimize thermal equilibration with the air. The alumina sleeve and glass wool combination allowed the oven to maintain stable temperatures and to function more efficiently.

4. Alternative sampling system

The alternative sampling system, as included in Figure 9, provided a means of introducing vapors of reference compounds, a regulated supply of argon carrier gas, and a gauge for monitoring backing pressure. For alternative sampling mode experiments, the 0.16 cm stainless steel line mounted in the base of the 0.16 cm Swagelok vacuum feedthrough was

connected to a 0.64 x 46 cm stainless steel sampling line by way of a reducing union. The other end of the sampling line was connected to a Swagelok tee fitting from which was mounted a 0.64 x 5.1 cm Pyrex tube, sealed at one end to create a sample vial. An air-tight connection was made between the vial and the base of the tee, utilizing either a teflon or graphite ferrule and a 0.64 cm nut. The tee was connected to a union cross that provided access to a 0-760 torr pressure gauge, a small cryotrap and roughing pump via a shut-off valve, and two compressed gas cylinders via a metering and two shut-off valves. All components were linked with 0.64-cm(o.d.) stainless steel tubing.

A Variac-controlled, flexible electric heating tape, coiled around the sampling line and tee, served to volatilize the sample in the vial and provided efficient transfer of the resulting vapors to the vacuum envelope oven. In these experiments, the metering valve provided a few torr of argon carrier gas that served to direct the flow of vapor through the sampling line. The roughing pump was used to evacuate the sampling system upon the completion of experiments.

Provisions were included for operation in a seeded, free-jet expansion mode. To make this possible, the extended oven probe of the GC-high vacuum interface had to be replaced by the extended oven probe nozzle (Figure 10c). The basic probe nozzle dimensions were identical to the original probe, to the point where they were physically interchangeable. However, the probe nozzle had a 2 mm(o.d.) platinum disc, with a 50 μm pinhole in the center, implanted in its tip. This pinhole served as a continuous-flow(cw) nozzle in free-jet expansion experiments. The probe nozzle tip was machined to a taper in order to facilitate better local

pumping speed near the nozzle. The argon backing pressure was controlled through the adjustment of the metering valve. A standard gas mixture for 5 % $NO_2$ in argon was also made accessible to the sampling lines, by way of this valve, and was utilized to demonstrate the cooling effects on the jet (Appendix B).

## C. TOF/MS Cation Detection System

The basic components of a commercially available TOF/MS instrument were adapted for use as a detection system for laser ionization studies. The primary components of this assembly, minus the associated electronic components, are shown in Figure 11. An itemized list of these commercial components, including the electronic components, is given in Table 5. The instrument, from which most of these components were acquired, was equipped with an electron-beam ionization (EI) source. After assembly, the mass spectral resolution and ion throughput were roughly optimized using EI. However, the principles and design of the EI source components, as they relate to this particular instrument, will not be presented here, as they are available elsewhere (198-200).

After optimizing the EI source for maximum resolution, the horizontal and vertical deflection plate potentials were adjusted to maximize ion throughput. The magnetic electron multiplier(MEM) magnet and compensating magnet assemblies were then finely positioned to maximize detector sensitivity. The primary purpose of the compensating magnet assembly is to empirically negate the effects of the detector magnetic field on the ions moving through the flight tube.

The EI-TOF mass spectrum shown in Figure 12 provides a rough

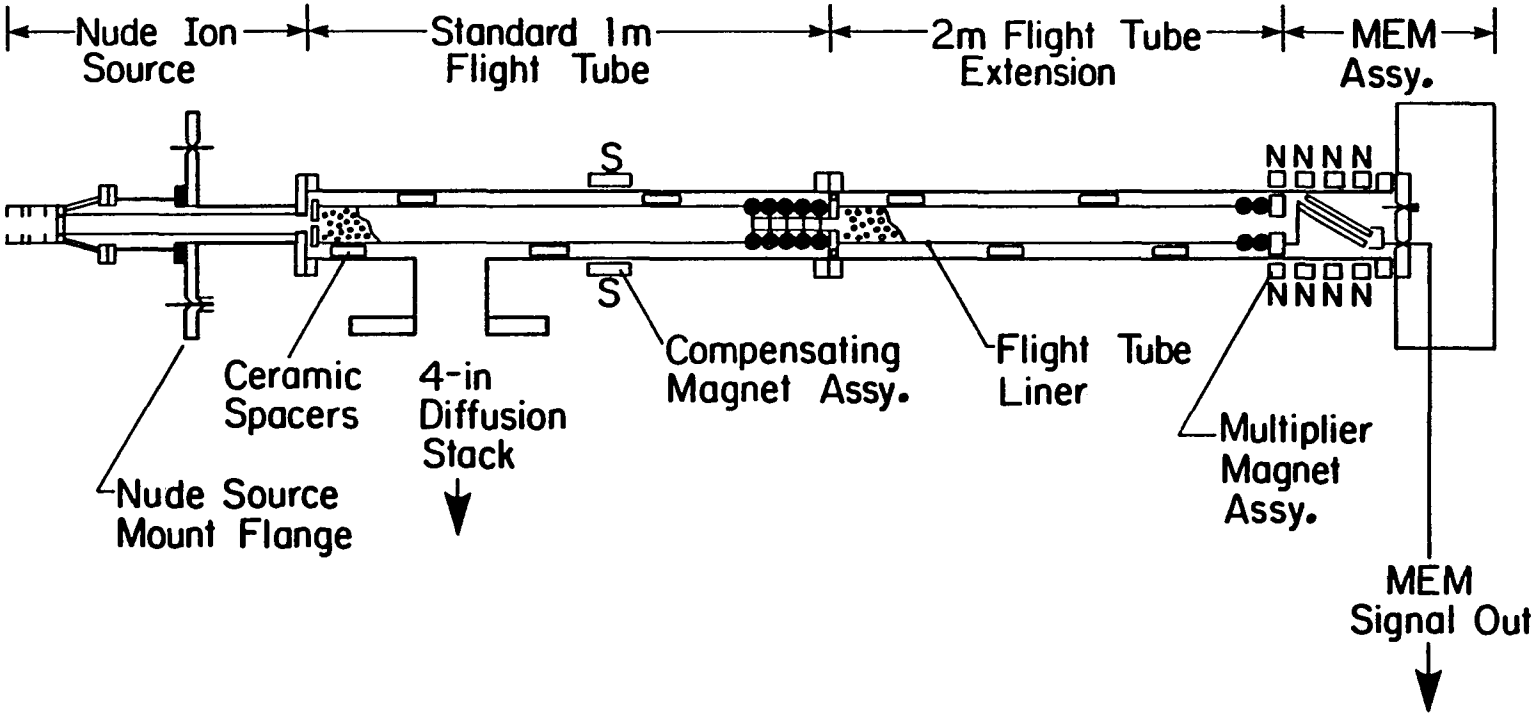


Figure 11. Basic components of commercial TOF/MS adapted for photoionization studies. Itemized list of these components, plus electronics, is provided in Table 5. Nude ion source details are provided in Figure 14

Table 5. Components of commercial TOF/MS instrument, including electronics, utilized in laser ionization studies

| Component[a] | Model Number | Part Number |
|---|---|---|
| Nude Source Assembly | MA-017 | 5504422-2 |
| Flight Tube Assembly | | 5508320 |
| Two-Meter Flight Tube Extension | MA-022 | 5505683 |
| Magnetic Electron Multiplier Assembly | | 5503678 |
| Multiplier Magnet Assembly | | 5502561 |
| Compensating Magnet Assembly | | 5507104 |
| Electronics Chasis Assembly | | 5503772 |
| Analog Output Scanner[b] | MA-010A | 5503733-1 |

[a]All components supplied by CVC Products, Inc., Rochester, NY.

[b]Used only in EI-TOF/MS experiments.

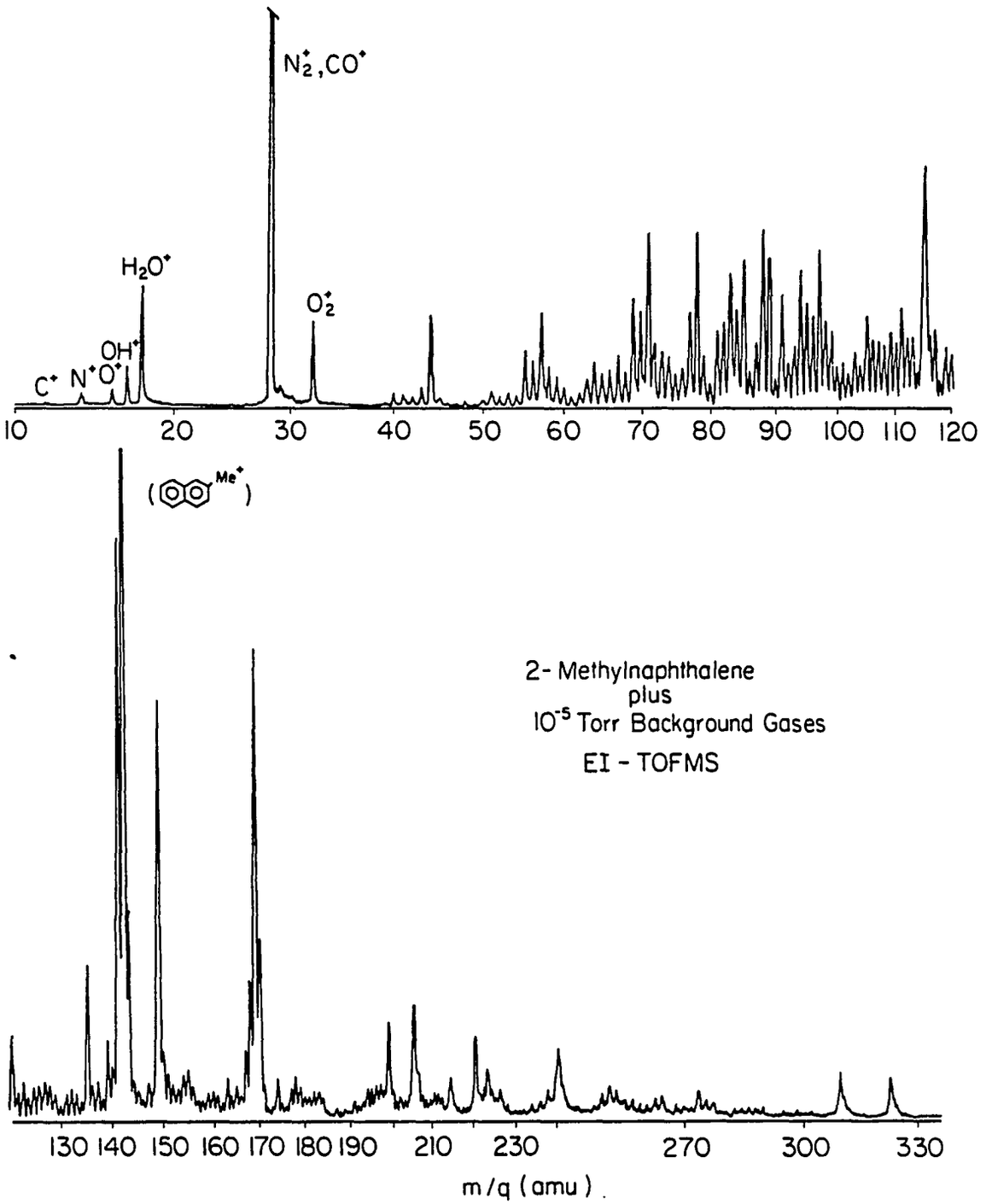


Figure 12. EI-TOF/MS of 2-methylnaphthalene plus $10^{-5}$ torr background gases. EI source: 80 eV at 10 kHz repetition rate

indication of the mass resolution available with this instrument when a 10 kHz, 80 eV EI source was used. This mass spectrum was taken at a source pressure of approximately $10^{-5}$ torr, while the vacuum system was in the process of pumping down to its ultimate pressure of $10^{-7}$ torr, after having been vented to atmosphere. The MEM signal was processed by an analog output scanner (200), before being recorded on a strip chart recorder. In addition to vacuum system residuals, including air, water vapor, $CO_2$, and background pump oils, vapors of 2-methylnaphthalene were also present by way of the alternative sampling system. Thus, this background mass spectrum was very complicated, consisting of parent ions of each of these species as well as a multitude of fragment ions. In this particular mass spectrum, adjacent mass peaks were easily distinguishable up to approximately 220 u. The more intense peaks were broader than the weaker peaks, resulting in a "local" degradation in mass resolution. This peak broadening was likely due to coulombic repulsion within isobaric "ion packets" as they traversed the flight tube. Naturally, this effect was expected to be more pronounced when the number of ions within a particular packet was greater.

The discussions to be presented in the following subsections will center around three primary topics. First, basic principles of the MEM detector will be briefly summarized. Following this is a description of the primary alterations that were implemented in order to incorporate the TOF/MS components into the multidimensional detection scheme. Finally, the data acquisition systems utilized with the laser ionization-TOF/MS system will be described.

1. Magnetic electron multiplier(MEM) detector

To appreciate the principles of operation of MEM detectors one must first understand the basic theory related to the movement of charged particles in crossed electric and magnetic fields. As this theory has been adequately presented elsewhere (198,201), only qualitative consideration will be given to the very simple case shown in Figure 13a. A static electric field ($\underline{E}$) is established between two parallel plates by positively biasing one with respect to the other. An electron at rest between the two plates will experience a force due to this electric field ($\underline{F}_E$),

$$\underline{F}_E = -e\underline{E},$$

where e is the charge of an electron and the "bars" label vector quantities. Thus, the electron will initially be accelerated in the direction of the more positive plate. Given a homogeneous magnetic field ($\underline{B}$), aligned perpendicular to $\underline{E}$, the electron, now moving with an increasing velocity ($\underline{v}$), will experience a second force ($\underline{F}_B$),

$$\underline{F}_B = -e\underline{v} \times \underline{B}.$$

Alone, $\underline{F}_B$ would cause the electron to follow a circular path, in a plane perpendicular to $\underline{B}$. However, in the presence of $\underline{F}_E$, the electron slows down when directed back toward the negatively biased plate and must momentarily come to rest at a point that is equal in potential to that of its original starting point (conservation of energy). This process will repeat itself until the electron escapes the influence of $\underline{E}$ and/or $\underline{B}$. Thus, the electron travels in a cycloidal path, with the cusps of the cycloids directed along an equipotential line.

A simplistic schematic view of an MEM detector is given in Figure

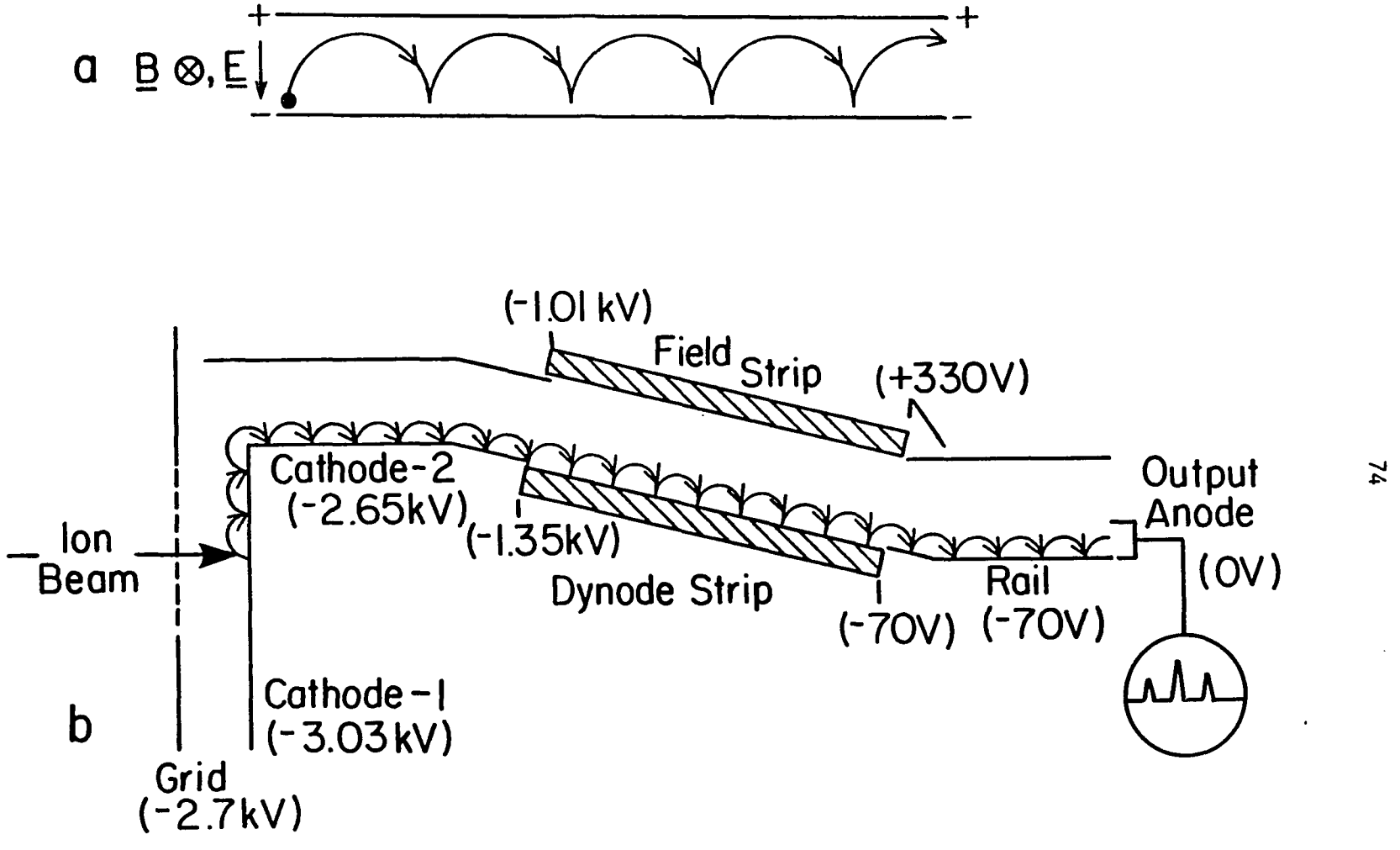


Figure 13. MEM detection. a) Electron moving in crossed electric and magnetic fields. b) Simplified schematic view of an MEM detector

13b. The magnetic field is furnished by a permanent magnet assembly positioned outside of the flight tube (Figure 11). The electric fields are provided by metal plates and other conductive surfaces within the vacuum housing. Cations initially strike the surface of cathode-1 with 3.03 keV of energy, causing electrons to be released. In a manner similar to that described for Figure 13a, these electrons follow a cycloidal path along an equipotential line just above the surface of cathode-1. Cathode-2 is held at a potential of approximately 400 V more positive than cathode-1, thus the equipotential line of cathode-1 is, in effect, a virtual line that is beneath the surface of cathode-2. Therefore, electrons entering the cathode-2 region will hit the cathode surface with 400 eV of energy, liberating secondary electrons with an approximate yield of 3:1 (198). These electrons then proceed along a new equipotential line, just above the surface of cathode-2.

There is a sharp potential rise in going from the end of cathode-2 to the front of the dynode strip. Therefore, the transition cycloid results in the electrons being slammed into the dynode surface with an energy of approximately 1.3 keV, resulting in a single high-gain step, with several secondary electrons being produced for each incident electron. The dynode and field strips are resistively coated glass plates with a high potential difference applied across each of them (approximately 1.3 kV for a multiplier gain setting of 5). Thus, a uniform potential gradient is set up along these strips, so that the equipotential point, from the reference frame of the cycloiding electrons, is always virtual. This results in the premature termination of each cycloid by 35-40 eV collisions between the electrons and the surface of the dynode strip. Depending on the gain

setting of the multiplier, this process may liberate secondary electrons with an approximate efficiency of 1.4:1. Normally, 40 to 60 cycles will occur from one end of the dynode to the other, resulting in typical gains of from $10^5$ to $10^9$. The dynode strip terminates at a -70 V rail that provides an equipotential line for the resultant electrons to follow to the grounded output anode.

The low gain per cycloid allows the use of nonactivated resistive coatings on the glass strips. This makes the MEM an ideal detector for use in the developmental stage of a new instrument that must be frequently vented to the atmosphere for adjustments, as it is resistant to moisture and oxidation. Further, the inertness of the MEM results in high durability, and may be routinely "baked out" at up to 350 $^{o}$C with no subsequent degradation in performance.

2. Alterations to design of commercial nude ion source

The nude ion source, as utilized in the laser ionization studies, is shown in Figure 14. Sufficient detail is included to indicate the primary alterations of the original commercial design that were necessary to best incorporate the TOF/MS instrument into the analytical system. A stainless steel cylinder, 7.6 cm in length, was added between the 20 cm(o.d.) nude source mount flange and the source mount pyramid. This enabled the ion drawout grid assembly to be precisely centered directly beneath the extended oven probe that was mounted in the base of the vacuum envelope oven, as described in the previous section. The layout of the high vacuum chamber is given in Appendix C, along with a description of the pumping systems. In order to maintain electrical contact between the deflection plate housing and the flight tube liner contact plate, the deflection

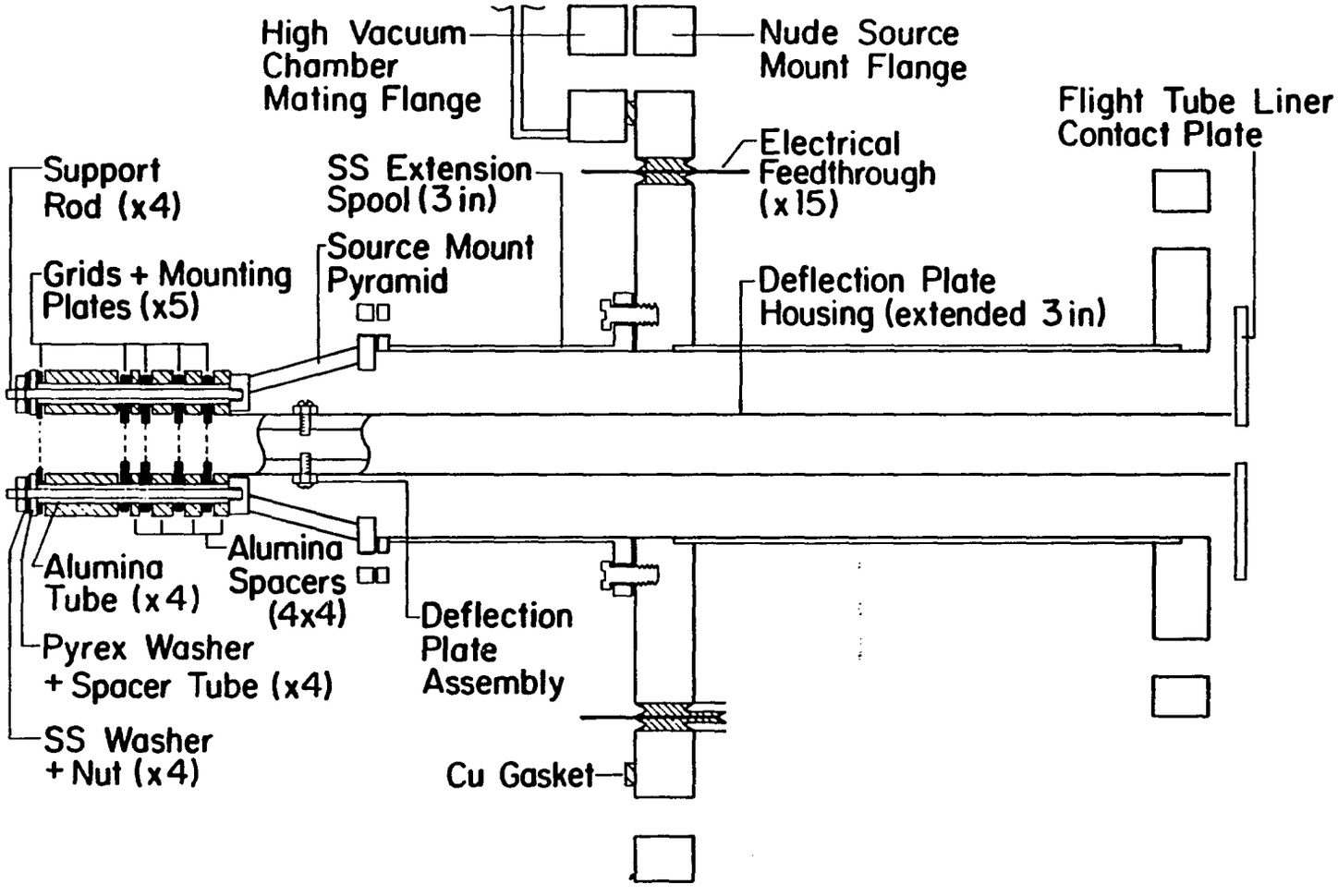


Figure 14. Nude ion source with alterations for photoionization studies

plate housing was also extended by 7.6 cm. Thus, upon the addition of the 2-m flight tube extension, a field-free drift region of approximately 210 cm in length resulted.

To minimize the interaction between the free-jet expansion and the nude ion source structure, the spacing between the grids that define the ionization region was increased from the standard 3 mm to 15 mm. This revised dimension was similar to that used by Lubman and Kronick (162) and Dietz et al. (168) in their so-called optical time-of-flight mass spectrometers. The wider spacing also somewhat relaxed the ionizing beam diameter restrictions (Chapter III) of the instrument and, therefore, allowed variations in the diameter of the laser beam without significant degradation in mass spectral resolution. To supply the additional ion source spacing, both the stainless steel support rods and the long alumina insulating tubes were 15 mm longer than the standard nude ion source dimensions. Four Pyrex tubes (4 mm i.d. x 6 mm o.d.), precisely 15 mm in length, were used as spacers between the backing grid and ion grid (IG) 1. Also, the backing grid was electrically isolated from the remainder of the source components by including 1 mm thick Pyrex washers (4 mm i.d. x 6 mm o.d.) between the stainless steel mounting washers and the backing grid. This allowed the backing grid to be conveniently used as an electron collector for the TECD, as discussed in the next section.

All ion source components associated with electron beam ionization (EI), including the EI source collimating magnet, filament and slit, and electron beam trap assemblies, were removed to allow optimum local pumping speed and to provide unobstructed access to the ionization region by the laser beam. In the EI mode, it was necessary to employ pulsed ion drawout

potentials on IG1 and IG2 (Figure 14) to prevent any electron beam deviation. The use of d.c. drawout potentials posed no difficulties for laser ionization. Laser beams are not effected by static high voltage fields and the temporal width of the Nd:YAG-pumped dye laser beam (<15 ns) was comparable to the rise time of the ion drawout pulses used in the EI configuration, resulting in no corresponding degradation in mass spectral resolution. Thus, all laser ionization were drawn out of the source immediately upon formation.

The d.c. drawout potentials were adjusted to empirically optimize ion throughput (sensitivity), while monitoring the 2-methylnaphthalene parent ion (142 u) signal provided by REMPI at an excitation wavelength of 286 nm. The 2-methylnaphthalene vapor was introduced as an effusive expansion via an alternative sampling system. The backing grid was held at ground potential. Two independent power supplies controlled the d.c. potentials on IG1 and IG2, respectively. Three general observations were made regarding this optimization process, listed as follows:

a) obviously, IG1<0 in order to transmit ions;

b) |IG2|>|IG1|, otherwise no signal was detected; and

c) the strongest 142 amu signal was produced when IG2 was approximately 165 Vd.c. more negative than IG1.

In effect, the ions were drawn out of the ionization region by the static electric field provided by IG1, while the IG1:IG2 combination served as an ion lens to optimize cation transmission through the entire instrument (202). The empirically optimized d.c. potentials were established to be -335 V and -500 V for IG1 and IG2, respectively, while IG3 and IG4 (including the flight tube liner) were maintained at their standard d.c.

values of -1.5 kV and -2.7 kV, respectively. The use of d.c. potentials on all grids had the additional advantage of eliminating difficulties due to sporadic drawout pulses, which are often a problem with commercial TOF/MS instruments.

3. Data acquisition for TOF/MS detection

The MEM output anode provided the TOF/MS signal for data processing. For each pulse of the ionizing beam an entire mass spectrum was delivered to the anode, in order of increasing mass, over a period of less the 100 μs, for the case of the TOF/MS instrument employed in these studies. Typical isobaric ion packets had temporal width of slightly less than 100 ns. The signal processing electronic components, therefore, had to have very fast response and recovery characteristics so as not to degrade the intrinsic mass spectral resolution of the instrument. Because fast response oscilloscopes have been used to provide a real-time monitor of TOF/MS signals (190,191,198), such an oscilloscope was incorporated into the TOF/MS data acquisition system to serve as a real-time monitor while optimizing experimental parameters. However, simple oscilloscopes have no provision for hard-copy data output and, therefore, have little use in a practical analytical sense, particularly for GC applications.

After being processed by a fast preamplifier, the MEM signal was made available to a gated integrator/boxcar averager system. (Such an integrator will be given further consideration in the next section.) This gated integrator provided access to a narrow mass window, typically 1 u, as it was utilized in the TOF/MS selective ion monitoring (SIM) studies. This electronic system was synchronized with the laser system via a fast photodiode trigger that was actuated by an in-house designed and assembled

1-101 μs variable delay generator (Figure 15). The mass window of interest was first roughly accessed by adjusting this delay generator and then fine-tuned via the aperture delay controls of the boxcar mainframe. The averaged SIM signal was then supplied to an X-Y recorder to provide hard-copy output. This data acquisition mode was primarily utilized for collection of REMPI-TOF/MS(SIM) chromatograms and, occasionally, for instrument optimization procedures.

The boxcar systems used in these studies were all capable of aperture delay scanning. In this mode, an entire mass spectrum could be collected by selecting the appropriate scanning rate and range. However, such an approach negates the intrinsic advantage of utilizing TOF/MS, in that most of the ion signal is wasted during a scan. Extremely poor signal-to-noise ratios (S/N) are the result, particularly at the low laser repetition rate (10 Hz) employed. Further, it would be hopeless to use this scanning detection mode in conjunction with a dynamic sampling system, such as CC/GC.

To best utilize the information available from the TOF/MS, the preamplified MEM output was fed into a LeCroy System 3500SA200 signal analyzer system (see Table 2). This system served as a high speed waveform digitizer that also signal averaged, processed, and archived the MEM analog signals. Waveform, or transient, digitizing involved the periodic sampling of a waveform at a rate high enough to provide an accurate picture of its structure. At each sampling, the voltage level of the input analog waveform was digitized for storage and processing by the signal analyzer computer.

In the studies presented here, the waveforms to be analyzed were

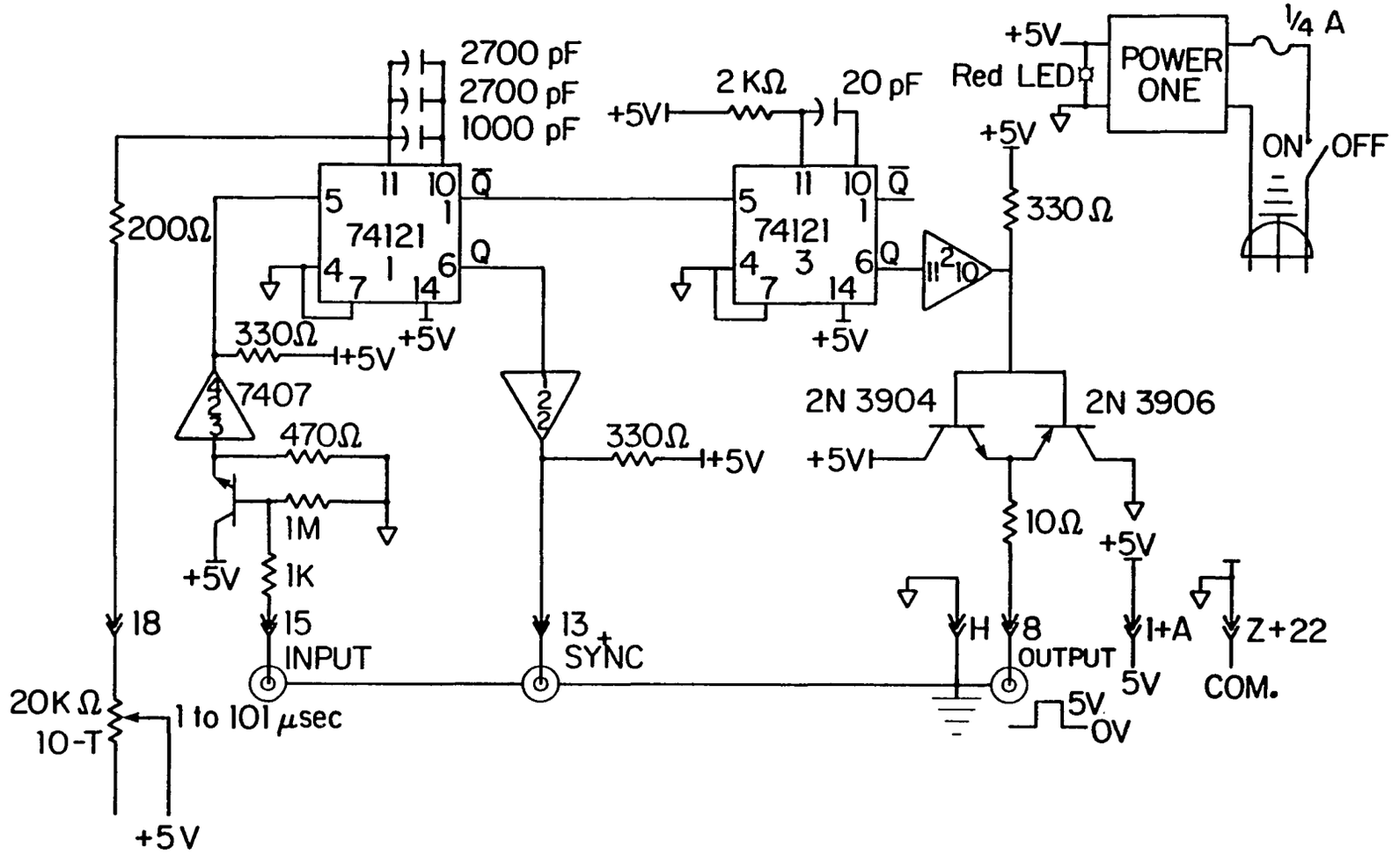


Figure 15. TTL variable delay generator (1-101μs), designed and constructed in the Ames Laboratory

simply time-of-flight mass spectra. The maximum sampling rate available with this signal analyzer system was 200 MHz (5 ns resolution), which was more than adequate to accurately profile the 100 ns mass peaks produced by the TOF/MS. Further, a maximum active memory of 8-K channels, with 8-bit dynamic resolution per channel, allowed up to 40 μs windows of the MEM output to be accessed while maintaining 5 ns temporal resolution. However, it was found that, even at this maximum resolution, 4-K or less of the active memory was normally more than sufficient to cover all mass windows of interest. Again, proper synchronization was provided by the photodiode trigger/variable delay generator (Figure 15) combination. By adjusting the delay generator, the active memory could be positioned, in time, to access any time-of-flight mass window.

The data processing system offered a choice of either exponential or summation signal averaging within respective memory locations, or "channels." In general, the exponential averaging option provides a preselected weighting factor to both incoming data and data already in each channel, such that data from earlier mass spectra becomes increasingly insignificant. Thus, the system gradually "forgets" old mass spectra. This mode of signal averaging may continue indefinitely, with a frequently updated mass spectrum being displayed on the cathode ray tube (CRT) of the system, as long as the signal analyzer continues to be triggered. Exponential signal averaging was most useful in establishing proper experimental parameters, such as the positioning of the mass windows and optimizing TOF/MS resolution, because changes in mass spectral features were discernible in real-time (approximately).

The summation-averaging, data-acquisition alternative was selected

for most of the TOF/MS work. In summation averaging, the 8-bit active memories of the transient digitizer were "dumped" into their corresponding 24-bit averaging memories within the signal processing system. In this manner, new data were summed with previously accumulated data, within the averaging memories, for a predetermined number of cycles. After completion of this summation process, the signal averaged mass spectra were archived onto a floppy disc for subsequent retrieval and processing. The mass spectra were available in hard copy via a CRT "screen-dump" to a LeCroy model 3931A printer. For the investigation of transient analytes, such as CC/GC effluents, the number of cycles was chosen to provide a total data acquisition time of on the order of chromatographic peak temporal widths, or less. Longer averaging periods were practical only when a continuous supply of analyte was available.

For the CC/GC-TOF/MS studies conducted thus far, it was deemed impractical to continuously collect and archive mass spectra throughout entire chromatographic runs, due to the unreasonable amount of floppy disc memory that would have been required. Therefore, data acquisition was initiated by manually triggering the system only upon the appearance of selected photoionizable chromatographic eluents, as indicated by a rise in the TECD signal. The TECD detection mode, as described in the next section, provided a reliable measure of the onset of REMPI.

By utilizing the signal analyzer system, as has been briefly described above, full advantage was taken of the high ion transmission efficiency of TOF/MS. Virtually all ions, within a preselected mass window, were detected and contributed to the archived mass spectra. In a sense, no ions were wasted, as would have been the case if other types of

mass spectrometers or data acquisition systems had been utilized for these pulsed laser-based studies.

An indication of the mass spectral resolution that was achieved by the TOF/MS, in conjunction with the transient digitizer data acquisition system, is provided by the laser ionization mass spectrum displayed in Figure 16. In this case, a small piece (<1 $cm^3$) of black sponge rubber (Durometer 35; Dunn Products, Chicago, IL) was inserted directly into the high vacuum chamber and a number of its volatile components were ionized by a 290 nm laser beam. The mass spectrum was obtained over a summation averaging period of three minutes (1800 laser shots) and covers a mass range of 120-325 u. The entire mass window is shown in Figure 16a, with apparently poor mass spectral resolution. However, the quality of the hard copy that is created by the screen-dump output mode is actually limited by the resolution of the CRT display. By expanding the time scales of two "regions of interest" (ROI), within this mass spectrum, a better picture of the true resolution is provided. Nearly baseline separation of all adjacent mass peaks shown in Figure 16c indicates unit mass resolution in excess of 300 u. The poorer-than-baseline resolution, shown in Figure 16b, is likely due to coulombic repulsion within isobaric ion packets as they traverse the flight tube. This peak broadening effect is quite common for high ion signals. No attempt has been made, thus far, to ascertain the identity of the easily ionizable components of this black sponge rubber sample. However, its complex spectrum illustrated that the mass resolution was more than adequate for these PAC studies and was useful in simplifying mass calibration procedures.

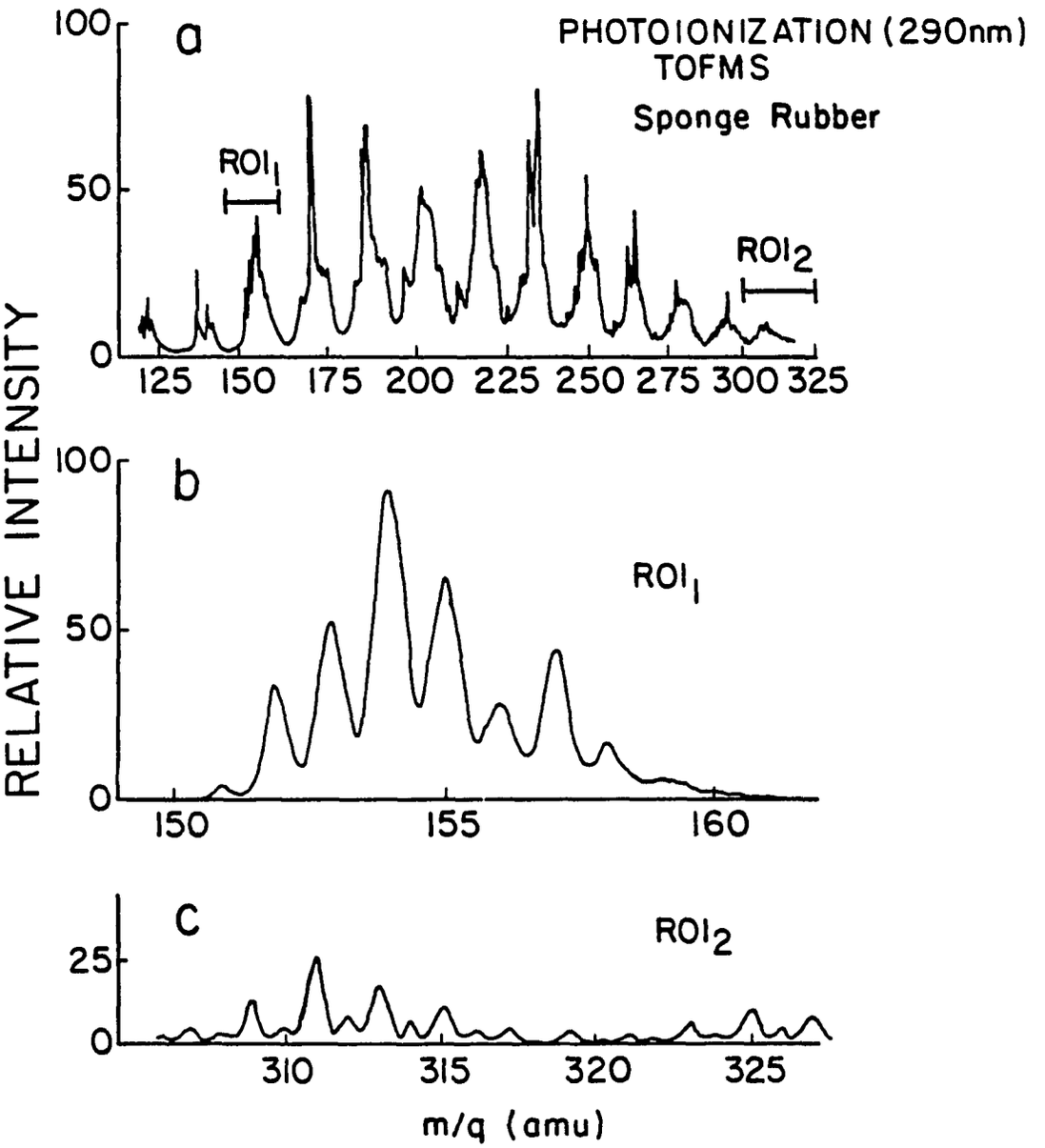


Figure 16. Photoionization-TOF/MS of black sponge rubber volatile components, summed over 1800 laser shots ($\lambda_{ex}$=290 nm). a) 120-325 u "screen dump"; b) $ROI_1$; c) $ROI_2$

## D. Total Electron Current Detection

All electrons resulting from photoionization of gaseous analyte within the static electric field of the enlarged nude ion source ionization region were efficiently collected on the backing grid and grid mount, which was grounded across a 10 kΩ resistor. A fast operational amplifier, current-to-voltage converter was directly attached to the backing grid via a 1 mm x 20 mm stainless steel rod that was welded to the rear of the backing grid mount. The circuit diagram for this source preamplifier and the arrangement of the high vacuum electrical feedthroughs is shown in Figure 17. The general circuit design was modeled after that employed by Havrilla and Green (203) as a preamplifier for studies of laser enhanced ionization in flames. The operational amplifier circuitry was constructed around a fast field effect transistor (FET) with high response characteristics (500 V/μA), high input impedance ($10^{12}$Ω), and a wide bandwidth (70 MHz). Such features are required for pulsed laser spectrometry because the operational amplifier must be able to respond to high frequency, fast risetime signals. The C, $R_F$ combination served as a high-pass active filter that minimized the possibility of low frequency interferences (e.g., 60 Hz). The opposed diodes on the FET input served to protect the circuit from any potentially damaging high voltage transients. The gain of this preamplifier was established by supplying a $2x10^{-5}$ A input current from a Model PB-2 Pulse Generator (Berkeley Nucleonics Co., Berkeley, California) that was set to provide a 1 mV square wave signal across 50 Ω. Under these conditions, the source preamplifier output was -0.3 V and, therefore, the gain was

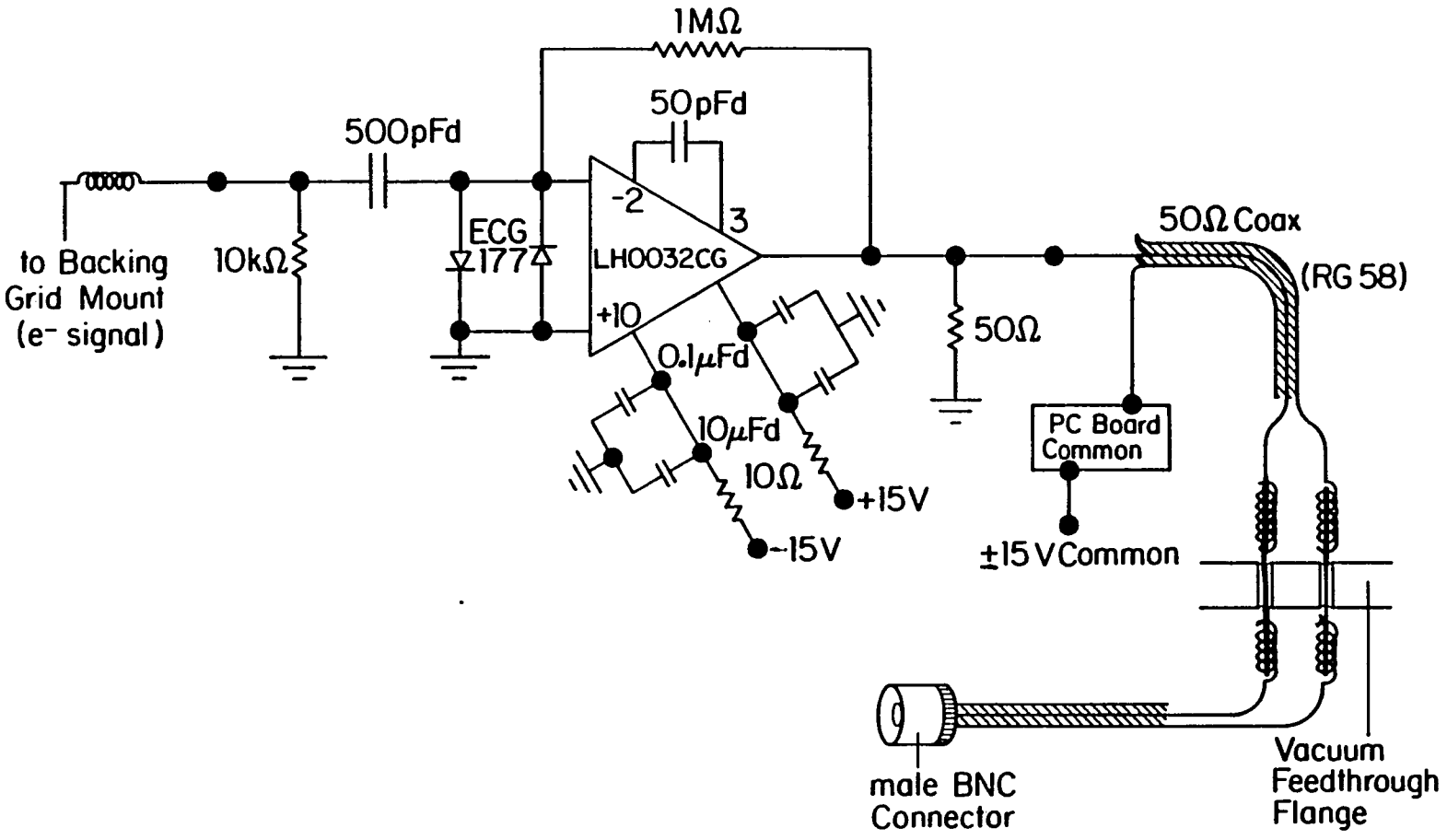


Figure 17. Source preamplifier circuit diagram plus high vacuum electrical feedthroughs for signal

determined to be approximately $-1.5 \times 10^4$ V/A.

Because small, transient electrical signals are measured in pulsed REMPI experiments, great care was taken to minimize ambient electrical "noise" resulting from radio frequency interference (RFI), which invariably accompanies pulsed laser operation. To this end, the preamplifier circuitry was assembled on a printed circuit board and mounted as close to the backing grid as possible. The possibility of forming "ground loops" was reduced by employing a single ground reference for all circuitry (204), that being the common of the 15 V power supply (Power-One Model HAA15-0.8 DC power supply). Also, all signal transmission lines and terminals were impedance matched to 50 Ω.

Even with the above precautions, appreciable RFI was still evident in the REMPI experiments. A qualitative illustration of an oscilloscope tracing of the source preamplifier output, resulting from both REMPI and high frequency RFI signals, is provided in Figure 18. The overall transient waveform was the superposition of 3 types of signals, the total electron signal, synchronous "ringing" RFI, and sporadic RFI noise, with characteristic frequencies of approximately 300-500 kHz, 10 MHz, and 100 MHz, respectively. In order to improve the signal-to-noise ratio, the output of the source preamplifier was connected to the input of an active filter preamplifier which is diagrammed in Figure 19. A tunable twin-T, electronic filter network in the feedback loop provided preferential amplification of the total electron signal, while discriminating against the high frequency RFI and any low frequency interferences.

Although the functionality of twin-T active filter networks has been described elsewhere (204), it is informative to define the characteristics

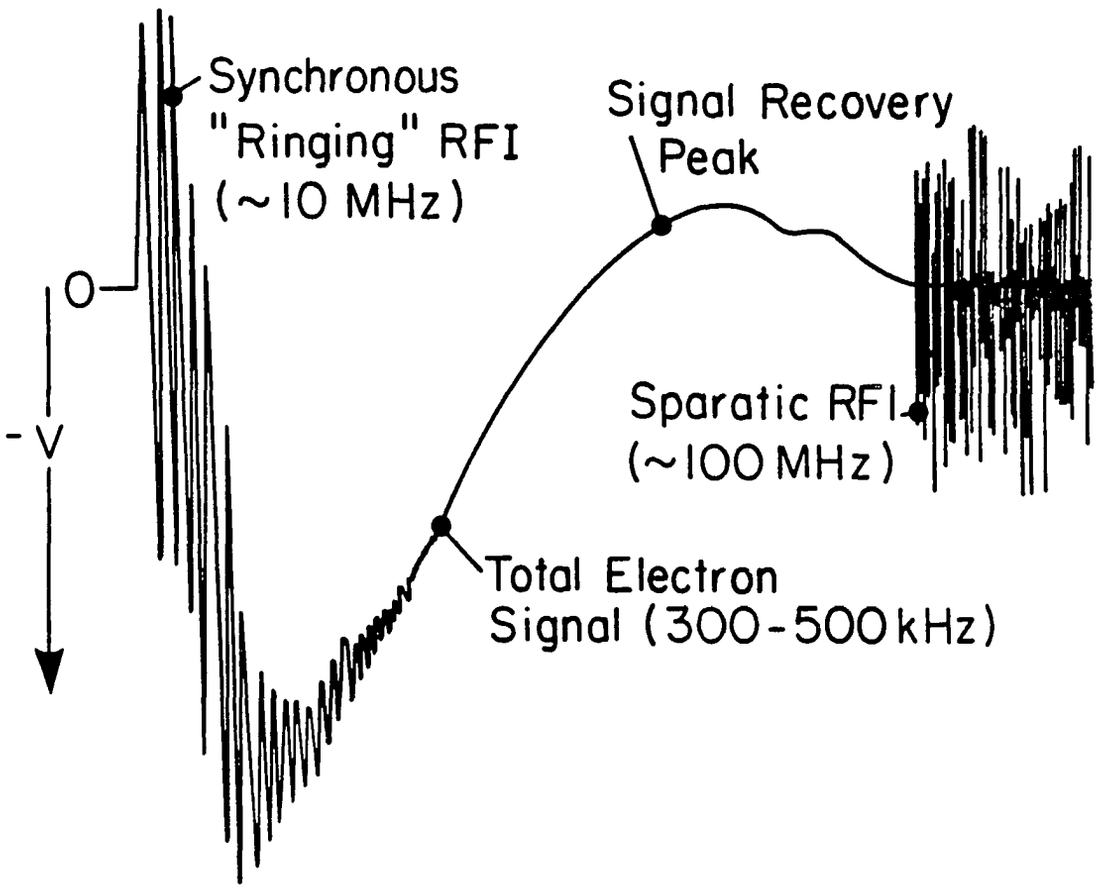


Figure 18. Sketch of oscilloscope trace of source preamplifier output resulting from laser ionization. Apparently, the waveform is the superposition of the signal and two types of RFI noise

of the circuit constructed for these studies. In general, a tunable twin-T filter tends to reject a narrow band of frequencies centered about the rejection frequency ($f_o$) given by:

$$f_o = 1/[2\pi RC(1-a^2)^{1/2}],$$

where a is the fractional setting of the potentiometer. In effect, this filter provided high impedance for signals with frequencies near $f_o$ and relatively low impedance to all other signals. Thus, such a filter placed in the feedback circuitry of an operational amplifier that provides inversion with gain, as is shown in Figure 19, resulted in amplification of $f_o$ signals to a greater extent than all other signals. All experimental measurements of total electron current were taken utilizing $a \approx 0.75$, which provided a rejection frequency of approximately 340 kHz. Thus, preferential amplification of the analytical signal was the result. This second preamplifier provided a voltage gain of approximately 10 for the analytical signal.

The output of the active-filter preamplifier was processed by a gated integrator/boxcar averager system. An input resistance of 50 Ω was selected for proper impedance matching and to minimize signal distortion. The voltage across the input load resistor was then applied to a unitary gain operational amplifier that in turn drove the gated integrator. Proper synchronization of the boxcar averager, gate delay circuitry was achieved via the fast photodiode trigger. Because of the gating action, the integrator only "saw" the signal for a selected aperture duration (or gate width) after each trigger. Thus, the output was proportional to the average value of the input signal over the gate width. By employing the exponential averaging mode (205), the boxcar output quickly reached a

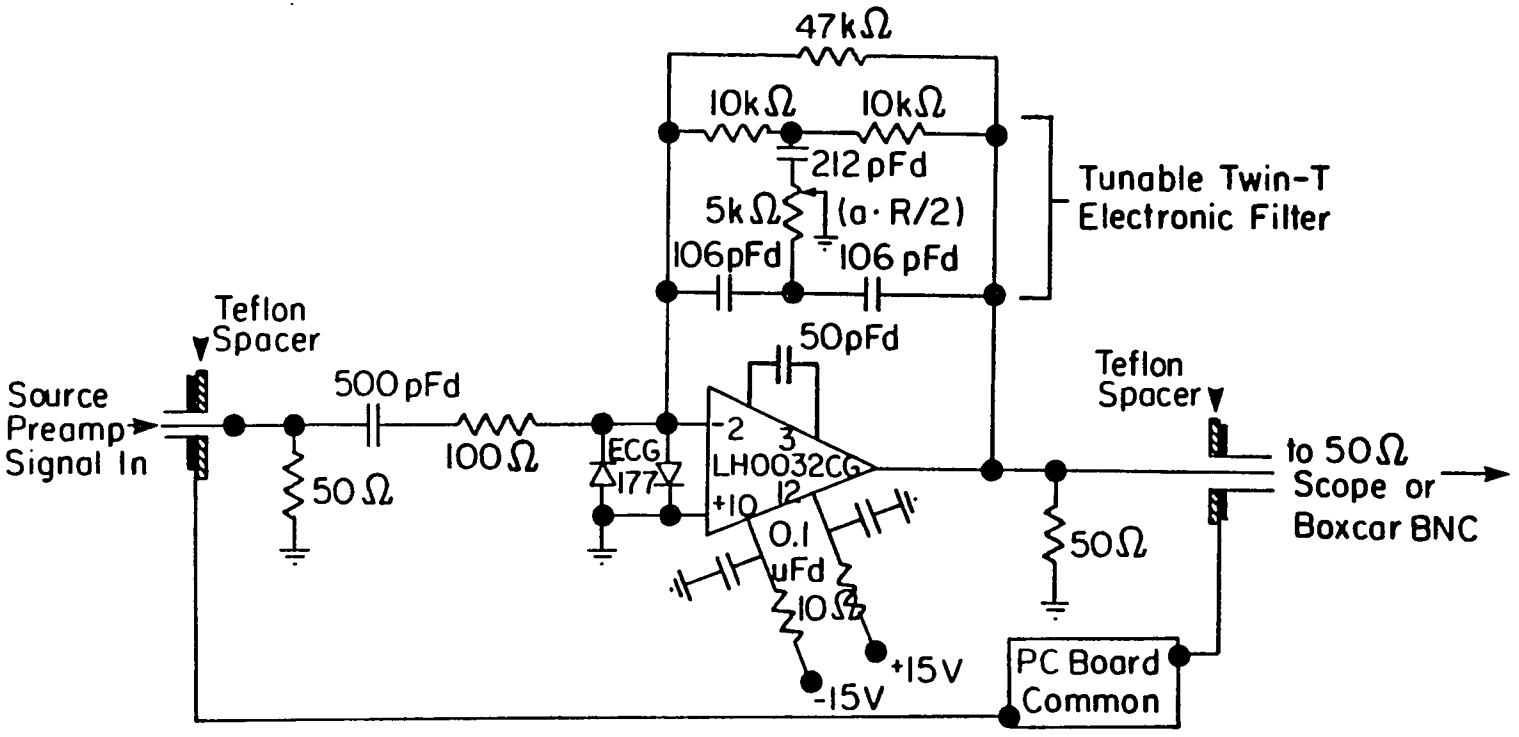


Figure 19. Active filter preamplifier for laser ionization experiments ($f_o$ = 150 kHz)

steady-state, exhibiting a simple linear relation with the input signal. The combination of variable gate width and delay allowed empirical optimization of this gated signal processing for each boxcar application.

The averagers were capable of scanning the position of a particular gate, in time, through a predetermined aperture delay range. In this manner, the profile of a repetitive transient signal could be recorded. Such scans were made to evaluate the total ion current and background RFI signals produced using this detection mode. With the laser firing ($\lambda_{ex}$=290 nm), a 100 ns gate was scanned over a 0-10 μs aperture delay range while monitoring the output of the second preamplifier. The background RFI "waveform", obtained with the laser beam blocked, is shown in Figure 20a. The RFI plus the total electron current produced by the ionization of residual PAC that were present in the dynamic gas sample cell is shown in Figure 20b. These results were helpful in choosing the optimum gate width and aperture delay of 200 ns and 0.87 μs, respectively, for this mode of detection.

The entire electron collection and signal processing data acquisition dimension, as has been described in this section, is termed total electron current detection (TECD). This system was primarily employed for the collection of TECD chromatograms. However, because it provided a reliable indication of the onset of photoionization, the TECD also served as a signal to initiate TOF/MS data acquisition.

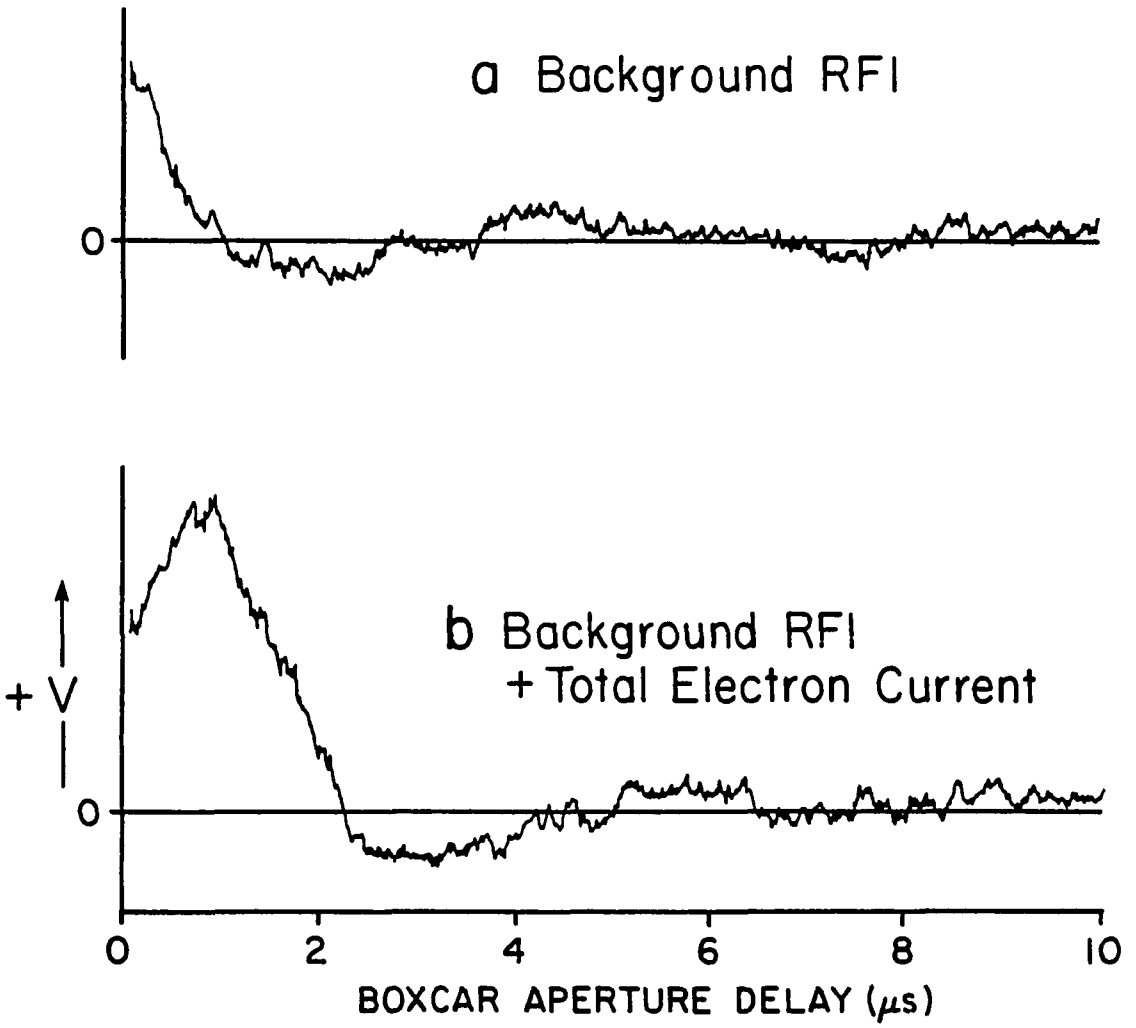


Figure 20. TECD output for 0-10 μs boxcar aperture delay scan, for a 100 ns gate width. a) Background RFI (laser beam blocked); b) Background RFI plus TEC. TEC due to photoionization 1 mJ/pulse, $\lambda_{ex}$=290 nm) of residual PAC in dynamic gas sample cell

## E. Laser-induced Fluorescence Detection System

The overall layout of the total fluorescence optical collection and detection system is shown in Figure 21a. A dual lens optical collection assembly was mounted behind the backing grid of the nude ion source (i.e. at an angle of 180° with respect to the TOF/MS flight tube). A 5-cm focal length (f.l.) fused silica lens, 2.5 cm in diameter, was positioned approximately 5 cm from the line of the ion source to collect and collimate fluorescence originating from the laser-analyte interaction region. A second fused silica lens (10 cm f.l. x 2.5 cm o.d.), positioned within the arm of a vacuum port, focused the fluorescence, through a quartz vacuum window and colored glass cut-off filters, onto a photomultiplier tube for detection. Each lens was mounted in a 1.9 cm brass Ultra-Torr adapter (Cajon Co., Solon, Ohio), which in-turn was mounted in an aluminum sleeve that was fitted with a pair of rubber o-rings. These assemblies were inserted into opposite ends of a 3.5 cm o.d. x 3.2 cm i.d. x 20 cm copper tube that was then snugly fit into the vacuum port arm. The o-rings allowed smooth and even positioning of the lens mounting assemblies, while keeping all optics precisely on-axis.

An end-on view of the filter holder mating flange is provided in Figure 21b. The 7 cm mating flange, machined to allow clearance for the six vacuum flange bolts, was mounted to the vacuum flange by three screws. A "light tight" o-ring seal was made between the two flanges. The mating flange was attached to the filter holder section via an aluminum tube, 3 cm in length. The filter holder consisted of four "sandwiched" 6 mm x 7 cm-square sections. The two Teflon spacer squares were machined to accommodate two colored glass filters. The interior of the aluminum end

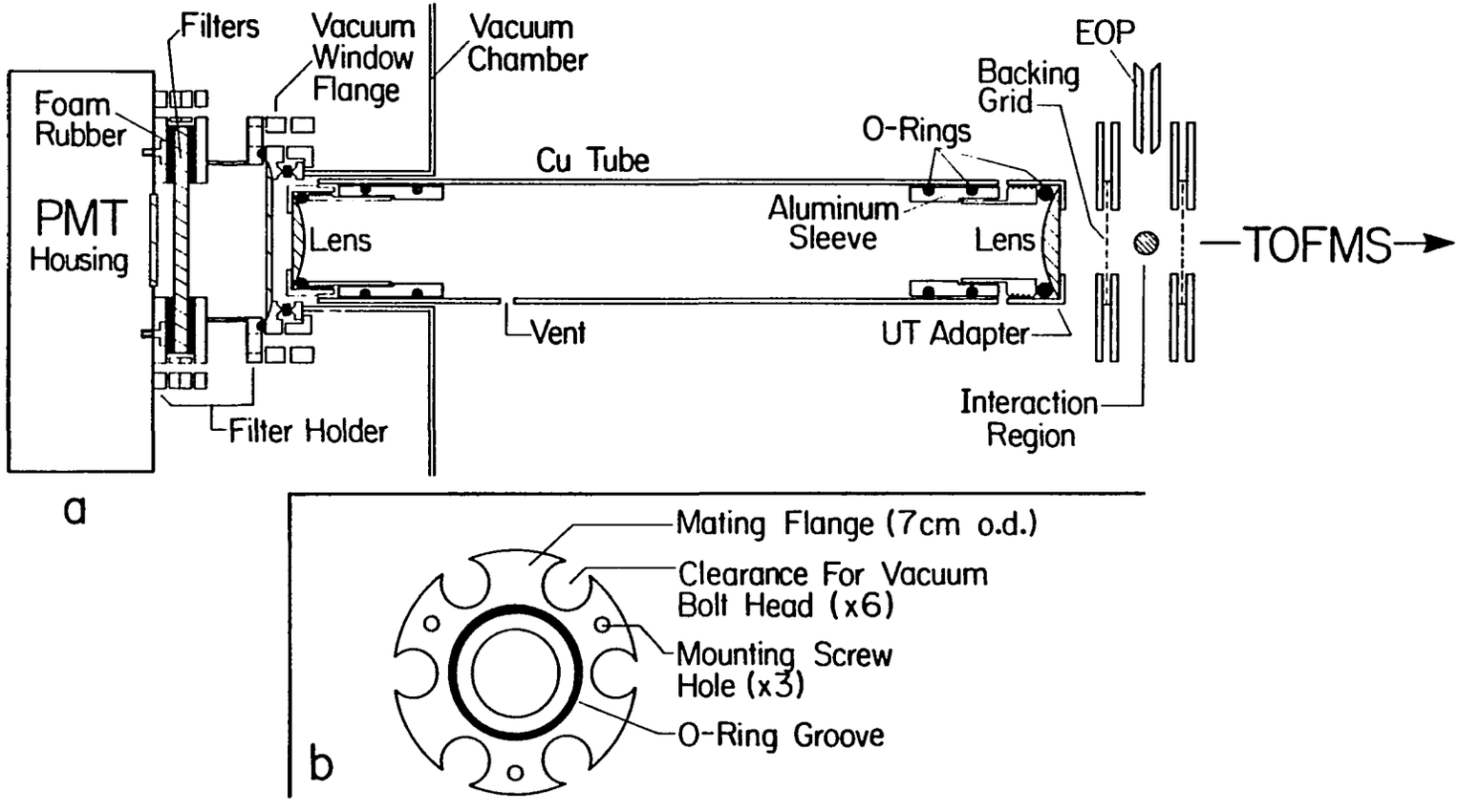


Figure 21. Total fluorescence optical collection and detection system. a) Overall layout; b) Filter holder mating flange (end-on view)

plates was lined with 3 mm thick, black foam rubber that provided a snug fit for and prevented scratching of the glass filters. The rear end plate served as a mount for a RFI-shielded sidewindow PMT housing (EMI-Gemcon, Inc., Plainview, New York). The sandwiched filter section was wrapped in black electrical tape to minimize stray light pickup.

A side-on PMT operated at -990 V was employed as the detector. The detector was capable of responding to fluorescence signals on a nanosecond time scale, without distortion, by replacing the standard "flat" voltage divider network with the network recommended by Lytle (206). A schematic diagram of the base wiring is shown in Figure 22. Essentially, signal distortion was prevented by assuring the delivery of sufficient charges to all dynodes so that response linearity was maintained, even at high photon flux levels.

The PMT output was conditioned by a LeCroy model 6102 preamplifier before being processed by a gated integrator/boxcar averager system. Again, synchronization was achieved via the use of a fast photodiode trigger. Although the preamplifier provided a variable gain to the LIF signal, its primary function was to delay the signal by approximately 80 ns. This delay was necessary because there was essentially no measurable temporal shift between the photodiode trigger and the beginning of the LIF signal. Hence, the boxcar could not respond quickly enough to measure the signal without employing an artificial delay.

In the LIF mode of detection, RFI, stray laser light, and LIF originating from residual PAC in the dynamic gas sample cell, all contributed to the background signal. This is shown clearly in Figure 23, in which two 0-300 ns scans of a 4 ns wide boxcar gate are displayed.

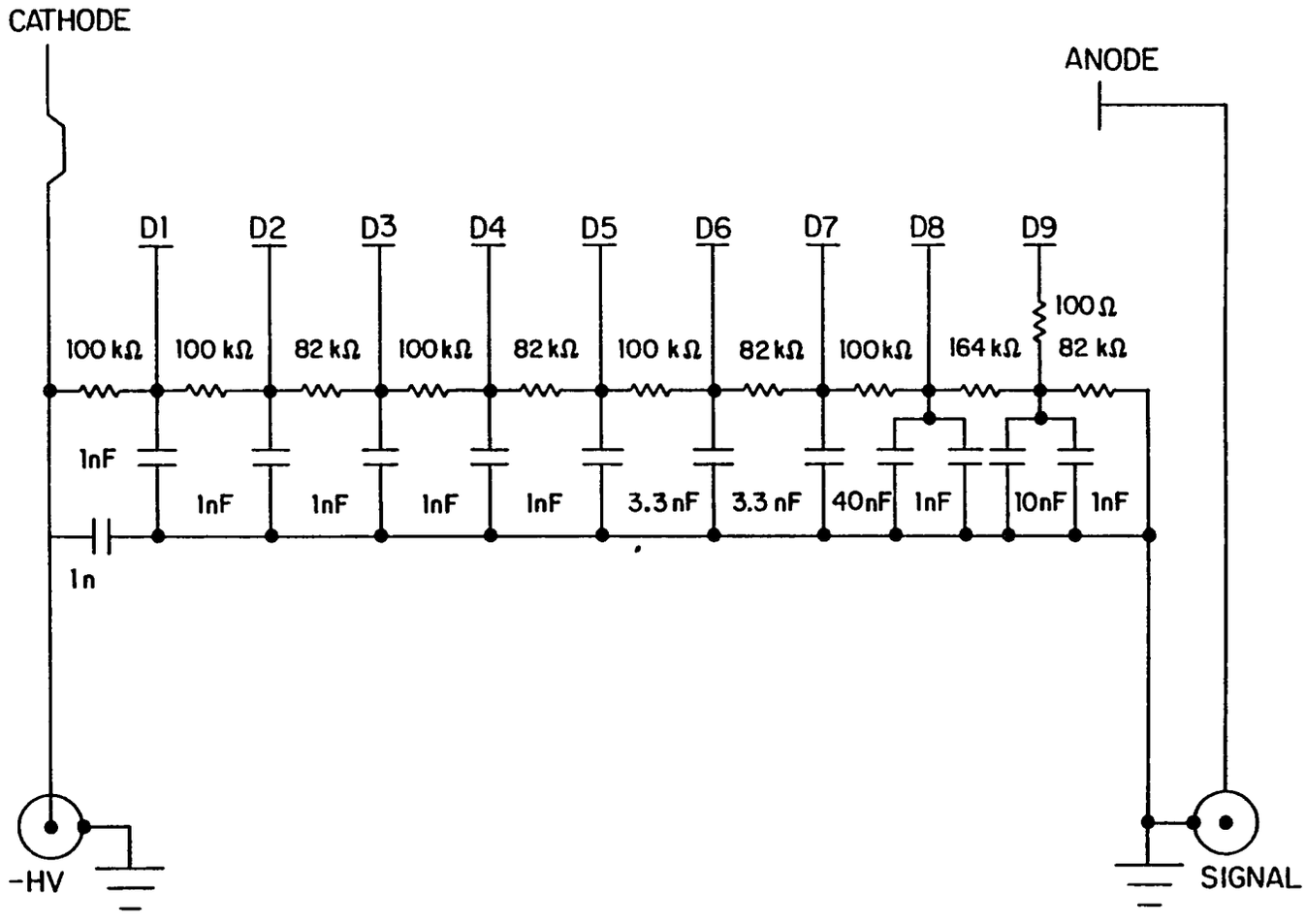


Figure 22. Schematic diagram of the base wiring for PMT as recommended by Lytle (206)

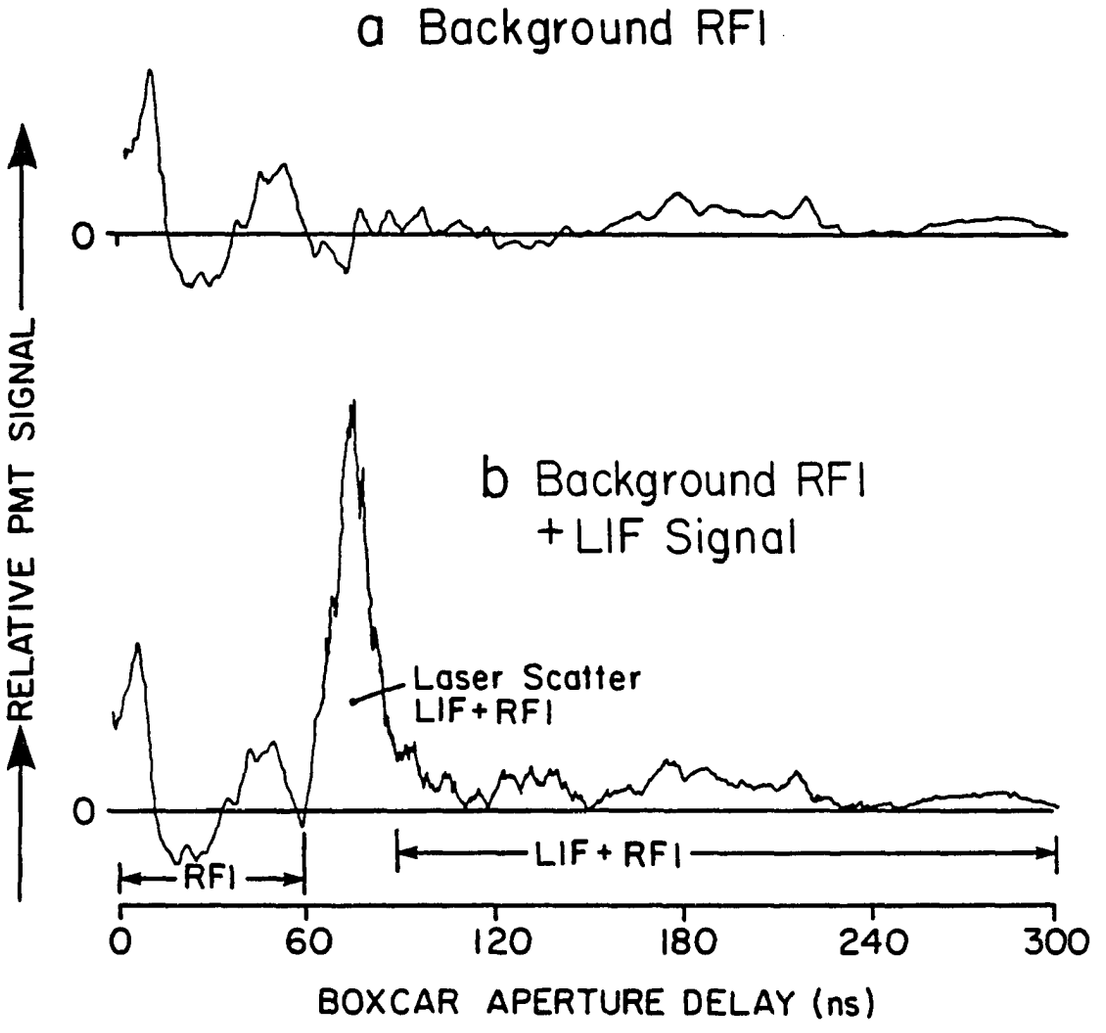


Figure 23. LIF output for 0-300 ns boxcar aperture delay scan, for a 4 ns gate width. a) Background RFI (laser beam blocked); b) Background RFI, laser scatter, plus LIF of residual PAC in dynamic gas sample cell (1 mJ/pulse, $\lambda_{ex}$=290 nm)

First, with the 290 nm laser beam blocked, the synchronous RFI was recorded (Figure 23a). Next, utilizing appropriate colored glass filters (Schott WG320 and WG335) to minimize stray laser light detection, the total background signal was collected over this time frame. The contributions from each general source of background are noted in Figure 23b. Typically, optimum signal processing parameters were selected with the boxcar gate positioned just beyond the time frame of the stray laser light background.

# V. EXPERIMENTAL PROCEDURES

## A. Chemicals and Solution Preparation

The PAC and other aromatic compounds studied in this investigation are listed in Table 6. A second set of organic compounds, used only in the chromatogram simplification demonstration, is listed in Table 7. The purity of each compound was greater than 97 percent, as verified by CC/GC-FID. The solvent used in all cases was methylene chloride (pesticide grade), obtained from Fisher Scientific Co., Fair Lain, NJ.

Stock solution of all reference compounds were prepared in volumetric flasks from weighed solid or pipetted liquid standards according to their physical state at room temperature, at concentrations of up to 5 mg/mL. A number of PAC tended to dissolve slowly and were, therefore, equilibrated overnight and/or vigorously stirred by an ultrasonic cleaner. Even with this additional agitation, perylene and dibenz(a,h)anthracene were not fully solvated in methylene chloride, at these high concentration levels (As this problem was left uncorrected for this work, only qualitative results are reported for these two compounds.). Concentrated stock solutions were prepared to minimize adsorption and decomposition effects commonly observed with very dilute solutions. All stock solutions and mixtures were prepared just prior to their use. All glassware was thoroughly washed, rinsed with ethanol, and dried with air.

Approximately 0.2 g of Crude Shale Oil A (Paraho Shale Oil): CRM-2, supplied by the DOE Fossil Fuels Research Material Facility (Oak Ridge National Laboratory) was fractionated according to the procedure of Later et al. (39). The A-2 fraction (neutral PAC in benzene) was evaporated to near dryness before being redissolved in approximately 10 mL methylene

Table 6. PAC and other aromatic compounds studied

| Compound | Formula | MW (g/Mole) | Source |
|---|---|---|---|
| p-Cresol | $C_7H_8O$ | 108 | [a] |
| Naphthalene | $C_{10}H_8$ | 128 | [b] |
| Acenaphthylene | $C_{12}H_8$ | 152 | [b] |
| Acenaphthene | $C_{12}H_{10}$ | 154 | [c] |
| Dibenzofuran | $C_{12}H_8O$ | 168 | [a] |
| Fluorene | $C_{13}H_{10}$ | 166 | [b] |
| p-Phenylphenol | $C_{12}H_{10}O$ | 178 | [a] |
| Dibenzothiophene | $C_{12}H_8S$ | 184 | [b] |
| Pentachlorophenol | $C_6HOCl_5$ | 264 | [a] |
| Phenanthrene | $C_{14}H_{10}$ | 178 | [c] |
| Phenanthrene-$d_{10}$ | $C_{14}D_{10}$ | 188 | [d] |
| Anthracene | $C_{14}H_{10}$ | 178 | [c] |
| Carbazole | $C_{12}H_9N$ | 167 | [a] |
| Fluoranthene | $C_{16}H_{10}$ | 202 | [b] |
| Pyrene | $C_{16}H_{10}$ | 202 | [c] |
| p-Terphenyl | $C_{18}H_{14}$ | 230 | [a] |
| Benz(a)anthracene | $C_{18}H_{12}$ | 228 | [b] |
| Triphenylene | $C_{18}H_{12}$ | 228 | [c] |
| Chrysene | $C_{18}H_{12}$ | 228 | [c] |
| Benzo(b)fluoranthene | $C_{20}H_{12}$ | 252 | [e] |
| Benzo(j)fluoranthene | $C_{20}H_{12}$ | 252 | [e] |
| Benzo(k)fluoranthene | $C_{20}H_{12}$ | 252 | [e] |
| Benzo(e)pyrene | $C_{20}H_{12}$ | 252 | [e] |
| Benzo(a)pyrene | $C_{20}H_{12}$ | 252 | [c] |
| Perylene | $C_{20}H_{12}$ | 252 | [c] |
| Indeno(1,2,3-cd)pyrene | $C_{22}H_{12}$ | 276 | [e] |
| Dibenz(a,h)anthracene | $C_{22}H_{14}$ | 278 | [b] |
| Dibenz(a,c)anthracene | $C_{22}H_{14}$ | 278 | [b] |
| Benzo(ghi)perylene | $C_{22}H_{12}$ | 276 | [b] |

[a]Chem Service, West Chester, PA.

[b]Aldrich Chemical Company, Inc., Milwaukee, WI.

[c]Zone refined at Ames Laboratory, Ames, IA.

[d]MDS Isotopes, Merek & Co., Inc., Rahway, NJ.

[e]Community Bureau of References, Commission of the European Communities.

Table 7. Other organic reference compounds utilized[a]

| Compound | Formula | MW(g/Mole) |
|---|---|---|
| 1,6-Hexanediol | $C_6H_{14}O_2$ | 118 |
| 3,4-Dimethylphenol | $C_8H_{10}O$ | 122 |
| 1-Decanol | $C_{10}H_{22}O$ | 158 |
| Biphenyl | $C_{12}H_{10}$ | 154 |
| m-Dinitrobenzene | $C_6H_4N_2O_4$ | 168 |
| n-Hexadecane | $C_{16}H_{34}$ | 226 |
| Diethylphthalate | $C_{12}H_{14}O_4$ | 222 |
| Phenylbenzoate | $C_{13}H_{10}O_2$ | 198 |
| 1-Tetradecanol | $C_{14}H_{30}O$ | 214 |
| Hexachlorobenzene | $C_6Cl_6$ | 282 |
| Benzylbenzoate | $C_{14}H_{12}O_2$ | 212 |
| Benzil | $C_{14}H_{10}O_2$ | 210 |
| n-Octadecane[b] | $C_{18}H_{38}$ | 254 |
| 1-Hexadecanol | $C_{16}H_{34}O$ | 242 |
| n-Nonadecane | $C_{19}H_{40}$ | 268 |
| Phenylsulphone | $C_{13}H_{12}SO$ | 232 |
| Dibutylphthalate | $C_{16}H_{22}O_4$ | 278 |
| 9,10-Anthraquinone | $C_{14}H_8O_2$ | 208 |
| 4,4'-Dibromobiphenyl | $C_{12}H_8Br_2$ | 312 |
| n-Eicosane[b] | $C_{20}H_{42}$ | 282 |
| Triphenylmethane | $C_{19}H_{16}$ | 244 |
| 1-Octadecanol | $C_{18}H_{38}O$ | 270 |
| Bis(2-ethoxyethyl)phthalate | $C_{16}H_{22}O_6$ | 310 |
| Methylstearate | $C_{19}H_{38}O_2$ | 298 |
| Dibutylsebacate | $C_{18}H_{34}O_4$ | 314 |
| n-Docosane[b] | $C_{22}H_{46}$ | 310 |
| n-Tetracosane[b] | $C_{24}H_{50}$ | 338 |
| Bis(2-ethylhexyl)phthalate | $C_{24}H_{38}O_4$ | 390 |
| n-Hexacosane[b] | $C_{26}H_{54}$ | 366 |
| n-Octacosane[b] | $C_{28}H_{58}$ | 394 |
| n-Triacontane[b] | $C_{30}H_{62}$ | 422 |
| n-Hentricontane | $C_{31}H_{64}$ | 436 |
| Cholesterol | $C_{27}H_{46}O$ | 386 |
| n-Dotriacontane[b] | $C_{32}H_{66}$ | 450 |
| n-Tritriacontane[b] | $C_{33}H_{68}$ | 464 |
| n-Tetratriacontane[b] | $C_{34}h_{70}$ | 478 |

[a]Chemicals obtained from Chem Service, West Chester, PA, unless otherwise denoted.

[b]Alltech Associates, Inc., Deerfield, IL.

chloride. Because only a qualitative demonstration was conducted on this sample, quantitative values of sample mass and precise dilution volume were not recorded.

## B. Capillary Column Gas Chromatography

All chromatographic analyses were conducted at a helium carrier gas average linear velocity of 50 cm/s (2.5 mL/min), measured at 100 °C. Typically, 1.2 µL samples were injected into the GC with a split ratio of approximately 50:1. For quantitative measurements, chromatographic peak heights were normalized to the precise sample volume injected. Various temperature programs were selected to best suit the particular study being conducted. As a result, conditions were commonly chosen to provide only moderate chromatographic resolution in the shortest possible analysis time.

The FID conditions, including gas flow rates and temperature, were optimized according to standard procedures prescribed elsewhere (207). The transfer line and GC-high vacuum interface portion of the sampling system were heated to temperature (typically 350 °C) greater than the final GC oven temperature to allow efficient transfer of analyte to the gas sample cell.

Zero Gas grade air, hydrogen, and helium were utilized in all chromatographic studies. Zero Gas hydrogen and helium were certified to have less than 0.5 ppm total hydrocarbon content (THC), while the Zero Gas air was certified with THC<2 ppm.

## C. Laser Power Density Manipulation

For most of the studies, no lens was placed at the laser entrance window of the high vacuum chamber. Hence, a constant beam diameter of approximately 2 mm was maintained, regardless of laser power. Laser power density was, therefore, directly proportional to laser pulse energy. Because lasing efficiency varied over the tuning of the laser dye and some experiments required a range of laser power densities, it was necessary to empirically manipulate laser pulse energies prior to many chromatographic runs. Both the tuning angle of the frequency doubler crystal and the high voltage applied to the Nd:YAG laser flashlamps controlled the UV laser beam pulse energy for any given wavelength. Normally, with the dye laser monochromator set at the desired wavelength, the frequency doubler was tuned to provide maximum UV output. The flashlamp high voltage was then adjusted, through a range of 1.5-1.9 kV, until the average UV pulse energy (i.e., power density) was at the desired value. Below 1.5 kV, the laser output became noticeably irregular. Thus, yet lower pulse energies were obtained by slightly detuning the frequency doubler. All investigations were conducted at UV laser beam energies in the 0.05-3.0 mJ ($1.3\text{-}80 \times 10^5$ $W/cm^2$ peak power density) range.

## D. System Start-up/Warm-up and Data Collection

The general stepwise procedure that was followed for start-up/warm-up, sample introduction, and data acquisition is outlined as follows:

a) The main vacuum chamber and flight tube were rough-pumped down to less than 30 mtorr.

b) After isolating the high vacuum chamber from the roughing pump line, the aluminum slide valves of the preheated and cryotrapped VHS-6 and M-4 diffusion pump stacks were opened.

c) While the vacuum system was pumping down:

   i) The GC oven operation conditions were set and the FID was started.

   ii) The transfer line and GC-high vacuum interface oven were heated to approximately 350 °C, by adjusting their respective Variac controllers. Typically, equilibration of the interface oven required 30-45 min.

   iii) All detection and data processing electronics (with the exception of the TOF/MS high voltage power supplies) were turned on and allowed to stabilize for at least 30 min.

d) The TOF/MS high voltage power supplies were turned on when the flight tube pressure had dropped to less than $10^{-5}$ torr. An MEM gain setting of 6 was used for all studies presented in this dissertation.

e) With the laser system operating at 10 Hz, the average UV laser beam pulse energy was adjusted, as described in the previous section.

f) With the proper preamplifier and/or boxcar sensitivity ranges set, a baseline tracing was established on all analog recorders. The mainframe time constant was set at 1 s, for all boxcar averagers, to minimize chromatographic

peak distortion and baseline noise in the TECD, LIF, and SIM evaluations.

g) Approximately 1.2 µL of sample was injected into the CC/GC and the temperature program initiated. The point of injection marked on all chromatographic baselines.

h) The collection of TOF/MS mass windows (summation mode) was initiated by operator interaction with the LeCroy 3500 system, upon observing the leading edge of the TECD signal of a selected chromatographic eluent.

## E. General Mass Scale Calibration For TOF/MS

For a given TOF/MS system, equation 3 (Chapter III) may be simplified to the following:

$$t_i = KM_i^{1/2}, \qquad (4)$$

where K represents all characteristic constants of the TOF/MS system and assumes that only singly charged ions are formed. The active memory of the LeCroy data acquisition system consists of a series of numbered channels. These channels may be thought of as representing ion flight times, $t_i$, each separated by a certain increment (5 ns in these studies). The precise flight time represented by a particular channel may be expressed in terms of both the channel number, $CN_i$, and the artificial delay imposed by the variable delay generator, $T_D$, as follows:

$$t_i = (CN_i)5 \text{ ns} + T_D. \qquad (5)$$

The combination of equations 4 and 5 provides a simple calibration relationship between $M_i$ and $CN_i$, expressed as follows:

$$(CN_i)5 \text{ ns} + T_D = KM_i^{1/2}. \qquad (6)$$

Equation 6 was used to provide mass scale calibration for each mass window of interest. Although approximate values for $T_D$ and K could have been determined directly from experimental parameters, precise values were needed to provide accurate calibration. To this end, a sample containing two photoionizable reference PAC was employed as a calibration standard. The PAC were chosen so that their respective molecular weights represented values at the high and low ends of the mass window. The channel number corresponding to the center of each parent ion peak was determined experimentally. These values were then inserted into their respective forms of equation 6 to provide two equations to solve for the two unknowns ($T_D$ and K). Appropriate manipulations resulted in the following:

$$K=[(CN_2-CN_1)5\ ns]/(M_2^{1/2}-M_1^{1/2}) \ , \quad (7)$$

and

$$T_D = KM_1^{1/2}-(CN_1)5\ ns \ , \quad (8)$$

where the numerical subscripts label values corresponding to a particular PAC. Equations 7 and 8 were, therefore, utilized to determine, in turn, K and $T_D$, thus establishing accurate mass scale calibration according to equation 6. For a given mass window, this calibration was quite stable (±2 channels) on day-to-day basis.

# VI. RESULTS AND DISCUSSION

The CC/GC-REMPI(TECD)-TOF/MS(SIM)-LIF-FID analytical instrument, as the acronym implies, can simultaneously generate a universal FID and selective TECD, LIF, and SIM chromatograms. Further, the TOF/MS signal may be processed by the transient digitizer and minicomputer system to yield, in effect, three-dimensional GC/MS chromatograms. To demonstrate its viability as an analytical technique, some fundamental instrument characterization studies were conducted and analytical figures of merit were determined. In addition, the utility of the various aspects fo this technique for simplification of complex chromatograms was qualitatively investigated.

## A. Laser Power Density Effects On REMPI Response and Fragmentation

The effects of laser power density on REMPI analytical signals were studied. With pulse energies of a 2 mm laser beam ranging from 0.1 to 2.6 mJ, at an excitation wavelength of 285 nm, representative PAC chromatographic eluents were photoionized while monitoring the TECD signal. Typical results of this study are shown graphically in Figure 24. The TECD chromatographic peak heights of acenaphthene and carbazole were linear with respect to laser pulse energy, with linear correlation coefficients (208) of 0.996 and 0.977, respectively. Precision was limited, in part, by pulse-to-pulse energy fluctuations of the laser beam. Although the background ionization signal was linear with laser power, as indicated by a 0.997 correlation coefficient, the precision for chromatographic eluents tended to degrade with increasing PAC size. For

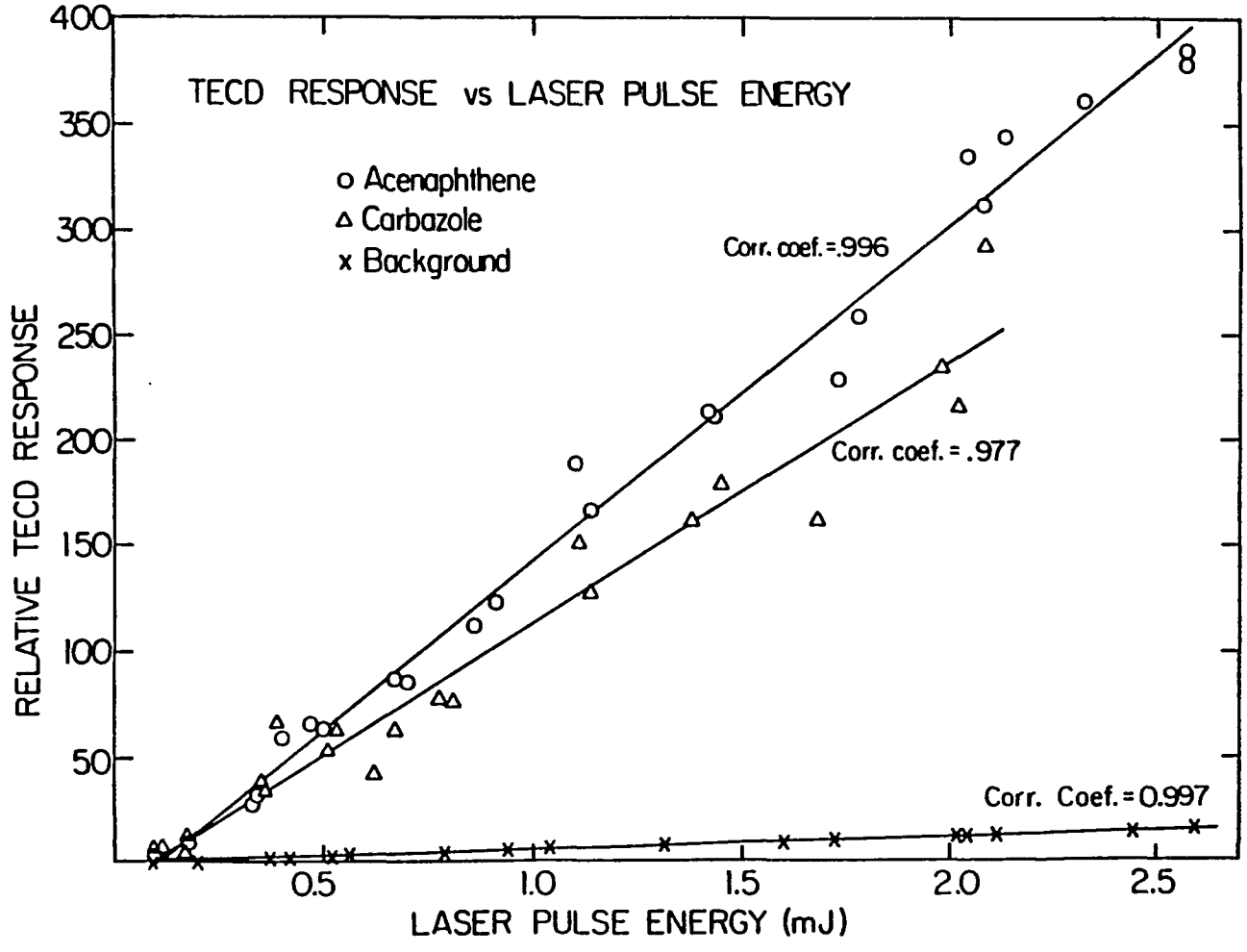


Figure 24. Relative TECD response versus laser pulse energy ($\lambda_{ex}$=285 nm) utilizing a 2 mm laser beam. Temperature program: column held at 100 °C for 1 min, then ramped to 320 °C at 14 °C/min, where it was held for 2 min

example, the correlation coefficient for the benz(a)anthracene TECD response versus laser pulse energy plot was 0.846, indicating that the primary detriment to precision was likely the method of sample injection (i.e., split mode).

Although the precision was not optimum, this initial study did show that the TECD response was linear with respect to laser power density, for a fixed laser beam diameter. Thus, the primary ionization mechanism was a stepwise one-photon-limited process for the range of power densities employed in this study. Hence, in subsequent work, the analytical signal was normalized with respect to laser pulse energies, in order to compensate for any drift in laser power.

The general effect of laser power density on the degree of cation fragmentation was also investigated. A simple PAC mixture, consisting of approximately 0.5 mg/mL each of acenaphthene, dibenzofuran, fluorene, and carbazole, in methylene chloride, was used in this study. The temperature program employed was as follows: the column temperature was held at 130 °C for 1 min and then programed to 190 °C at a rate of 14 °C/min, where it was held for 1 min.

Laser pulse energies (285 nm) were varied over a 0.18-2.40 mJ range while collecting complete mass spectra for each of the PAC eluents. The TOF/MS data acquisition system was manually actuated, upon the appearance of each TECD chromatographic peak, to sum and store mass spectra from five consecutive laser pulses (0.5 s). The percent of fragment ion formation was determined by ratioing the total fragment peak area to the total ion peak area. (Note: Obviously, 0.5 s was insufficient to collect ions resulting from every laser pulse during the elution of a chromatographic

peak. However, because an entire mass spectrum was collected for each of the five laser pulses, the resulting data were representative of the relative extent of fragmentation for a given pulse energy.)

As shown in Table 8, the extent of fragmentation increased slightly with laser pulse energy for each of these PAC. Although the heterocyclic compounds showed a greater fragmentation tendency, the parent ion peak dominated in all cases, even at 2.4 mJ. This indicated that the PAC analyte molecules largely experienced "soft ionization", absorbing just enough photons(two) to lose an electron, when the collimated 2 mm laser beam was used.

By installing an appropriate lens in front of the vacuum chamber entrance window, the laser beam diameter was reduced by a factor of four (down to 0.5 mm) within the laser-analyte interaction region. A comparison of the TECD and TOF/MS data obtained for this focused versus an unfocused laser beam, both at approximately 2 mJ/pulse, is given in Figure 25. Interestingly, the respective TECD peak heights were similar in both cases, indicating that approximately the same number of ions were created in both excitation modes. Because the sample volume interrogated was reduced by a factor of 16 while the laser power density was increased by an identical factor, linear response of the TECD with respect to laser power density was implied to still higher power densities. Also, this indicated that the TECD signal observed with an unfocused beam was far from saturation and that the efficiency of the analyte ionization process may be further increased, should a higher-power, tunable, UV laser source be employed.

Table 8. Laser pulse energy effect on fragmentation of a) acenaphthene; b) fluorene; c) dibenzofuran; and d) carbazole at $\lambda_{ex}$=285 nm and a 2 mm beam diameter

| Pulse Energy(mJ) | Fragmentation(%) | Pulse Energy(mJ) | Fragmentation(%) |
|---|---|---|---|
| a. Acenaphthene | | b. Fluorene | |
| 0.18 | 0.00 | 0.18 | 0.00 |
| 0.36 | 0.00 | 0.35 | 0.00 |
| 0.47 | 0.00 | 0.58 | 0.07 |
| 1.03 | 0.19 | 1.17 | 0.15 |
| 2.02 | 0.41 | 1.85 | 0.88 |
| 2.40 | 0.41 | 2.35 | 0.81 |
| c. Dibenzofuran | | d. Carbazole | |
| 0.18 | 0.00 | 0.18 | 0.00 |
| 0.35 | 0.09 | 0.35 | 0.25 |
| 0.59 | 1.76 | 0.61 | 0.32 |
| 1.02 | 5.91 | 1.22 | 3.65 |
| 1.94 | 8.25 | 1.95 | 5.54 |
| 2.37 | 10.85 | 2.40 | 8.06 |

As shown in Figure 25, the extent of fragmentation was significantly increased by condensing the laser beam, although the parent ion peak continued to dominate for these PAC. The option of obtaining a complete fragmentation pattern for a well-resolved chromatographic eluent should prove to be quite valuable for the identification of unknown PAC. However, the simplified mass spectra provided by the "soft ionization" alternative may be more practical when there exist a number of coeluting photoionizable species in complex PAC analyses. Hence, for the remainder of the work to be presented in this dissertation, a 2 mm laser beam with pulse energies of approximately 1 mJ was employed.

### B. Wavelength Selective Ionization at Ambient Temperatures

Selective ionization of ambient-temperature GC eluents may be achieved, in a number of cases, by exploiting differences in the respective REMPI spectra of various compounds. The TECD chromatographic peak heights represent relative REMPI responses, at a chosen excitation wavelength. Thus, TECD chromatograms of several simple PAC mixtures were accumulated over an excitation wavelength range of 282-350 nm, in 2.5 nm increments, and at a constant pulse energy of approximately 1 mJ. Each PAC mixture was chromatographed three times at each excitation wavelength and the averaged wavelength-dependent relative TECD peak heights were assembled into a REMPI spectrum for each of the 28 compounds listed in Table 6. The 2.5 nm spectral resolution was adequate to profile these broad-band, ambient-temperature REMPI spectra. These spectra, compiled in

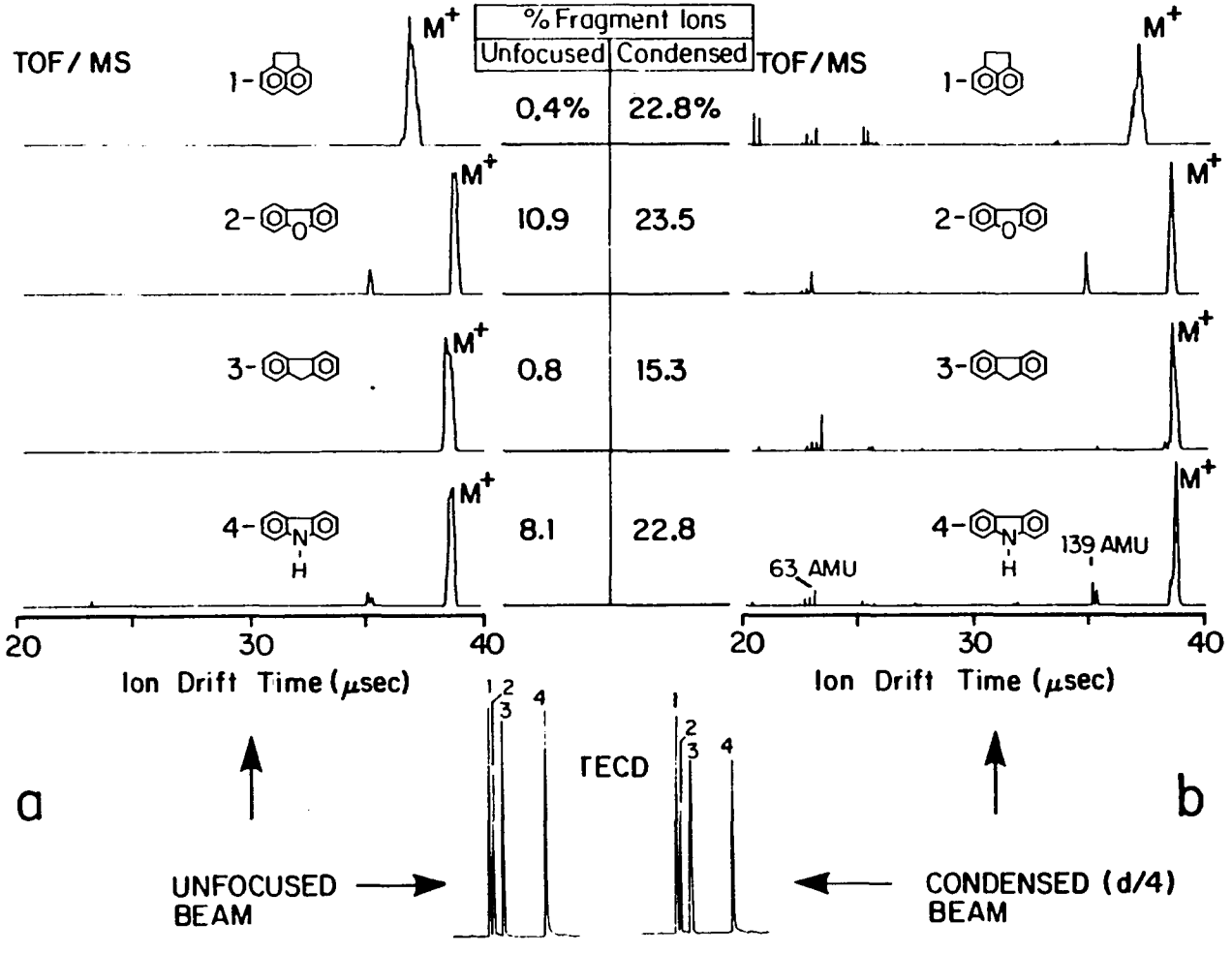


Figure 25. CC/GC-REMPI(TECD)-TOF/MS for mixture containing: 1)acenaphthene, 2)dibenzofuran, 3)fluorene, 4)carbazole. TOF/MS fragmentation data: 5 consecutive mass spectra summed (2 mJ/pulse, $\lambda_{ex}$=285 nm). a) 2 mm collimated beam; b) Condensed beam: 0.5 mm in laser-analyte interaction region

Figure 26, served as references to establish compromise excitation wavelengths for general PAC detection, or were consulted when choosing selective ionization conditions in order to distinguish between coeluting isomers.

The reconstructed REMPI spectra, shown in Figure 26 are not particularly elegant, however, they do provide a qualitative indication of the potential for selective ionization among various PAC. All TECD responses were zero in the 330-350 nm range for the compounds studied, therefore, these data were excluded from the REMPI plots. By utilizing a frequency-doubled, excimer-pumped dye laser system, capable of providing excitation wavelengths down to 240 nm (93,194), a clearer picture of the overall REMPI spectra could be established. Improved sensitivity and/or selectivity would likely result for many PAC.

The REMPI spectra of two closely eluting PAC isomers, anthracene and phenanthrene, are shown in Figure 26c. These spectra suggested that by choosing the laser excitation wavelength to be 300 nm, anthracene could be selectively ionized in the presence of phenanthrene. This prediction was verified by using both TECD and TOF/MS to monitor photoionization products of a chromatographic eluent consisting of a 1:1 mixture of these two PAC. In this study, the deuterated analog of phenanthrene was substituted to make obvious the identity of the ionized species. Each of the TOF/MS spectra shown in Figure 27 represents the summation of all ions produced, within a 42 u mass window, during the elution of both PAC peaks. Spectral selectivity factors (SF) were determined by ratioing mass spectral peak areas of the protonated species to those of phenanthrene-$d_{10}$. Photoexcitation at 300 nm provided selective ionization of anthracene, as

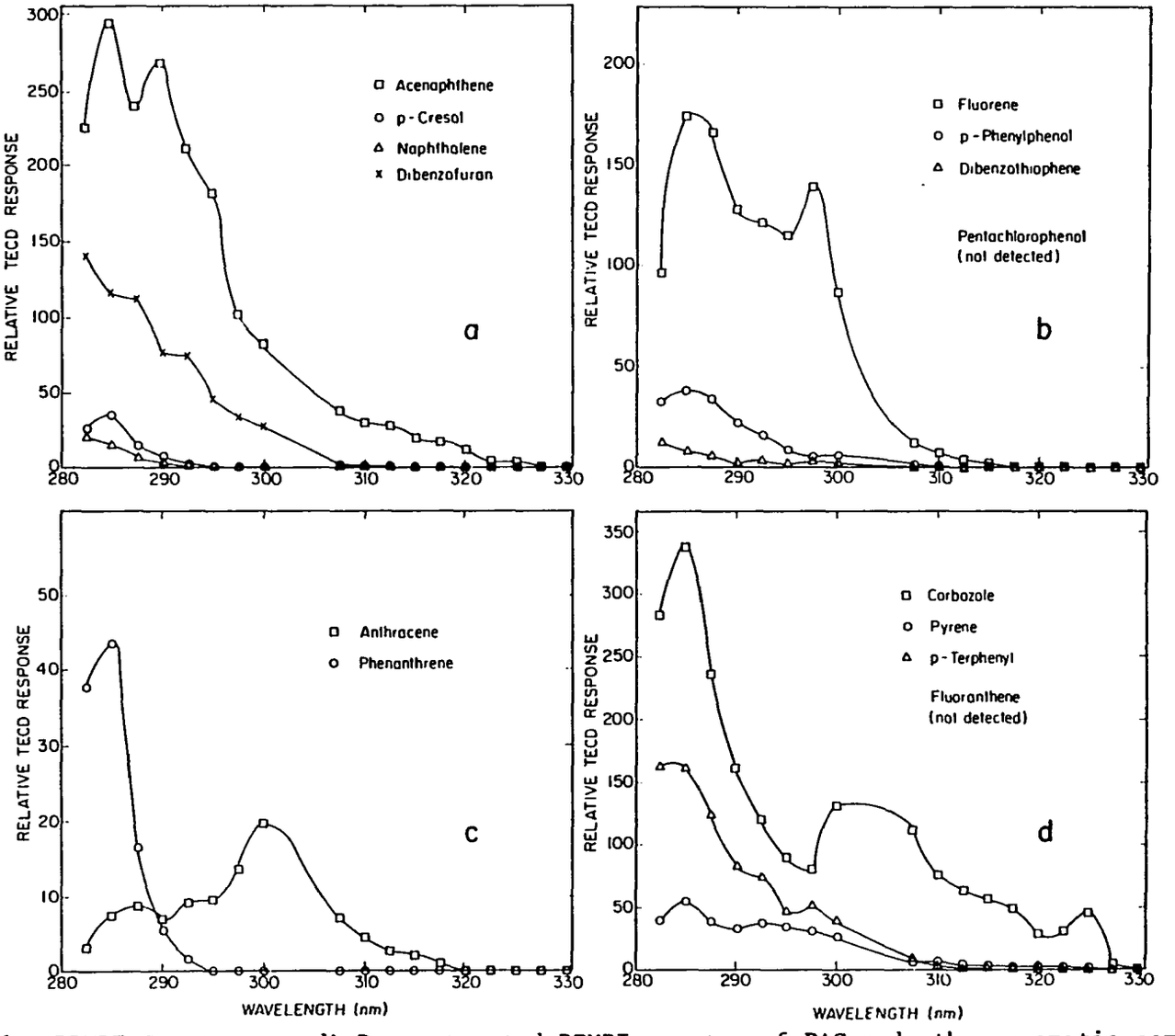


Figure 26. REMPI Spectra. a-d) Reconstructed REMPI spectra of PAC and other aromatic compounds

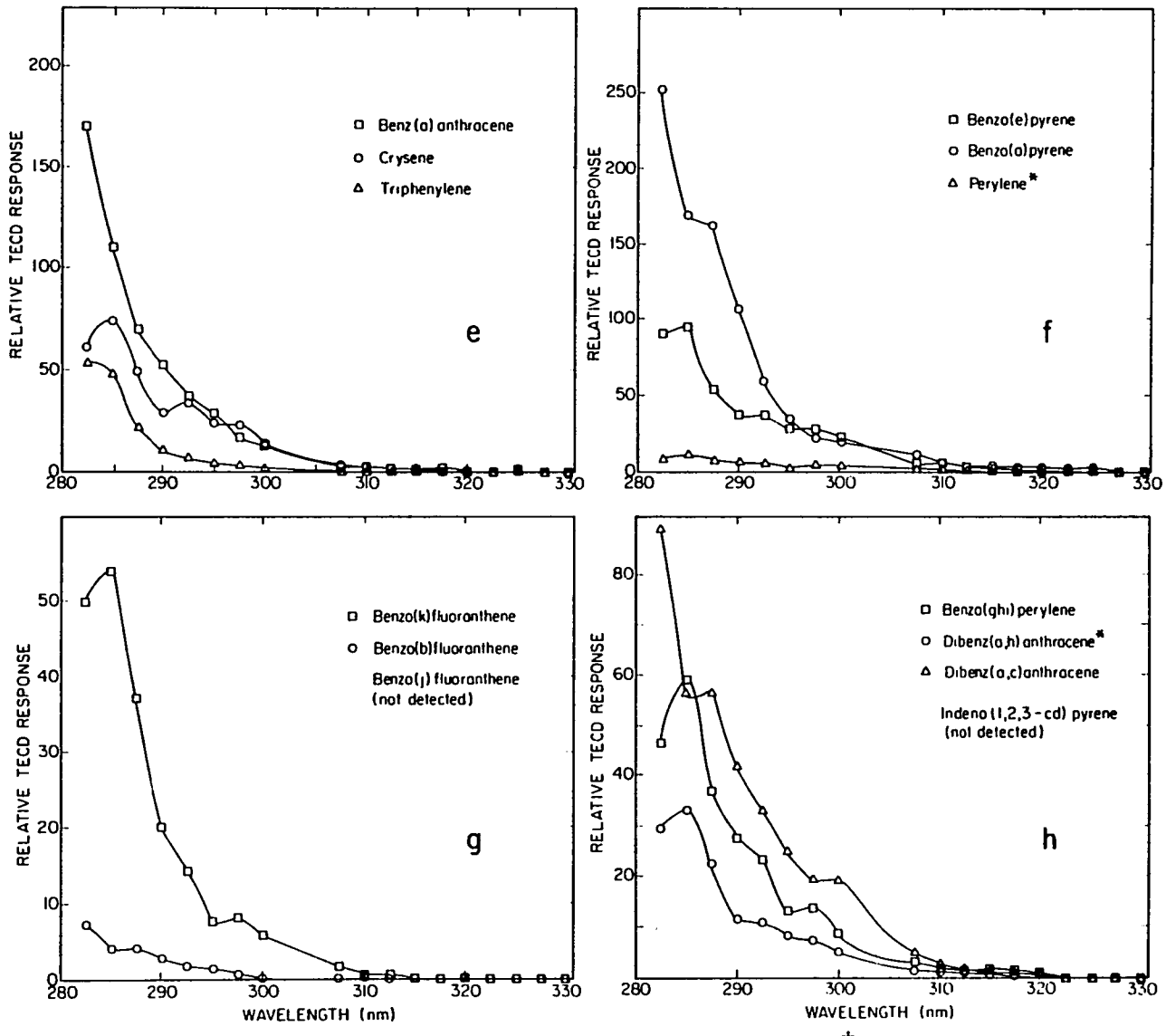


Figure 26. Continued. e-h) Reconstructed REMPI spectra of PAC. *Not fully solvated

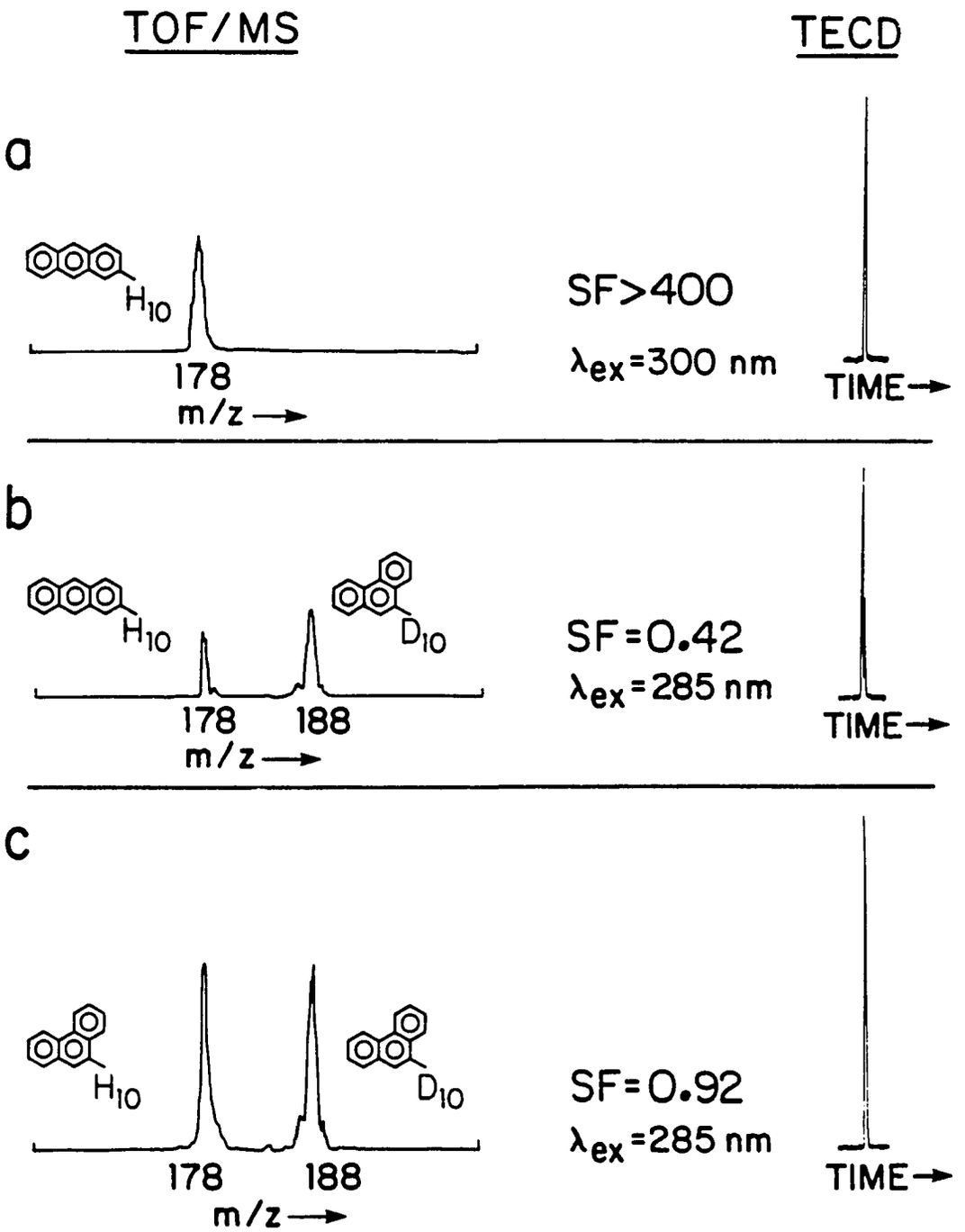


Figure 27. Comparison of TECD and TOF/MS (42 u mass window) REMPI (1 mJ/pulse) data for a) 1:1 anthracene: phenanthrene-$d_{10}$, $\lambda_{ex}$=300 nm; b) 1:1 anthracene: phenanthrene-$d_{10}$, $\lambda_{ex}$=285 nm; and c) 1:1 phenanthrene-$h_{10}$:phenanthrene-$d_{10}$, $\lambda_{ex}$=285 nm. Chromatographic conditions: 180 °C isothermal

is convincingly shown by the resulting mass spectrum (Figure 27a) and the calculated SF value of approximately 400. The actual SF value may be considerably higher than this, as it is not unreasonable to suspect that low level anthracene-$d_{10}$ impurities may be present in the phenanthrene-$d_{10}$ standard.

For comparison, both PAC isomers were detected utilizing 285 nm irradiation, as indicated by the 0.42 SF value (Figure 27b). A 1:1 mixture of phenanthrene and its deuterated analog was also run, under identical conditions, with the results shown in Figure 27c. A SF value of 0.92 indicated similar responses for both of these species at 285 nm. This, in part, justified the substitution of a deuterated analog in these selective ionization studies. Further, these observations imply that deuterated analogs should prove ideal for use as internal reference standards for quantitation, when the photoionization TOF/MS detection mode is used, as their physical, chemical, and ambient-temperature spectroscopic properties are nearly identical to those of the parent compound.

## C. Analytical Figures of Merit

The overall analytical figures of merit of the CC/GC-REMPI(TECD)-TOF/MS portion of the system, in its present form, were established through the determination of the linear dynamic range (LDR) of the TECD detector, as well as the absolute limits of detection (LOD) of the TECD and TOF/MS detectors, for a number of representative PAC. These measurements were conducted with a compromise laser excitation wavelength

of 285 nm and all analytical signals were normalized to a laser pulse energy of about 1 mJ.

1. Linear dynamic range

LDR study was performed under the same chromatographic conditions as employed in the power density/fragmentation study. The four-component PAC mixture, also used in the fragmentation study, was prepared at eleven different dilutions over a broad range of concentrations. The results of this study are tabulated in Table 9. The "quantity detected" value represents the absolute mass of analyte delivered to the gas sample cell, taking into account chromatographic inlet and outlet split ratios. Each relative TECD response represents an average of the "corrected" TECD chromatographic peak heights from five replicate chromatograms. (Peak heights were corrected for the boxcar averager and recorder sensitivity settings, the precise volume of sample injected, and the average laser pulse energy at the time of elution.) The calculated standard deviation for each of these averaged TECD responses was almost always less than 10 percent.

The TECD response for all four compounds was linear over approximately a four decade change in concentration. Linear correlation coefficients of 0.9992, 0.9998, 0.9996, and 0.9952, and slopes of 1.004, 1.067, 1.024, and 1.143, were calculated for acenaphthene, dibenzofuran, fluorene, and carbazole, respectively (208). The slight deviation from linearity reported for carbazole was likely due to chromatographic peak tailing, perhaps resulting from exposed adsorptive sites within the chromatographic system (197). For illustration, log-log plots of relative

Table 9. Dependence of TECD response on quantity of a) acenaphthene; b) fluorene; c) dibenzofuran; and d) carbazole detected

| Quantity Detected (pg) | Relative TECD Response | Quantity Detected (pg) | Relative TECD Response |
|---|---|---|---|
| a. Acenaphthene | | b. Fluorene | |
| 20.6 | 23.2 | 21.2 | 12.0[a] |
| 41.2 | 41.4 | 42.4 | 30.6 |
| 82.4 | 79.6 | 84.8 | 56.6 |
| 206 | 207 | 212 | 124 |
| 416 | 417 | 424 | 307 |
| 824 | 783 | 848 | 577 |
| 2060 | 2170 | 2120 | 1460 |
| 4120 | 4260 | 4240 | 3480 |
| 8240 | 8940 | 8480 | 7060 |
| 20600 | 26600 | 21200 | 17900 |
| 41200 | 37600 | 42400 | 29800 |
| c. Dibenzofuran | | d. Carbazole | |
| 22.5 | 10.7[a] | 21.1 | 11.7[a] |
| 45.0 | 15.6 | 42.2 | 16.6 |
| 90.0 | 33.8 | 84.4 | 20.8 |
| 225 | 98.5 | 211 | 70.5 |
| 450 | 191 | 422 | 254 |
| 900 | 402 | 844 | 470 |
| 2250 | 1110 | 2110 | 1790 |
| 4500 | 2100 | 4220 | 4100 |
| 9000 | 4750 | 8440 | 8850 |
| 22500 | 13200 | 21100 | 21200 |
| 45000 | 24200 | 42200 | 32700 |

[a]High uncertainty due to baseline noise.

TECD response as a function of the mass of acenaphthene and fluorene delivered to the dynamic gas sample cell are shown in Figure 28. Deviations from linearity were observed above 50 ng because of overloading of the TECD preamplifiers. The upper end of the LDR could certainly be extended by attenuating the signal or by changing the operational amplifier circuitry.

2. Limits of detection

The absolute LOD (S/N=3) were obtained for acenaphthene and fluorene by extrapolating their respective LDR plots to a relative TECD reponse equal to 3 multiplied by the baseline noise of the chromatogram (i.e., to S=3N). A value of N=2.3 was measured and, hence, the TECD LOD for acenaphthene and fluorene were determined to be 7 pg and 12 pg, respectively.

The LOD for several PAC and other aromatic compounds were determined by referencing the corrected TECD chromatographic peak heights ($H_x'$) of each species to that of acenaphthene ($H_a'$), according to:

$$LOD_x = (H_a'/H_x')(LOD_a), \qquad (9)$$

where the subscripts denote the compound of interest. Typical TECD chromatograms (285 nm excitation) that were used to determine $H_x'$ values for each compound are shown in Figure 29. Each of the reference mixtures contained approximately 0.5 mg/mL of various aromatic compounds. The TECD (285 nm) LOD for 21 compounds are listed in Table 10.

The absolute LOD for each of the 21 photoionizable compounds (Table 10) were determined for the TOF/MS detection system, using p-terphenyl as a reference compound. Approximately 1 µL of 10 µg/mL p-terphenyl in methylene chloride was injected and the chromatographic process was

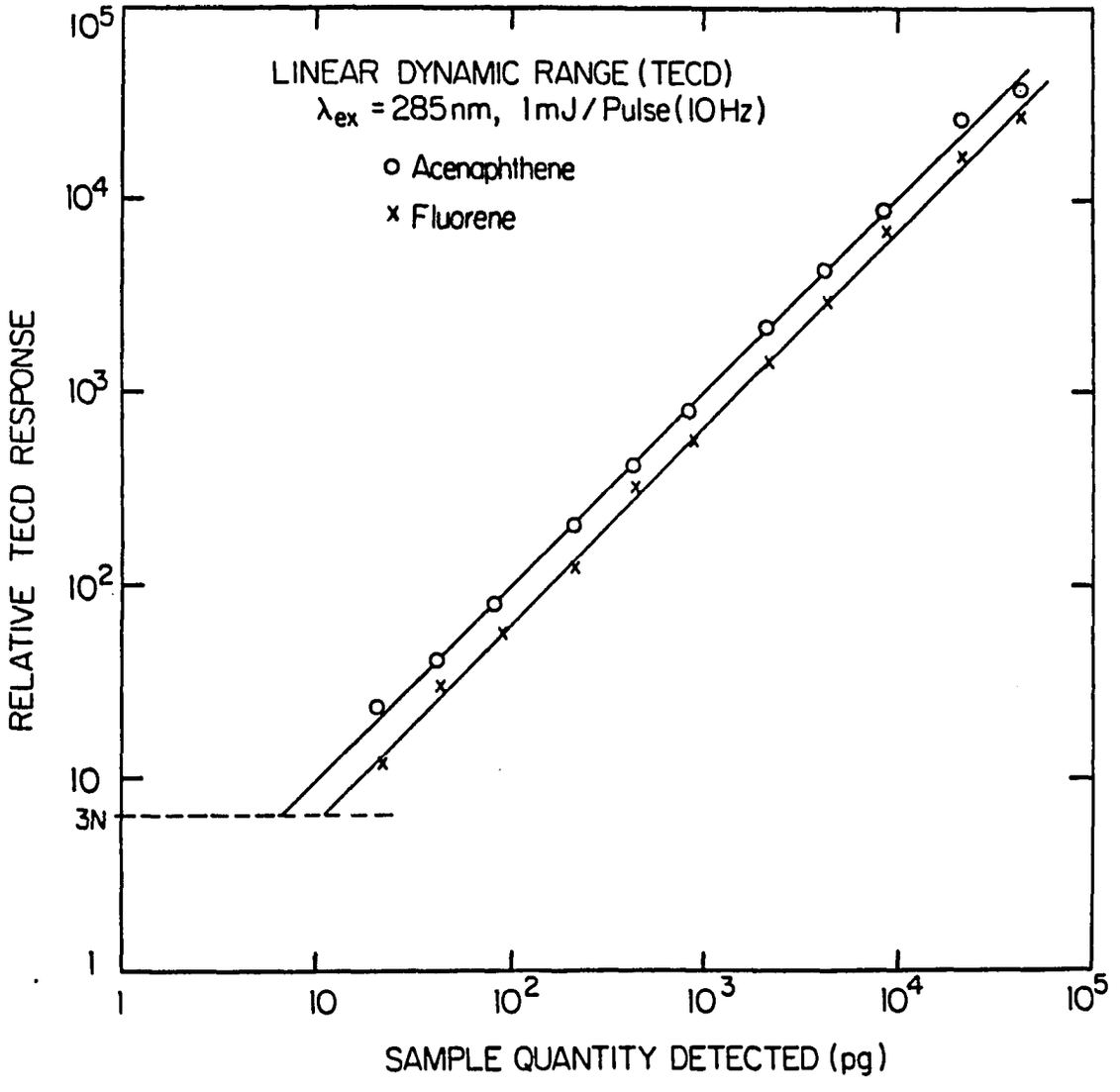


Figure 28. Log-log TECD LDR plots for acenaphthene and fluorene

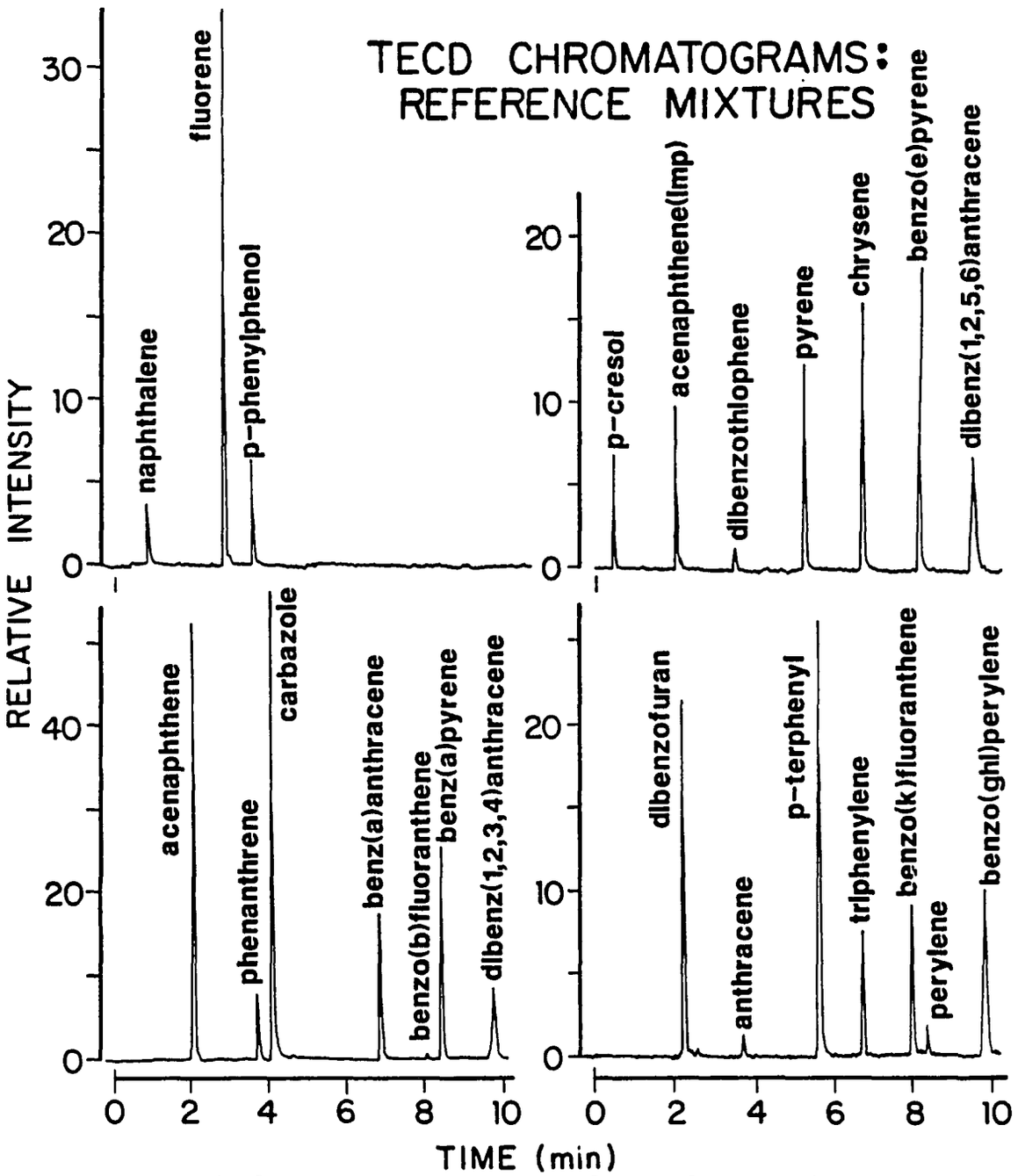


Figure 29. Typical TECD chromatograms of four reference mixtures. Approximately 5 ng of each species was delivered to the laser-based detector ($\lambda_{ex}$=285 nm, 1 mJ/pulse). Compounds not detected under these excitation conditions: acenaphthylene, pentachlorophenol, fluoranthene, benzo(j)fluoranthene, indeno(1,2,3-cd)pyrene. Temperature program: column held at 120 °C for 1 min, then ramped to 320 °C at 24 °C/min, where it was held for 2 min

Table 10. TECD and TOF/MS absolute limits of detection for PAC and other aromatic compounds at $\lambda_{ex}$=285 nm (1 mJ/pulse)

| Compound | Structure | LOD (pg) TECD | LOD (pg) TOF/MS |
|---|---|---|---|
| p-Cresol |  | 59 | 7 |
| Naphthalene |  | 130 | 16 |
| Acenaphthylene |  | N.D.[a] | |
| Acenaphthene |  | 7 | 1 |
| Dibenzofuran | 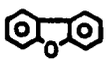 | 18 | 2 |
| Fluorene |  | 12 | 2 |
| p-Phenylphenol | 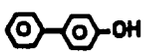 | 53 | 7 |
| Dibenzothiophene | 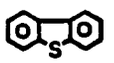 | 260 | 32 |
| Pentachlorophenol |  | N.D. | |
| Phenanthrene |  | 47 | 6 |
| Anthracene | 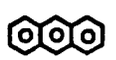 | 270 | 34 |
| Carbazole |  | 6 | 1 |
| Fluoranthene | 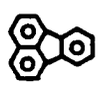 | N.D. | |
| Pyrene |  | 33 | 4 |

[a]N.D.=not detected.

Table 10. Continued

| Compound | Structure | LOD (pg) TECD | LOD (pg) TOF/MS |
|---|---|---|---|
| p-Terphenyl | 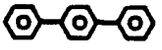 | 13 | 2 |
| Triphenylene |  | 43 | 5 |
| Benz(a)anthracene | 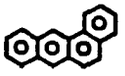 | 19 | 2 |
| Chrysene | 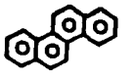 | 24 | 3 |
| Benzo(b)fluoranthene | 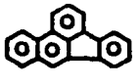 | 500 | 63 |
| Benzo(j)fluoranthene | 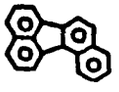 | N.D. | |
| Benzo(k)fluoranthene | 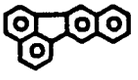 | 38 | 5 |
| Benzo(e)pyrene |  | 20 | 3 |
| Benzo(a)pyrene |  | 12 | 2 |
| Perylene | 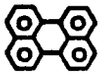 | _[b] | |
| Indeno(1,2,3-cd)pyrene | 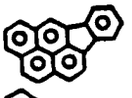 | N.D. | |
| Dibenz(a,h)anthracene | 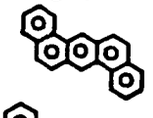 | _[b] | |
| Dibenz(a,c)anthracene |  | 37 | 5 |
| Benzo(ghi)perylene |  | 35 | 4 |

[b]Detected, not quantitated.

temperature programed as follows: the column temperature was held at 200 °C for 1 min and then ramped to 240 °C, at a rate of 24 °C/min, where it was held for 2 min. The TOF/MS data acquisition system was set to sum only the ion signal of the p-terphenyl parent peak (230 u) for ten consecutive laser pulses (1s). The system was manually triggered many times throughout the chromatogram, with a peak area value being recorded for each summation. The signal areas obtained when no analyte was eluting constituted a baseline and the standard deviation of these values defined the baseline noise (N). The peak area resulting from the photoionization of the p-terphenyl eluent, $A_{PTP}$, provided a measure of the signal. Thus, the TOF/MS LOD were simply calculated according to:

$$LOD_{PTP} = (10\ ng)(SR)(3N/A_{PTP}),$$

where 10 ng was the mass of p-terphenyl injected and SR was the overall split ratio of the chromatographic system.

Typical results obtained according to the above procedure are summarized as follows: For 164 baseline points, the standard deviation was 30.3 area units (au), while the signal was 5669 au. Thus, the TOF/MS LOD for p-terphenyl was calculated to be approximately 2 pg. This value was then used as a reference for the calculation of LOD for other photoionizable compounds, utilizing equation 9. The results are summarized in Table 10. These TOF/MS LOD values were restricted, in large part, by the manual triggering process of the data acquisition system. By automating this mechanism, no signal would be lost due to human reaction time. Thus, the LOD values would certainly decrease and the run-to-run precision would greatly improve.

In summary, under the compromise excitation/ionization conditions

employed in this study, the absolute LOD for most of these species were in the low picogram range. These LOD values were limited by ionization of background molecules (likely residual PAC) within the gas sample cell, as well as by stray electronic noise picked up by the preamplifiers. It must be stressed that these LOD were expected to be wavelength and laser power dependent. Therefore, 285 nm did not necessarily represent an optimum value for most of these PAC.

## D. Simplification of Chromatograms

One of the more obvious consequences of the inherent selectivity of this analytical system is its potential for simplification of chromatographic data. To qualitatively demonstrate this simplification, a 64-component mixture containing a wide variety of organic compounds, including PAC and other aromatic compounds, aliphatic hydrocarbons, alcohols, sulphones, and esters, was prepared. Each of these components are listed in Table 11, in order of retention time, for the chromatographic conditions employed. The numbered compounds label those species for which a measurable REMPI signal obtained for 1 mJ/pulse laser excitation at 285 nm.

Graphic demonstration of the various degrees of chromatogram simplification provided by this instrumentation is displayed in Figure 30. The FID chromatogram (Figure 30a) was complex, with many unresolved peaks, including peaks at higher retention times(>14 min) due to septum bleed. The laser-based portion of the detection system provided selective excitation/ionization based largely on characteristic molecular absorption coefficients and ionization cross sections at the selected excitation

Table 11. Components of a synthetic mixture consisting of 64 organic compounds in methylene chloride. Sample: 0.2-2 ng of each component (on column). Temperature program: column held at 100 °C for 1 min, then ramped to 320 °C at 14 °C/min, where it was held for 6 min

| Compound | Peak Number[a] | FID Retention Time (min) |
|---|---|---|
| p-Cresol | 1 | 0.80 |
| 1,6-Hexanediol | | 1.02 |
| 3,4-Dimethylphenol | | 1.25 |
| Naphthalene | 2 | 1.28 |
| 1-Decanol | | 1.80 |
| Biphenyl | 3 | 2.72 |
| Acenaphthylene | | 3.05 |
| m-Dinitrobenzene | | 3.33 |
| Acenaphthene | 4 | 3.37 |
| Dibenzofuran | 5 | 3.60 |
| Fluorene | 6 | 4.23 |
| n-Hexadecane | | 4.38 |
| Diethylphthalate | | 4.42 |
| Phenylbenzoate | | 4.98 |
| 1-Tetradecanol | | 5.02 |
| Hexachlorobenzene | | 5.35 |
| p-Phenylphenol | 7 | 5.40 |
| Dibenzothiophene | 8 | 5.68 |
| Pentachlorophenol | | 5.73 |
| Benzylbenzoate | | 5.82 |
| Phenanthrene | 9 | 5.95 |
| Anthracene | 10 | 5.98 |
| Benzil | | 6.10 |
| n-Octadecane | | 6.13 |
| Carbazole | 11 | 6.45 |
| 1-Hexadecanol | | 6.62 |
| n-Nonadecane | | 6.75 |
| Phenylsulphone | | 7.07 |
| Dibutylphthalate | | 7.45 |

[a]Numbered peaks refer to Figure 30 chromatograms. This labels those species for which a measurable REMPI signal was obtained utilizing 285 nm (1 mJ/pulse) laser excitation.

Table 11. Continued

| Compound | Peak Number[a] | FID Retention Time (min) |
|---|---|---|
| 9,10-Anthraquinone | | 7.52 |
| 4,4'-Dibromobiphenyl | | 7.58 |
| n-Eicosane | | 7.75 |
| Triphenylmethane | | 7.95 |
| Fluoranthene | | 8.18 |
| 1-Octadecanol | | 8.38 |
| Pyrene | 12 | 8.45 |
| Bis(2-ethoxyethy)phthalate | | 8.73 |
| Methylstearate | | 8.77 |
| Dibutylsebacate | | 9.05 |
| p-Terphenyl | 13 | 9.07 |
| n-Docosane | | 9.20 |
| n-Tetracosane | | 10.63 |
| Benz(a)anthracene | 14 | 10.77 |
| Chrysene | 15 | 10.80 |
| Triphenylene | 16 | 10.80 |
| Bis(2-ethylhhexy)phthalate | | 11.55 |
| n-Hexacosane | | 11.82 |
| Benzo(b)fluoranthene | 17 | 12.68 |
| Benzo(j)fluoranthene | | 12.68 |
| Benzo(k)fluoranthene | 18 | 12.68 |
| n-Octacosane | | 12.97 |
| Benzo(e)pyrene | 19 | 13.07 |
| Benzo(a)pyrene | 20 | 13.17 |
| Perylene | 21 | 13.28 |
| n-Triacontane | | 14.17 |
| n-Hentricontane | | 14.68 |
| Cholesterol | | 14.82 |
| Indeno(1,2,3-cd)pyrene | | 14.83 |
| Dibenz(a,h)anthracene | 22 | 14.83 |
| Dibenz(a,c)anthracene | 23 | 14.90 |
| Benzo(ghi)perylene | 24 | 15.12 |
| n-Dotriacontane | | 15.30 |
| n-Tritriacontane | | 15.90 |
| n-Tetratriacontane | | 16.50 |

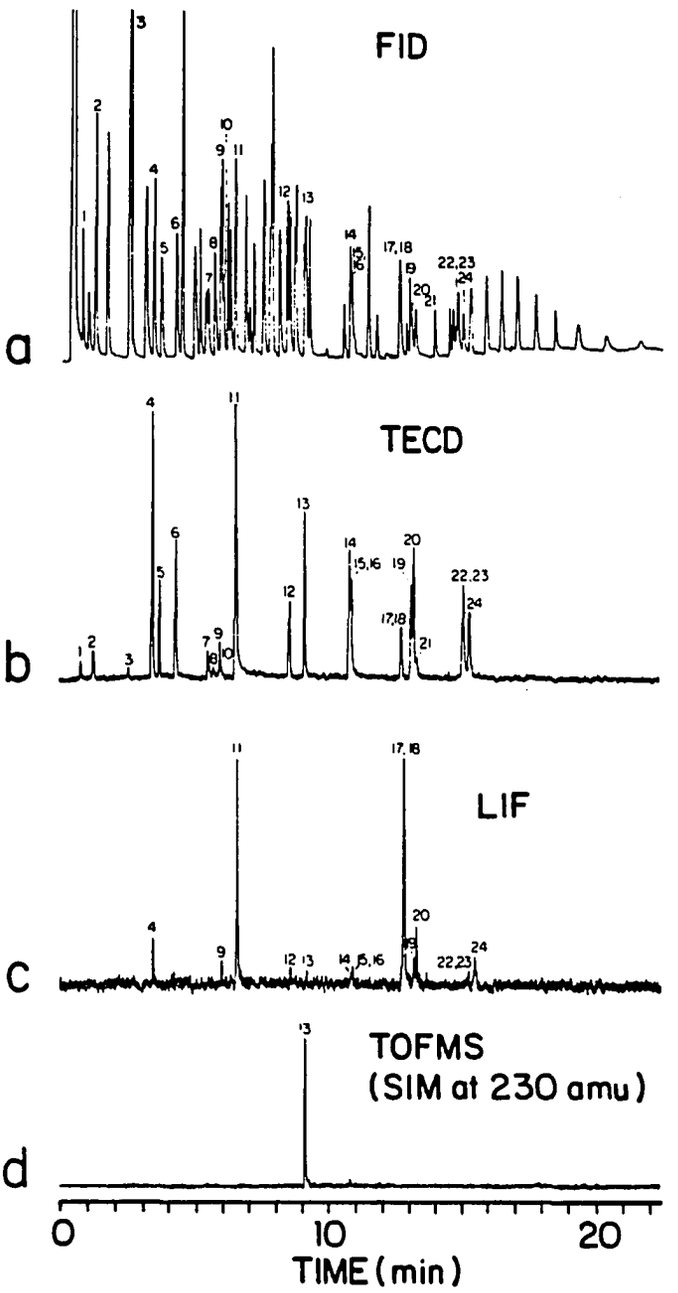


Figure 30. Simultaneous chromatograms of 64-component mixture ($\lambda_{ex}$=285 nm, 1 mJ/pulse). Numbered peaks are identified in Table 11. a) FID; b) TECD; c) TOF/MS with SIM at 230 u; d) LIF with WG320 and WG335 cut-off filters (Boxcar: Gate width=40 ns; gate delay=80 ns, Refer to Figure 23.)

wavelength. Thus, at an excitation wavelength of 285 nm, the TECD chromatogram (Figure 30b) indicates that only 24 of these compounds, mostly PAC, were ionized. The LIF chromatogram (Figure 30c) was obtained under compromise detector gate width/delay and emission filtering conditions, all of which effect selectivity and sensitivity for each compound. Again, this LIF mode of detection responded only to a select group of compounds.

The SIM chromatogram (Figure 30d) illustrates, in part, the additional selectivity offered by the incorporation of a mass spectrometer. In this case, only p-terphenyl was detected by preselecting only a 1 u mass window (i.e., boxcar gate), at 230 u, for monitoring. When the transient digitizer data acquisition system is employed, full advantage of the TOF/MS detector may be realized, as an entire mass spectrum may then be collected for each photoionizable chromatographic effluent. Thus, all of these chromatograms (FID, TECD, LIF, and TOF/MS-SIM or full mass spectra) are simultaneously available for each injection of analyte.

Unfortunately, most real samples are far more complex than this 64-component synthetic mixture. To provide a qualitative indication of the practical level of chromatogram simplification obtainable, the A-2 fraction (neutral PAC) of Crude Shale Oil A (Paraho Shale Oil):CRM-2 was examined. The overwhelming complexity of this sample was apparent in the FID chromatogram (Figure 31). Obviously, most of the components of this fraction were hopelessly unresolved, under the chromatographic conditions employed. Although the TECD provided a somewhat simplified chromatogram (Figure 31b), it was still far too complex for complete PAC

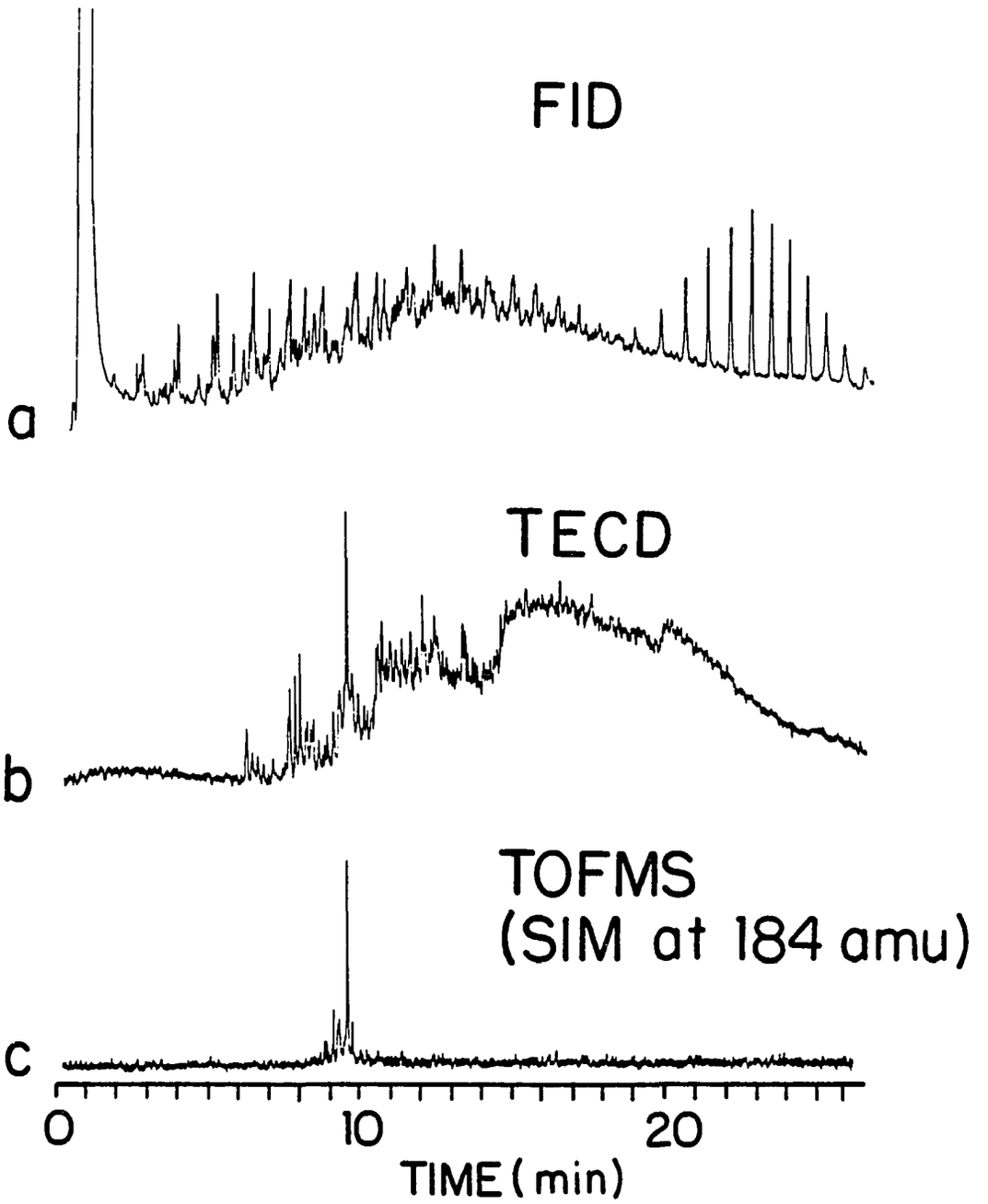


Figure 31. Simultaneous chromatograms of Paraho Shale Oil(CRM-2): Neutral PAC fraction ($\lambda_{ex}$=285 nm, 1 mJ/pulse). a) FID; b) TECD; c) TOF/MS with SIM at 184 u. Temperature program: column held at 60 °C for 1 min, then ramped to 340 °C at 12 °C/min, where it was held for 2 min

characterization, even under optimized CC/GC conditions. This is not surprising, as this fraction typically contains hundreds of different PAC species, including a variety of PAH and N-, O-, and S-heterocyclic compounds (39). However, as is shown by the SIM chromatogram in Figure 31c, the ability to isolate a narrow (±1 u) mass window allowed the targeting of a specific PAC for detection. In this case, dibenzothiophene (184 u) was the targeted molecule. A match of chromatographic retention time, along with REMPI and mass spectral data verified the identification. Fluorescence data are not presented for this application, as this aspect of the system was not sufficiently optimized.

# VII. SUMMARY AND RECOMMENDATIONS FOR FUTURE WORK

This dissertation has described preliminary results stemming from the development of a multidimensional analytical instrument for trace PAC characterization in complex mixtures. This is the first report of instrumentation that combines high resolution CC/GC with tunable laser-induced fluorescence/ionization and mass spectrometry for the simultaneous collection of cations, electrons, and photons. The picogram detection limits, combined with a four decade LDR, enhance the potential of this analytical approach. Further, the use of deuterated analog compounds as internal references for quantitation shows promise for improving accuracy and precision.

Although examination of samples at ambient temperatures by this instrument can, in many cases, provide selective excitation/ionization and detection of coeluting isomers, it is unlikely that this approach will be able to do so as a general rule. This is particularly important when complete characterization of PAC distributions in complex environmental samples is the goal. However, even these extremely demanding problems may be solved completely by utilizing a rotational cooling sampling system to provide selectivity enhancement in the excitation/ionization process. To this end, a high temperature (>350 °C), low dead-volume, pulsed jet sampling valve (designed and fabricated in the Ames Laboratory) is presently being tested. It is anticipated that this valve will provide not only efficient cooling of the CC/GC effluent, but will also achieve at least a two decade gain in sensitivity, in comparison to the continuous flow approach, as a result of a marked improvement in duty cycle. With or without the incorporation of a pulsed jet sampling valve, the use of a

higher repetition rate laser source would certainly improve S/N and provide a more reliable profile of transient CC/GC eluents.

Additional reduction in stray light and background electronic noise should improve the S/N ratios for LIF detection. Also, by partially enclosing the gas sampling cell within a $LN_2$-cooled cryoshield, the background levels of PAC and other residual interferences will be greatly reduced (168,187), which should result in improvement of LOD values for all of the laser-based detection schemes. Other dimensions of LIF emission, such as observation of fluorescence lifetime and characteristic emission spectra, remain to be exploited. With the addition of a monochromator/photodiode array detection system, an entire fluorescence emission spectrum can be made available, on-line, for each fluorescing chromatographic eluent. These spectra should be particularly useful if employed with a rotational cooling sampling system, as the resulting narrow band emission spectra would serve as "fingerprints" to assist in the identification of various species.

The wealth of analytical information provided by this instrument, and its future adaptations, should be very valuable in solving complex PAC characterization problems. The deluge of information that must be collected, processed, and collated in order to achieve identification and accurate quantitation of each component in a complex mixture, will require sophisticated data acquisition and reduction techniques, including chemometrics (209). The implementation of such schemes, including appropriate computer software, must be a high priority.

An on-column injection system will replace the split mode injector used in these studies. This replacement should greatly improve the

precision of analytical measurements, particularly for larger compounds. The CC/GC appears to be an ideal sampling system for most applications. The development of alternative sampling systems, such as capillary column supercritical fluid chromatography (CC/SFC) and microbore HPLC-thermospray (210) should extend the range of applicability to include the determination of nonvolatile and/or thermally labile compounds.

The most urgent need is to develop a low-pressure, gas-phase PAC excitation/ionization spectral data base, particularly if rotational cooling is to be employed. Diagnostic and mechanistic studies should also be helpful in the prediction of detector responses for various species and to assist in developing analytical methodologies for specific applications. Such a mechanistic study, involving simple halogenated aromatics, has recently been reported by Tembreull et al. (200).

The studies presented in this dissertation only begin to describe the analytical utility of the multidimensional instrument. The potential for high selectivity in the excitation/ionization process, coupled with the selectivity and sensitivity of the multidimensional detection scheme, clearly indicate the promise of utilizing CC/GC-REMPI-TOF/MS-LIF-FID for a wide variety of analytical applications involving trace PAC characterization. Ultimately, the wealth of information available from such a system may provide the means for complete, unambiguous identification and quantitation of trace-level, UV-absorbing species in extremely complex mixtures.

# VIII. BIBLIOGRAPHY


1. Birdbord, K.; French, J. G. In "Carcinogensis, Vol. 3: Polynuclear Aromatic Hydrocarbons;" Jones, P. W.; Freundanthal, R. I., Eds.; Raven Press: New York, NY, 1978; p 451.

2. Haddow, A. In "The Physiopathology of Cancer," 2nd Edition; Homburger, F., Ed.; Harper: New York, NY, 1959; Chapter 14.

3. Jones, D. W.; Mathews, R. S. Prog. Med. Chem. 1974, 10, 159.

4. White, C. In "Polyaromatic Hydrocarbons, Third International Symposium;" Jones, P., Ed.; Ann Arbor Science: Ann Arbor, MI, 1979.

5. Borgen, A.; Darvey, H.; Castagnok, N.; Crocker, T. T.; Rassmussen, R. E.; Wang, I. Y. J. Med. Chem. 1973, 16, 502.

6. Ho, C. -h.; Clark, B. R.; Guerin, M. R.; Barkenbus, B. D.; Rao, T. K.; Epler, J. L. Mutat. Res. 1981, 85, 335.

7. Guerin, M. R.; Rubin, I. B.; Rao, T. K.; Clark, B. R.; Epler, J. L. Fuel 1981, 60, 282.

8. "Chemical Carcinogens, Vols. 1 and 2," 2nd Edition; Searle, C. E., Ed.; American Chemical Society: Washington, DC, 1984.

9. Willey, C.; Iwao, M.; Castle, R. N.; Lee, M. L. Anal. Chem. 1981, 53, 400.

10. Woo, C. S.; D'Silva, A. P.; Fassel, V. A.; Oestreich, J. G. Environ. Sci. Technol. 1978, 12, 173.

11. Blumer, M. Scientific American 1976, 234 (3), 34.

12. Hoffman, D.; Wynder, E. L. Analytical and Biological Studies on Gasoline Engine Exhaust Nat. Cancer Inst. Monogr. 9:91-116, 1962.

13. Long, R. Studies On Polycyclic Aromatic Hydrocarbons In Flames; U.S.N.T.I.S. No. PB-220151, 1972.

14. Koppenaal, D. W.; Manahan, S. E. Envron. Sci. Technol. 1976, 10, 1104.

15. Guerin, M. R.; Griest, W. H.; Ho, C.-h.; Shutts, W. D. In Third ERDA Environmental Protection Conference, Oak Ridge, TN, Sept. 1975.

16. Panalaks, T. J. Environ. Sci. Health 1976, b11, 299.

17. Giger, W.; Blumor, M. Anal. Chem. 1974, 46, 1663.

18. Giger, W.; Schaffner, G. Anal. Chem. 1978, 50, 243.

19. Borneff, J. Der Landarzt 1964, 40, 109.

20. Howard, J. W.; Fazio, T.; White, R. H.; Klimeck, B. A. J. Ass. Off. Anal. Chem. 1968, 51, 122.

21. Griest, W. H.; Tomkins, B. A.; Epler, J. L.; Rao, T. K. In "Polynuclear Aromatic Hydrocarbons;" Jones, P. W.; Leber, P., Eds.; Ann Arbor Science: Ann Arbor, MI, 1979, p. 395.

22. Dripple, A. In "Chemical Carcinogens;" Searle, C. E., Ed.; American Chemical Society: Washington, D. C., 1976, p. 245.

23. Pelroy, A. A.; Gandolfi, A. Mutat. Res. 1980, 72, 329.

24. Hoffman, D.; Wynder, E. L. Cancer 1971, 27, 848.

25. Hirschfeld, T. Anal. Chem. 1980, 52, 297A.

26. Sonnefeld, W. J.; Zoller, W. H.; May, W. E.; Wise, S. A. Anal. Chem. 1982, 54, 723.

27. Wise, S. A.; May, W. E. Anal. Chem. 1983, 55, 1479.

28. Thomson, J. S.; Reynolds, J. W. Anal. Chem. 1984, 56, 2434.

29. Ogan, K.; Katz, E. Anal. Chem. 1981, 53, 160.

30. Das, B. S.; Thomas, G. H. Anal. Chem. 1978, 50, 967.

31. Fenimore, D. C.; Davis, C. M. Anal. Chem. 1981, 53, 252A.

32. Eganhouse, R. P.; Ruth, E. C.; Kaplan, I. R. Anal. Chem. 1983, 55, 2120.

33. Butler, H. T.; Coddens, M. E.; Khatib, S.; Poole, C. E. J. Chrom. Sci. 1985, 23, 200.

34. Novotny, M.; Springston, S. R.; Peaden, P. A.; Fjeldsted, J. C.; Lee, M. L. Anal. Chem. 1981, 53, 407A.

35. Peaden, P. A.; Fjeldsted, J. C.; Lee, M. L.; Springston, S. R.; Novotny, M. Anal. Chem. 1982, 54, 1090.

36. Fjeldsted, J. C.; Lee, M. L. Anal. Chem. 1984, 56, 619A.

37. Karasek, F. W.; Clement, R. E.; Sweetman, J. A. Anal. Chem. 1981, 53, 1050A.

38. Crowley, R. J.; Siggia, S.; Uden, P. C. Anal. Chem. 1980, 52, 1224.

39. Later, D. W.; Lee, M. L.; Bartle, K. D.; Kong, R. C.; Vassilaros, D. L. Anal. Chem. 1981, 53, 1612.

40. Yergey, J. A.; Risby, T. H.; Lests, S. S. Anal. Chem. 1982, 54, 354.

41. Grimmer, G.; Jacob, J.; Naujack, K.; Dettbarn, G. Anal. Chem. 1983, 55, 892.

42. Later, D. W.; Andros, T. G.; Lee, M. L. Anal. Chem. 1983, 55, 2126.

43. Rosenthal, D. Anal. Chem. 1982, 54, 63.

44. Fox, M. A.; Staley, S. W. Anal. Chem. 1976, 48, 992.

45. Lee, M. L.; Vassilaros, D. L.; White, C. M.; Novotny, M. Anal. Chem. 1979, 51, 768.

46. Cairns, T.; Siegmund, E. G. Anal. Chem. 1981, 53, 1183A.

47. Dunn, W. J.; Stalling, D. L.; Schwartz, T. R.; Hogan, J. W.; Petty, J. D.; Johansson, E.; Wold, S. Anal. Chem. 1984, 56, 1308.

48. Karasek, F. W.; Onuska, F. I. Anal. Chem. 1982, 54, 309A.

49. Albert, D. K. Anal. Chem. 1978, 50, 1822.

50. Paputa-Peck, M. C.; Marano, R. S.; Schuetzle, D.; Riley, T. L.; Hampton, C. V.; Prater, T. J.; Skewes, L. M.; Jensen, T. E.; Ruehle, P. H.; Bosch, L. C.; Duncan, W. P. Anal. Chem. 1983, 55, 1946.

51. Driscoll, J. N.; Ford, J.; Jaramillo, L. F.; Gruber, E. T. J. Chromatography 1978, 158, 171.

52. Nutmagul, W.; Cronn, D. R.; Hill, Jr., H. H. Anal. Chem. 1983, 55, 2160.

53. Krull, I. S.; Swartz, M.; Hilliard, R.; Xie, K. -H.; Driscoll, J. N. J. Chromatography 1983, 260, 347.

54. Novotny, M.; Schwend, F. J.; Hrtigan, M. J.; Purcell, J. E. Anal. Chem. 1980, 52, 736.

55. Uden, P. C.; Barnes, R. M.; Disanzo, F. P. Anal. Chem. 1978, 50, 852.

56. Quimby, B. D.; Uden, P. C.; Barnes, R. M. Anal. Chem. 1978, 50, 2112.

57. Rice, G. W.; Richard, J. J.; D'Silva, A. P.; Fassel, V. A. Anal. Chem. 1981, 53, 1519.

58. Fredriksson, S.; Cedergren, A. Anal. Chem. 1981, 53, 614.

59. McGaughey, J. F.; Gangwal, S. K. Anal. Chem. 1980, 52, 2079.

60. Aue, W. A.; Flinn, C. G. Anal. Chem. 1980, 52, 1537.

61. Wells, G. Anal. Chem. 1983, 55, 2112.

62. Baim, M. A.; Hill, Jr., H. H. Anal. Chem. 1982, 54, 38.

63. Ithakissios, D. S. J. Chromatogr. Sci. 1980, 18, 88.

64. Baim, M. A.; Eatherton, R. L.; Hill, Jr., H. H. Anal. Chem. 1983, 55, 1761.

65. Burlingame, A. L.; Baillie, T. A.; Derrick, P. J.; Chizhov, O. S. Anal. Chem. 1980, 52, 214R.

66. Lubman, D. M. Anal. Chem. 1984, 56, 1298.

67. Revercomb, H. E.; Mason, E. A. Anal. Chem. 1975, 47, 970.

68. Erickson, M. D. Appl. Spectrosc. Revs. 1979, 15, 261.

69. Griffiths, P. R.; deHaseth, J. A.; Azarraga, L. V. Anal. Chem. 1983, 55, 1361A.

70. Sparks, D. T.; Lam, R. B.; Isenhour, T. L. Anal. Chem. 1982, 54, 1922.

71. Lam, R. B.; Sparks, D. T.; Isenhour, T. L. Anal. Chem. 1982, 54, 1927.

72. Shafer, K. H.; Hayes, T. L.; Brasch, J. W.; Jakobsen, R. J. Anal. Chem. 1984, 56, 237.

73. Hembree, D. M.; Garrison, A. A.; Crocombe R. A.; Yokley, R. A.; Wehry, E. L.; Mamantov, G. Anal. Chem. 1981, 53, 1783.

74. Cooper, J. R.; Taylor, L. T. Anal. Chem. 1984, 56, 1989.

75. Romanowski, T.; Funcke, W.; Konig, J.; Balfanz, E. Anal. Chem. 1982, 54, 1285.

76. Hertz, H. S.; Brown, J. M.; Chesler, S. N.; Guenther, F. R,; Hilpert, L. R.; May, W. E.; Paris, R. M.; Wise, S. A. Anal. Chem. 1980, 52, 1650.

77. Choudhury, D. R.; Bush, B. Anal. Chem. 1981, 53, 1351.

78. Tong, H. Y.; Karasek, F. W. Anal. Chem. 1984, 56, 2129.

79. Later, D. W.; Lee, M. L.; Wilson, B. W. Anal. Chem. 1982, 54, 117.

80. Novotny, M.; Kump, R.; Merli, F.; Todd, L. J. Anal. Chem. 1980, 52, 401.

81. Tomkins, B. A.; Ho, C. -h. Anal. Chem. 1982, 54, 91.

82. Vassilaros, D. L.; Stoker, P. W.; Booth, G. M.; Lee, M. L. Anal. Chem. 1982, 54, 106.

83. Novotny, M.; Hirose, A.; Wiesler, D. Anal. Chem. 1984, 56, 1243.

84. Romanowski, T.; Funcke, W.; Grossmann, I.; Konig, J.; Balfanz, E. Anal. Chem. 1983, 55, 1030.

85. Cram, S. P.; Risby, T. H.; Field, L. R.; Yu, W. Anal. Chem. 1980, 52, 324R.

86. Hilpert, L. R.; Byrd, G. D.; Vogt, C. R. Anal. Chem. 1984, 56, 1842.

87. Simonsick, W. J.; Hites, R. A. Anal. Chem. 1984, 56, 2749.

88. Wilkens, C. L.; Giss, G. N.; White, R. L.; Brissey, G. M.; Onyiriuka, E. C. Anal. Chem. 1984, 54, 2260.

89. Crawford, R. W.; Hischfeld, T.; Sanborn, R. H.; Wong, C. M. Anal. Chem. 1982, 54, 817.

90. Chem. Eng. News 1983, 61 (15), 28.

91. Wright, J. C.; Wirth, M. J. Anal. Chem. 1980, 52, 988A.

92. Wright, J. C.; Wirth, M. J. Anal. Chem. 1980, 52, 1087A.

93. Adhav, R. S. Laser Focus 1983, June, 73.

94. Yeung, E. S.; Sepaniak, M. J. Anal. Chem. 1980, 52, 1465A.

95. Klimcak, C. M.; Wessel, J. E. Anal. Chem. 1980, 52, 1233.

96. Rhodes, G.; Opsal, R. B.; Meek, J. T.; Reilly, J. P. Anal. Chem. 1983, 55, 280.

97. Shpol'skii, E. V.; Il'ina, A. A.; Klimora, L. A. Dokl. Akad. Nauk SSSR 1952, 87, 935.

98. Svischev, G. M. Opt. Spectrosc. 1965, 18, 350.

99. Colmsjo, A.; Stenberg, V. J. Chromatography 1979, 169, 205.

100. Stenberg, V. R.; Alsberg, T. E. Anal. Chem. 1981, 53, 2067.

101. Colmsjo, A. L.; Ostman, C. E. Anal. Chem. 1980, 52, 2093.

102. Rima, J.; Lamotte, M.; Joussol-Dubien, J. Anal. Chem. 1982, 54, 1059.

103. Kirkbright, G. F.; de Lima, C. G. Analyst 1974, 99, 338.

104. Kirkbright, G. F.; de Lima, C. G. Chem. Phys. Lett. 1976, 37, 165.

105. Lee, M. L.; Novotny, M. V.; Bartle, K. In "Analytical Chemistry of Polycyclic Aromatic Compounds;" Academic Press: New York, 1981; Chapter 9.

106. D'Silva, A. P.; Oestreich, G. J.; Fassel, V. A. Anal. Chem. 1976, 48, 915.

107. Woo, C. S.; D'Silva, A. P.; Fassel, V. A. Anal. Chem. 1980, 52, 159.

108. Yang, Y.; D'Silva, A. P.; Fassel, V. A.; Iks, M. Anal. Chem., 1980, 52, 1350.

109. Yang, Y.; D'Silva, A. P.; Fassel, V. A. Anal. Chem. 1981, 53, 894.

110. Yang, Y.; D'Silva, A. P.; Fassel, V. A. Anal. Chem. 1981, 53, 2107.

111. D'Silva, A. P.; Fassel, V. A. Anal. Chem. 1984, 56, 985A.

112. Colmsjo, A. L.; Zebuhr, U. Y.; Ostman, C. E. Chem. Sci. 1982, 20, 123.

113. Personov, R. I. In "Spectroscopy and Excitation Dynamics of Condensed Molecular Systems;" Agranovich, V. M.; Hochstrasser, R. M., Eds.; North Holland: New York, NY, 1983; Chapter 10.

114. Brown, J. C.; Hayes, J. M.; Warren, J. A.; Small, G. J. In "Lasers and Chemical Analysis;" Hieftje, G. M.; Lytle, F. E.; Travis, J. C., Eds.; Humana Press: Clifton, NJ, 1981; Chapter 12.

115. Hayes, J. M.; Chiang, I.; McGlade, M. J.; Warren, J. A.; Small, G. J. In "Laser Spectroscopy for Sensitive Detection;" Gelbwach, J. A., Ed.; SPIE: Bellingham, WA, 1981; Vol. 286, p 117.

116. Brown, J. C.; Edelson, M. C.; Small, G. J. Anal. Chem. 1978, 50, 1394.

117. Brown, J. C.; Duncanson, J. A.; Small, G. J. Anal. Chem. 1980, 52, 1711.

118. McGlade, M. J. M.S. Thesis, Iowa State University, Ames, Iowa, 1983.

119. Personov, R. I. In "Spectroscopy and Excitation of Condensed Molecular Systems;" Agranovich, V. M.; Hochstrasser, R. M., Eds.; North Holland: New York, NY, 1983; Chapter 10.

120. Meyer, B. "Low Temperature Spectroscopy"; American Elsevier: New York, NY, 1971.

121. Bykovskaya, L. A.; Personov, R. I.; Romanovskii, Y. V. Anal. Chim. Acta 1981, 125, 1.

122. Sanders, M. J.; Cooper, R. S.; Small, G. J.; Heisig, V.; Jeffrey, A. M. Anal. Chem. 1985, 57, 1148.

123. Stroupe, R. C.; Tokousbalides, P.; Dickinson, R. B.; Wehry, E. L.; Mamantov, G. Anal. Chem. 1977, 49, 701.

124. Mamantov. G.; Wehry, E. L.; Kemmerer, R. R.; Hinton, E. R. Anal. Chem. 1977, 49, 86.

125. Tokousbalides, P.; Hinton, E. R.; Dickinson, R. B.; Bilotta, P. V.; Shery, E. L.; Mamantov, G. Anal. Chem. 1978, 50, 1189.

126. Wehry, E. L.; Mamantov, G. Anal. Chem. 1979, 51, 643A.

127. Dickinson, R. B.; Wehry, E. L. Anal. Chem. 1979, 51, 778.

128. Wehry, E. L.; Mamantov, G. Anal. Chem. 1979, 51, 643A.

129. Maple, J. R.; Wehry, E. L. Anal. Chem. 1981, 53, 266.

130. Maple, J. R.; Wehry, E. L. Anal. Chem. 1981, 53, 1244.

131. Perry, M. B.; Wehry, E. L.; Mamantov, G. Anal. Chem. 1983, 53, 1893.

132. Pace, C. F.; Maple, J. R. Anal. Chem. 1985, 57, 940.

133. Maple, J. R.; Wehry, E. L.; Mamantov, G. Anal. Chem. 1980, 52, 920.

134. Richards, J. L.; Rice, S. A. J. Chem. Phys. 1971, 54, 2014.

135. Personov, R. I.; Al'Shits, E. I.; Bykovskaya, L. A. Opt. Commun. 1972, 6, 169.

136. McColgin, W. C.; Marchetti, A. P.; Eberly, J. H. J. Am. Chem. Soc. 1978, 100, 5622.

137. Cunningham, K.; Morris, J. M.; Funfschilling, J.; Williams, D. F. Chem. Phys. Lett. 1975, 32, 581.

138. Zandee, L.; Bernstein, R. B.; Lictin, D. A. J. Chem. Phys. 1978, 69, 3427.

139. Levy, D. H. Science 1981, 214, 263.

140. Smalley, R. E.; Wharton, L.; Levy, D. H. Acc. Chem. Res. 1977, 10, 139.

141. Levy, D. H. Ann. Rev. Phys. Chem. 1980, 31, 197.

142. Johnston, M. V. Trends Anal. Chem. 1984, 3, 58.

143. Leutwyler, S.; Even, U.; Jortner, J. Chem. Phys. Lett. 1982, 86, 439.

144. Leutwyler, S.; Even, U.; Jortner, J. J. Chem. Phys. 1983, 79, 5769.

145. Lichtin, D. A.; Datta-Ghosh, S.; Newton, K. R.; Bernstein, R. B. Chem. Phys. Lett. 1980, 75, 214.

146. Yamada, S.; Winefordner, J. D. Spectroscopy Letters 1985, 18, 139.

147. Amirav, A.; Even, U.; Jortner, J. Chem. Phys. Lett. 1979, 67, 9.

148. Amirav, A.; Even, U.; Jortner, J. Optics Communications 1980, 32, 266.

149. Amirav, A.; Even, U.; Jortner, J. J. Chem. Phys. 1979, 71, 2319.

150. Amirav, A.; Even, U.; Jortner, J. J. Chem. Phys. 1981, 75, 3770.

151. Amirav, A.; Even, U.; Jortner, J. Chem. Phys. Lett. 1980, 72, 16.

152. Amirav, A.; Even, U.; Jortner, J. Optics Communications 1980, 32, 266.

153. Amirav, A.; Even, U.; Jortner, J. Chem. Phys. Lett. 1980, 72, 21.

154. Bersohn, R.; Even U.; Jortner, J. J. Chem. Phys. 1983, 79, 2163.

155. Amirav, A.: Even, U.; Jortner, J. Chem. Phys. Lett. 1980, 69, 14.

156. Warren, J. A.; Hayes, J. M.; Small, G. J. Anal. Chem. 1982, 54, 138.

157. Hayes, J. M.; Small, G. J. Anal. Chem. 1982, 54, 1202.

158. Hayes, J. M.; Small, G. J. Anal. Chem. 1983, 55, 565A.

159. Amirav, A.; Even, U.; Jortner, J. Anal. Chem. 1982, 54, 1666.

160. Imasaka, T.; Fukuoka, H.; Hayashi, T.; Ishibashi, N. Anal. Chim. Acta 1984, 156, 111.

161. D'Silva, A. P.; Iles, M.; Rice, G.; Fassel, V. A. Ames, Iowa, April 1984, Ames Laboratory Report IS-4556.

162. Lubman, D. M.; Kronick, M. N. Anal. Chem. 1982, 54, 660.

163. Tembreull, R.; Lubman, D. M. Anal. Chem. 1984, 56, 1962.

164. Sin, C. H.; Tembreull, R.; Lubman, D. M. Anal. Chem. 1984, 56, 2776.

165. Lubman, D. M.; Tembreull, R.; Sin, C. H. Anal. Chem. 1985, 57, 1084.

166. Imasaka, T.; Shigezumi, T.; Ishibashi, N. Analyst 1984, 109, 277.

167. Dietz, T. G.; Duncan, M. A.; Liverman, M. G.; Smalley, R. E. Chem. Phys. Lett. 1980, 70, 246.

168. Dietz, T. G.; Duncan, M. A.; Liverman, M. G.; Smalley, R. E. J. Chem. Phys. 1980, 73, 4816

169. Evan, U.; Magen, J.; Jortner, J. J. Chem. Phys. 1982, 77, 4374.

170. Evan, U.; Magen, J.; Jortner, J.; Friedman, J. J. Chem. Phys. 1982, 77, 4384.

171. Evan, U.; Jortner, J. J. Chem. Phys. 1982, 77, 4391.

172. Smith, R. D.; Felix, W. D.; Fjeldsted, J. C.; Lee, M. L. Anal. Chem. 1982, 54, 1883.

173. Schek, I.; Jortner, J. J. Chem. Phys. 1979, 70, 3016.

174. Johnson, P. M. Acc. Chem. Res. 1980, 13, 20.

175. Robin, M. B. Applied Optics 1980, 19, 3941.

176. Seaver, M.; Hudgens, J. W.; Decorpo, J. J. Int. J. Mass Spectrom. Ion Phys. 1980, 34, 159.

177. Brophy, J. H.; Rettner, C. T. Optics Letters 1979, 4, 337.

178. Cotter, R. J. Anal. Chem. 1984, 56, 485A.

179. Siebrand, W. In "Dynamics Of Molecular Collisions, Part A;" Miller, W., Ed.; Plenum: New York, NY, 1976; Chapter 6.

180. Kasha, M. Discuss. Faraday Soc. 1950, 9, 14.

181. Lubman, D. M.; Naaman, R.; Zare, R. N. J. Chem. Phys. 1980, 72, 3034.

182. Brophy, J. H.; Rettner, C. T. Chem. Phys, Lett. 1979, 67, 351.

183. McGilvery, D. C.; Morrison, J. O. Int. J. Mass Spectrom. Ion Phys. 1978, 28, 81.

184. Antonov, V. S.; Letokhov, V. S. Appl. Phys. 1981, 24, 89.

185. Antonov, V. S.; Knyazev, I. N.; Letokhov, V. S.; Matiuk, V. M.; Movshev, V. K.; Potapov, V. K. Opt. Lett. 1978, 3, 37.

186. Mukhtar, E. S.; Griffiths, I. W.; Harris, F. M.; Beynon, J. H. Int. J. Mass Spectrom. Ion Phys. 1982, 42, 77.

187. Lubman, D. M.; Jordan, R. M. Rev. Sci. Instrum. 1985, 56, 373.

188. Irion, M. P.; Bowers, W. D.; Hunter R. L.; Rowland, F. S.; McIver, R. T., Jr. Chem. Phys. Lett. 1982, 93, 375.

189. Carlin, T. J.; Freiser, B. S. Anal. Chem. 1983, 55, 955.

190. Wiley, W. C.; McLaren, I. H. Rev. Sci. Instrum. 1955, 26, 1150.

191. "Time-Of-Flight Mass Spectrometry;" Price, D.; Williams, J. E., Eds.; Pergamon Press: New York, 1969.

192. Linder, B.; Seydel, U. Anal. Chem. 1985, 57, 895.

193. Tailliez, B. Y.; Hume, S. H. In "Dynamic Mass Spectrometry;" Price, D.; Todd, J. F. J., Eds.; Heyden & Son Ltd.: London, England, 1981; Vol. 6, Chapter 15.

194. Bernhardt, A. F.; Herbst, R. L.; Kronick, M. N. Laser Focus 1982, October, 59.

195. Hartig, W. Opt. Commun. 1978, 27, 447.

196. Maeda, M. "Laser Dyes;" Academic Press, Inc.: Tokyo, Japan, 1984.

197. Jennings, W. "Gas Chromatography with Glass Capillary Columns;" 2nd Edition; Academic Press: New York, NY; 1980.

198. CVC Instruction Manual No. 20-21; CVC Products, Inc.: Rochester, NY.

199. CVC Instruction Manual No. 20-8-A; CVC Products, Inc.: Rochester, NY.

200. Tembreull, R.; Sin, C. H.; Li, P.; Pang, H. M.; Lubman, D. M. Anal. Chem. 1985, 57, 1186.

201. Sears, F. W.; Zemansky, M. W. "University Physics;" 3rd Edition; Addison-Wesley Publishing Company, Inc.: Reading, Mass; 1964; Chapter 30.

202. Robaz, J. "Introduction To Mass Spectrometry: Instrumentation and Techniques;" Interscience Publishers: New York, NY, 1964.

203. Havrilla, G. J.; Green R. B. Chem., Biomed., and Environ. Instrumentation 1981, 11(4), 273.

204. Malmstadt, H. V.; Enke, C. G.; Crouch, S. R.; Horlick, G. "Optimization Of Electronic Measurements-Instrumentation For Scientists Series-Module 4"; W. A. Benjamin, Inc.: Menlo Park, CA, 1974.

205. Letzter, S. Laser Focus/Electro-Opt. 1983, 19(12), 76.

206. Lytle, F. Anal. Chem. 1974, 46, 545A.

207. Model 560 Gas Chromatograph Operation Manual Number 114806B; Tracor Instruments: Austin, TX, October 1975.

208. Bevington, P. R. "Data Reduction and Error Analysis for the Physical Sciences;" McGraw Hill: New York, NY; 1969.

209. Ramos, L. S.; Burger, J. E.; Kowalski, B. R. Anal. Chem. 1985, 57, 2920.

210. Blakley, C. R.; Vestal, M. L. Anal. Chem. 1983, 55, 750.

211. Levine, I. N. "Quantum Chemistry;" 2nd Edition; Allyn and Bacon, Inc.: Boston, MA, 1974; Chapter 15.

212. Ramsey, N. F. "Molecular Beams;" Oxford University Press: Oxford, England, 1956.

213. Pauly, H.; Toennies, J. P. Methods Exp. Phys. 1968, 75, 237.

214. Maeda, M. "Laser Dyes"; Academic Press, Inc.: Tokyo, Japan, 1984.

215. Anderson, J. B.; Fenn, J. B. Phys. Fluids 1965, 8, 780.

216. Gentry, W. R.; Giese, C. F. Rev. Sci. Instrum. 1978, 49, 595.

217. Lasertechnics Model LPV Pulsed Molecular Beam Valve; Lasertechnics, Inc.: Albuquerque, NM, July 1982.

218. Quanta-Ray PSV-2 Pulsed Supersonic Valve; Quanta-Ray: Mountain View, CA, April 1982.

219. Dushman, S. In "Scientific Foundations of Vacuum Technique;" 2nd Edition; Lafferty, J. M., Ed., Wiley: New York, NY, 1962, Chapter 2.

# IX. ACKNOWLEDGMENTS

I take great pleasure in acknowledging those who were involved with this research, either directly or indirectly. This work was supported by the U. S. Department of Energy, Office of Health and Environmental Research. Also, the financial support provided by the Standard Oil Company of Ohio, in the form of a graduate fellowship, is greatly appreciated.

I wish to express my sincere gratitude to Professor Velmer A. Fassel and Mr. Arthur P. D'Silva for their guidance and critical review of the work presented in this dissertation. Further, their trust in my judgement and abilities was instrumental in making "Dobson's Folly" a success.

Special thanks to Dr. R. Sam Houk who gave me "real good" advice, free of charge, throughout my graduate career. I would also like to thank Dr. Stephan J. Weeks for his assistance in the later stages of this work and particularly for taking the time to offer critical review of the documentation thereof.

Thanks to my fellow graduate students, particularly Greg Sevenich, Kim and Bryant LaFreniere, and Moi Leong, for their friendship and encouragement, and to the members of the Pizza Pit Softball Team that provided a needed diversion from the occasional doldrums of graduate study.

The patience and understanding of my parents, Robert and Genevieve Dobson, as well as my sisters and brother, Judy, Cindy, and Gary, in coping with their son and brother, "the professional student", is sincerely appreciated.

Above all, I am deeply indebted to my wife, Marilyn, for her love,

patience, encouragement, and the sacrifices she made over the past several years, and to our new daughter, Jessica, for being a pleasant distraction (usually) during the preparation of this dissertation.

# X. APPENDIX A: REFERENCE FOR ACRONYMS AND ABBREVIATIONS

Below is a summary of acronyms and abbreviations that were used in this dissertation. In general, standard units are not included. Also, the instrumental components were itemized previously (Tables 2 and 4).

Table A1. Acronyms and abbreviations

| Term | Definition | Term | Definition |
|---|---|---|---|
| CC | Capillary column | MPI | Multiphoton ionization |
| CE | Charge-exchange | Nd:YAG | Neodynium: yttrium aluminum garnet |
| CI | Chemical ionization | | |
| CRT | Cathode ray tube | NI | Negative ion |
| ECD | Electron capture detector | NPD | Nitrogen-phosphorous detector |
| EI | Electron-beam ionization | PAC | Polynuclear aromatic compound(s) |
| FET | Field effect transistor | | |
| FID | Flame ionization detector | PAH | Polynuclear aromatic hydrocarbon(s) |
| FLNS | Fluorescence line narrowing spectrometry | PCB | Polychlorinated biphenyl(s) |
| | | PID | Photoionization detector |
| FPD | Flame photometric detector | RC | Rotationally-cooled |
| FT | Fourier transform | RE | Resonance enhanced |
| FWHM | Full-width at half-maximum | SF | Selectivity factor |
| GC | Gas chromatography | SFC | Supercritical fluid chromatography |
| HPLC | High performance liquid chromatography | | |
| | | SIM | Selective ion monitoring |
| ICP | Inductively-coupled plasma | S/N | Signal-to-noise ratio |
| IG | Ion grid | SR | Chromatographic split ratio(overall) |
| IMS | Ion mobility spectrometry | | |
| IP | Ionization potential | | |
| IR | Infrared | TECD | Total electron current detector |
| KE | Kinetic energy | | |
| KDP | Potassium dihydrogen phosphate | THC | Total hydrocarbon content |
| | | TLC | Thin layer chromatography |
| LDR | Linear dynamic range | TOF | Time-of-flight |
| LESS | Laser-excited Shpol'skii spectrometry | UV | Ultraviolet |
| | | VQ | Vibrational quasicontinuum |
| LIF | Laser-induced fluorescence | | |
| LOD | Limit(s) of detection | Miscellaneous: | |
| MS | Mass spectrometry | cw | continuous flow |
| MIFS | Matrix-isolation fluorescence spectrometry | d.c. | direct current |
| | | f.l. | focal length |
| MIP | Microwave induced plasma | i.d. | inside diameter |
| | | o.d. | outside diameter |

# XI. APPENDIX B: SPECTROSCOPIC SELECTIVITY AND PRINCIPLES OF ROTATIONAL COOLING

No matter which particular analytical spectroscopic technique is considered for the characterization of PAC in a mixture, selectivity is ultimately limited by the characteristic molecular absorption band cross sections of each species present. Therefore, the absorption spectra of the respective PAC are indicative of the specificity with which each may be determined. Certainly, any distinctive differences in their characteristic spectra may be exploitable, in the case of very simple mixtures. However, for very complex mixtures at ambient temperatures, the absorption spectra are far too broad and congested to allow even a reasonable degree of selectivity. The processes that are responsible for these broad, ambient-temperature spectra and the basic principles involved in the rotational cooling process are briefly described in this Appendix. Although the focus here is on gas phase spectral broadening, many of the concepts are analogous to those of the condensed phase condition.

## A. Deterrents to Spectroscopic Selectivity

The sources of gas-phase, ambient-temperature spectroscopic broadening must be understood in order to appreciate the potential benefits offered by rotationally-cooled, jet spectroscopy. Figure B1a displays an energy level diagram of the ground and first excited singlet states for an arbitrary PAC. At ambient temperatures (chromatographic or room temperatures), a number of ground state vibrational levels are thermally populated. Thus, not only is the molecule able to undergo "zero point" vibronic transitions, but also a multitude of "hot band"

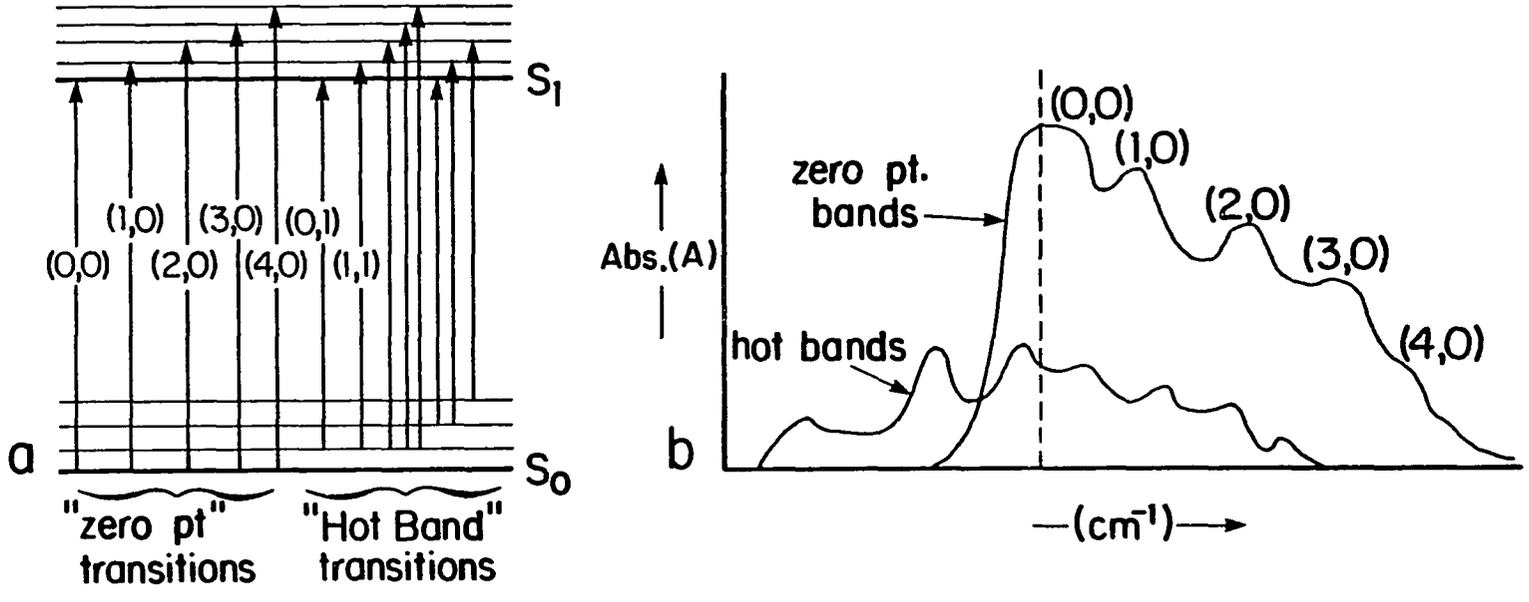


Figure B1. Arbitrary PAC in gas-phase at ambient temperature. a) Energy level diagram (simplified) representing several possible transitions; b) Ambient-temperature absorption profile (Note: Obviously, the superposition of hot bands and zero point bands represents the net profile.)

transitions are possible. While not all vibronic transitions are quantum mechanically allowed, many of them are and each of these allowed transitions will be represented in the molecular absorption spectrum. Normally, this results in heavy congestion of the spectrum, particularly in the case of large PAC molecules that typically may have hundreds of vibrational degrees of freedom (152).

To further complicate the situation, each of the molecular vibronic bands has a broad, essentially continuous, structure at these temperatures. In the gas phase, this broadness is primarily the result of thousands of rotational levels, within each vibrational level of the ground electronic state, being thermally populated. Thus, the exact energy required for a rovibronic transition will vary slightly, from molecule to molecule, depending upon the precise level of origin. Therefore, each vibronic band in an ambient-temperature, gas-phase molecular absorption spectrum is broad, typically 300 $cm^{-1}$ FWHM, due to its rotational "structure". Such a congested absorption spectrum is represented in Figure B1b. It is apparent that it would be quite difficult to satisfactorily resolve vibronic bands of a pure sample, let alone distinguish between characteristic absorption bands of two different PAC isomers, in which the difference in their respective origins might be as little as 10 $cm^{-1}$.

The spectroscopic effects of cooling a gas phase sample to a temperature of 0 K are illustrated in Figure B2. By definition, at 0 K there are no thermally populated vibrational or rotational levels in the ground electronic state. Thus, all transitions must originate at the zero point rovibronic level. Further, the selection rules of quantum mechanics

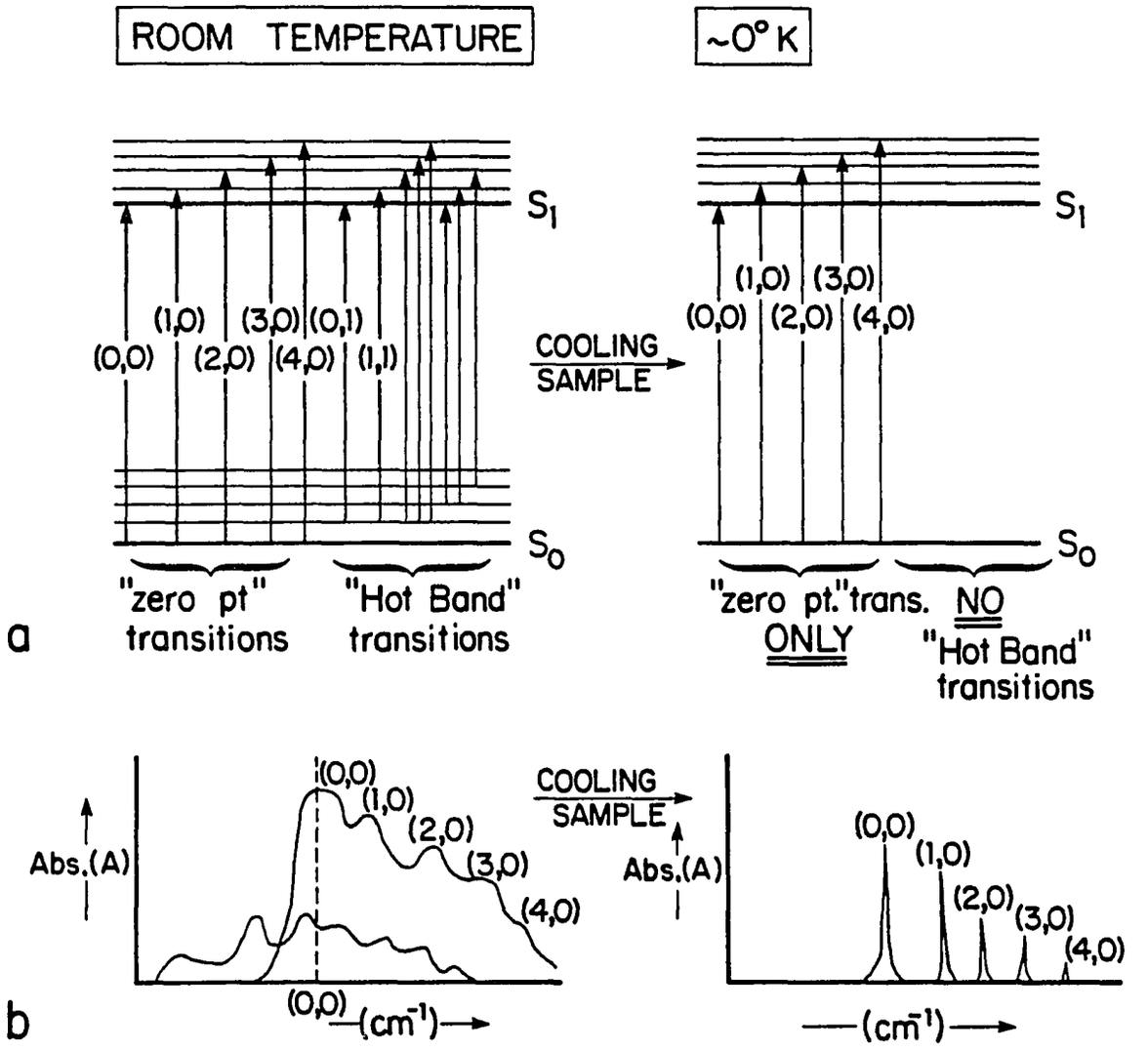


Figure B2. Effects of cooling gas-phase PAC to a temperature of absolute zero. a) Energy level diagram comparison; b) Absorption profile comparison

greatly restrict the number of possible energetically different transitions that originate from any particular level (211). The net effects, of cryogenic temperatures, on a gas-phase molecular absorption spectrum are the elimination of all hot bands and a tremendous narrowing of each allowed zero point band due to the elimination of all rotational structure. This results in a narrow-band or "quasiline" spectrum, which may be exploited to provide high selectivity in spectroscopic characterization studies.

## B. General Principles of the Rotational Cooling Process

When a reservoir of gas, pressurized to $P_0$, is provided access to a high vacuum chamber by way of a small orifice of a given diameter (D), those molecules near the orifice and with a velocity component in the forward direction may pass into the chamber. If $D<<\lambda_0$ (the mean free path of the gas at $P_0$), the molecules will flow through the orifice with essentially no collisions. Therefore, the velocity distribution of these molecules will be a Boltzmann distribution that is determined by the temperature of the reservoir ($T_0$). Under these so-called effusive source conditions, it is apparent that no cooling occurs.

In the case where $D>>\lambda_0$, molecules undergo many collisions while passing through the orifice and for a short distance downstream, as the gas expands. This dynamic situation, termed free-jet expansion, is depicted on a microscopic scale in Figure B3. The molecules emerge from the orifice or nozzle, as it is more commonly termed, with a wide range of positive velocities. These molecular velocities rapidly equilibrate into a narrow distribution by way of a number of two-body collisions. A

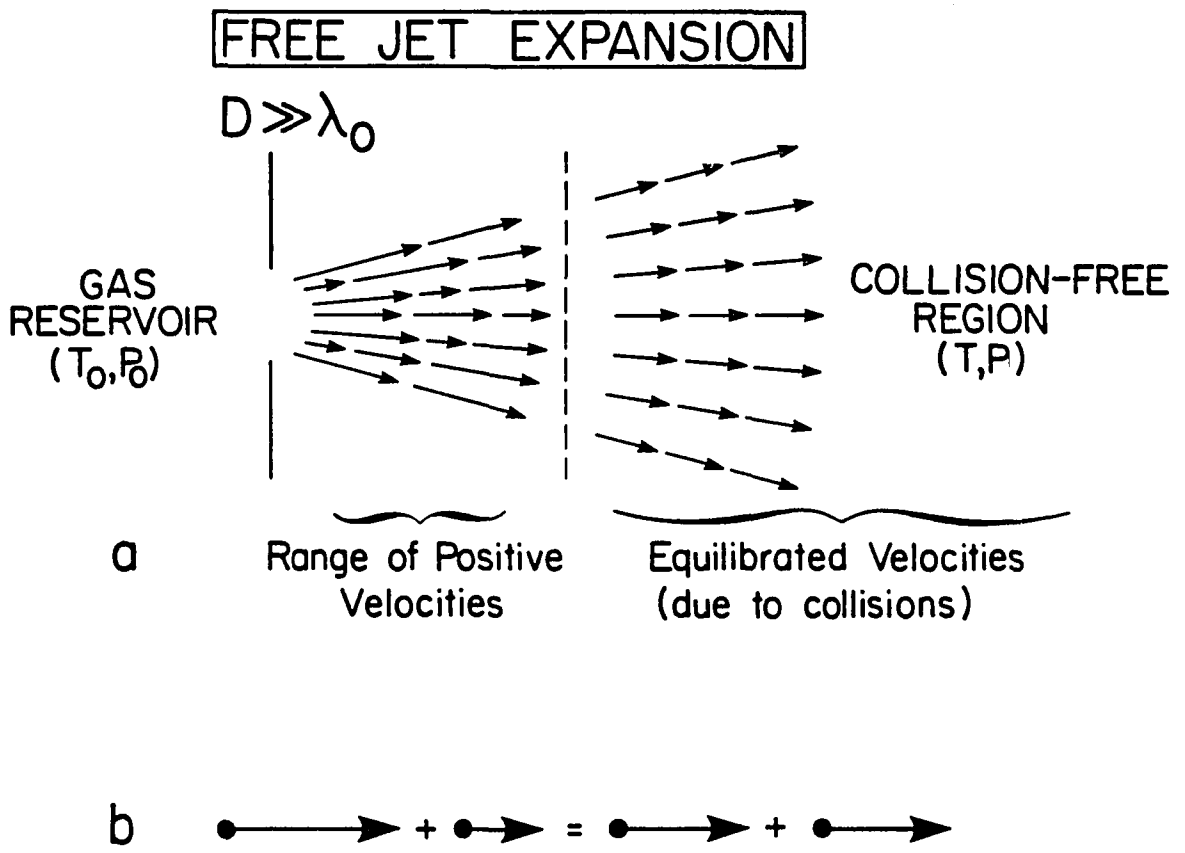


Figure B3. Free jet expansion on a microscopic scale. a) Three primary regions of flow: Reservoir; Collision Region (hydrodynamic flow); Collision Free Region (free flow); b) Typical binary collision, leading to velocity equilibration

simplified explanation is that molecules initially traveling faster than average most often collide with slower molecules, with a net result of decreasing the velocity of the fast molecules and increasing the velocity of the slow molecules. Such collisions become less frequent and less energetic as the velocity distribution narrows. Translational temperature (T) is defined in terms of the standard deviation of the velocity distribution ($\sigma_v$),

$$\sigma_v=(0.47\ kT/m)^{1/2}, \qquad (b1)$$

where k is the Boltzmann constant and m is the molecular mass. Therefore, the translational temperature drops as a result of this collisional equilibration process (212). Thermodynamically, the enthalpy required for directed mass flow is provided at the expense of the random thermal motion of the molecules. This also leads to the conclusion that the molecules must cool in such a "hydrodynamic" expansion (213).

Noble (monatomic) gases are capable of achieving much lower temperatures in a free-jet expansion than polyatomic molecules, because they cannot store energy in rotational and vibrational degrees of freedom. The ultimate translational temperature attainable in such an expansion may be determined utilizing the following equation (214):

$$T/T_o=(P/P_o)^{(\gamma-1)/\gamma}=[1+1/2(\gamma-1)M_T^2]^{-1}, \qquad (b2)$$

where $\gamma$ is the heat capacity ratio of the gas ($C_p/C_v$), P is the pressure in the high vacuum chamber, and $M_T$ is the terminal Mach number. The terminal Mach number is defined as the ratio of the mean velocity of the gas to the local speed of sound. An expression for $M_T$, as derived by Anderson and Fenn (215) for the case of argon, is given as follows:

$$M_T=133(P_oD)^{0.4}, \qquad (b3)$$

where $P_o$ and D are expressed in atmospheres and cm, repectively. The lowest temperatures are, therefore, achieved when $P_o$ and D are large, while maintaining a low value for P. However, equations b2 and b3 are valid only when the jet-background gas interaction is negligible, requiring values of P on the order of $10^{-3}$ torr or lower. Thus, the practical limitation in selection of $P_o$ and D values is the pumping capacity of the high vacuum system. Temperatures as low as 2 K have been reported for jet-cooled argon (140).

By mixing vapors of a polyatomic analyte with the rare gas carrier in the reservoir, the supersonic jet becomes seeded with these molecules. In the early stages of expansion, each molecule will undergo a number of binary collisions with translationally cold carrier atoms. Such collisions serve to equilibrate the various degrees of freedom of the molecule, resulting in tremendous vibrational and rotational relaxation (cooling) of the analyte molecules. Although the efficiency of rotational cooling is much higher than that of vibrational cooling, the corresponding temperature drops are both substantial. Typically, by the time these molecules enter the collision-free region of the jet (Figure B3), their rotational and vibrational temperatures may be as low as 1 K and 150 K, respectively (140).

To demonstrate the effect of rotational cooling on the absorption characteristics of the polyatomic molecule, a portion of the fluorescence excitation spectrum of a 5 % $NO_2$ in argon mixture was obtained utilizing the supersonic jet option and the alternative sampling line of the multidimensional analytical instrument (Chapter IV). This spectrum is displayed in Figure B4, along with corresponding ambient-temperature,

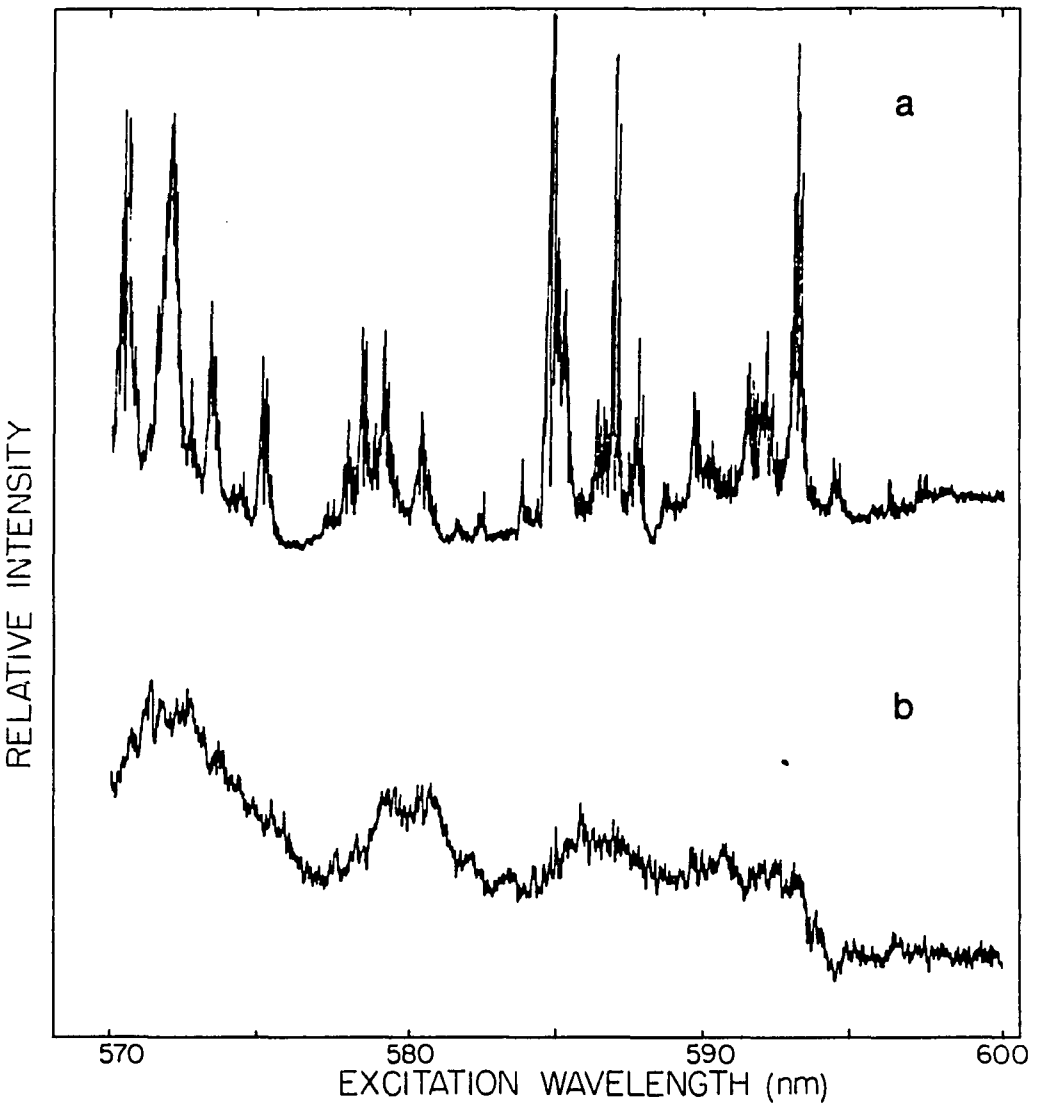


Figure B4. $NO_2$ fluorescence excitation spectra (5 % $NO_2$ in Ar) utilizing RG630 and RG610 cut-off filters and 800 V PMT high voltage. a) Free jet expansion (rotational cooling): 50 μm nozzle, 600 torr backing pressure; b) Static gas at room temperature, 60 mtorr of gas mixture in vacuum chamber. Spectra are not normalized to laser power

fluorescence excitation spectrum of the same gas mixture. Thus, the rotational-vibrational cooling process provides access to a characteristic spectrum that is considerably more defined than the broad, almost featureless, static gas spectrum.

Although the cooling effects demonstrated in Figure B4 are substantial considerable improvement could be provided, in principle, by optimizing the experimental parameters of equations b2 and b3. However, if $P_o$ and/or D were increased much further, the chamber pressure would rise well above $10^{-3}$ torr, due to the limited pumping capacity of the vacuum system, and the integrity of the supersonic jet would be disturbed due to its interaction with the background gas. This pumping capacity problem can be circumvented, in some applications, through the use of a pulsed nozzle or valve (216). In this case, a valve repeatedly opens and closes to allow pulses of gas, typically 150 μsec or less in duration, to enter the vacuum chamber. By synchronizing such a valve with a pulsed laser excitation source, a supersonic jet is created only as often as the laser fires. This results in reduction of the load on the pumping system by orders of magnitude. Hence, D and $P_o$ valves may be increased to provide more efficient cooling conditions, while maintaining a very low background pressure in the vacuum chamber.

The improvement in cooling efficiency gained through the use of a pulsed nozzle was demonstrated, again utilizing the 5 % $NO_2$ in argon mixture, by employing a Lasertechnics Model LPV pulsed nozzle in place of the continuous-flow (cw) nozzle that was used in the previous experiment. Baseline resolution of most of the $NO_2$ spectral features in the corresponding fluorescence excitation spectrum, as shown in Figure B5, is

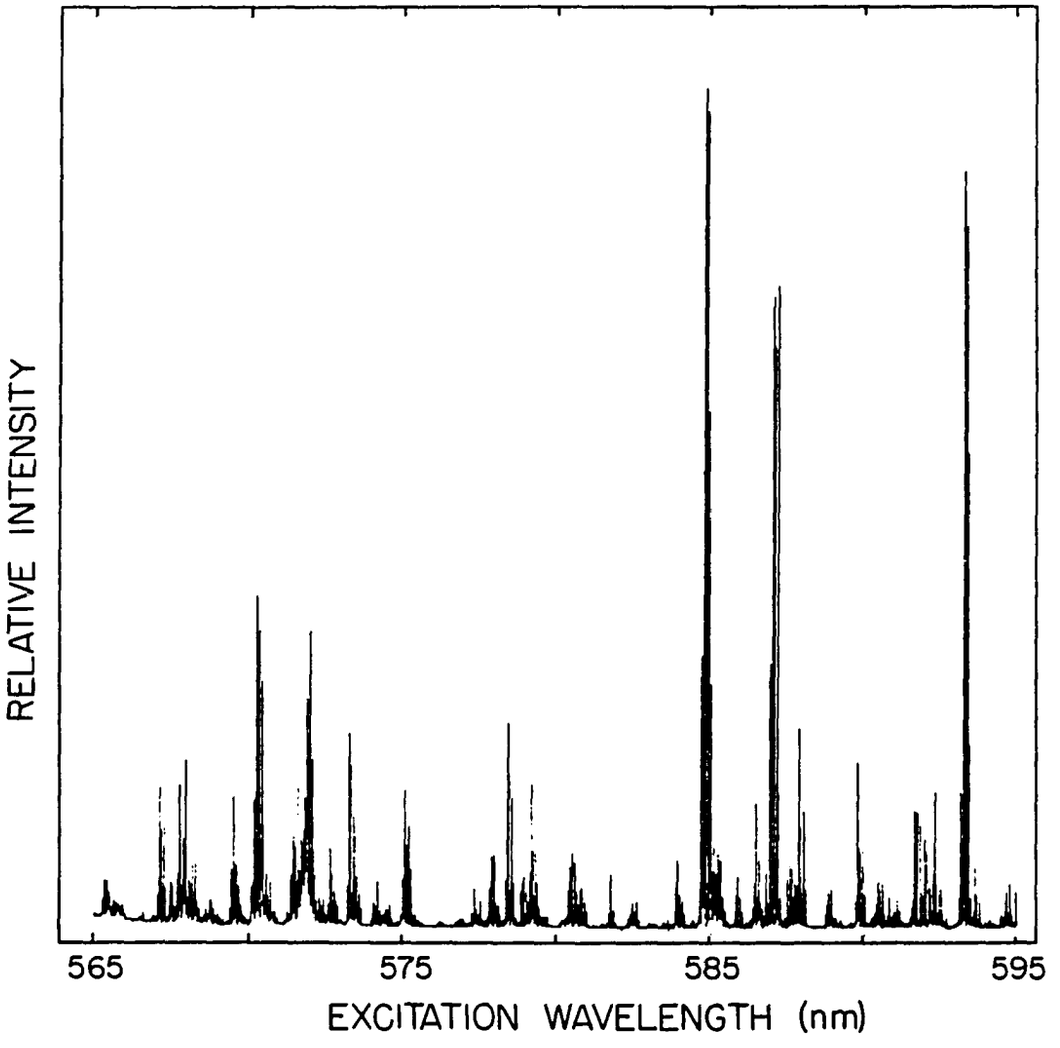


Figure B5. $NO_2$ fluorescence excitation spectra (5 % $NO_2$ in Ar) with same detection parameters as Figure B4. Rotational cooling provided by Lasertechnics LPV pulsed nozzle (D=300 μm) $P_o$=760 torr. Spectrum is not normalized to laser power

indicative of the improvement in cooling offered by this pulsed nozzle approach.

Currently, there are two primary shortcomings of commercially-available pulsed valves that prevent their use in analytical systems designed for detection of high molecular weight PAC. First, these valves often have dead volumes of on the order of several milliliters. This may pose difficulties stemming from intrinsically slow response and relatively long cleanout times. This aspect becomes particularly significant when such a pulsed valve is considered for use in chromatographic applications, in which severe broadening of chromatographic elution peaks would certainly result. The most formative obstacle that precludes the utilization of a commercial pulsed valve in such applications are their upper-temperature limits of operation. These limits are typically somewhere in the 50-70 $^{o}$C range (217,218), which is far too low for use in applications involving high molecular weight PAC. Thus, the incorporation of a pulsed nozzle into an analytical instrument designed for gas phase PAC determinations must await the development of a reliable, high-temperature, low dead volume, pulsed valve.

# XII. APPENDIX C: HIGH VACUUM SYSTEM DESIGN

The high vacuum chamber was designed to accommodate all of the accessories included in the multidimensional analytical system. This chamber was also an integral part of a high vacuum system that provided more-than-adequate pumping speed to maintain sufficiently low operating pressures for optimum performance of the instrument. The high vacuum chamber is diagrammed, to scale, in Figure C1. The chamber consisted of three nonmagnetic stainless steel sections that, when bolted together, formed vacuum-tight seals with rubber o-rings in place. Because the high vacuum chamber was originally designed to be pumped by a 10-in.(25.4 cm) diffusion stack, a high vacuum adapter spool was included to facilitate pumping with 6-in.(15.2 cm) diffusion stack that was employed in these studies.

The top plate section included a 7.5-in.(19.1 cm) o.d. flange to accommodate the vacuum envelope oven (Chapter IV). An 8-in.(20.3 cm) vacuum flange housed the nude ion source mount flange. Two opposing 2.75-in.(7.0 cm) vacuum flanges served to mount the laser access ports. The optical axis of the laser beam and the center line of the vacuum envelope oven intersected, at right angles, precisely 5.56 in.(14.1 cm) from the face of the nude source mount flange. This intersection coincided with the center of the ionization region (i.e., the dynamic gas sample cell) of the nude ion source.

A 2.75-in.(7.0 cm) vacuum flange, positioned opposite the nude ion source mount flange, housed the components of the LIF collection assembly. Also, two off-axis auxiliary ports were included in this high vacuum chamber. One port housed a Bayard-Alpert type ionization gauge tube that

was utilized in conjunction with a Granville-Phillips Model 270004 ionization guage to monitor pressures in the $10^{-8}$ - $10^{-3}$ torr range (An identical system was used to independently monitor flight tube pressures during operation.). The second auxiliary port provided access for additional high vacuum electrical feedthroughs.

The 6-in.(15.2 cm) diffusion pumping stack employed in this work consisted of an aluminum slide valve, a liquid nitrogen ($LN_2$) cryotrap, and a VHS-6 diffusion pump (Varian Industrial Products, Northbrook, IL). This stack was backed by a 500 L/min mechanical roughing pump (Welch Model 1397) that included a TX-150 coaxial metal adsorbant foreline trap (MDC Mfg., Inc., Hayward, CA). The primary purpose of this trap and the $LN_2$ cryotrap was to minimize the backstreaming of pump oils into the high vacuum chamber and flight tube. A 4-in.(10.2 cm) diffusion pumping stack, also consisting of an aluminum slide valve and a cryotrap, as well as an M-4 diffusion pump, was used to maintain the flight tube at a lower pressure than the main chamber. The M-4 stack was backed by a 160 L/min mechanical roughing pump (Welch Model 1402) that also utilized a TX-150 foreline trap.

Theoretical pumping speeds were determined for the vacuum system by employing standard molecular flow (low pressure) vacuum formulas (219). The conductance, C, of a pipe of diameter, D, and length, L, (for air), is given by:

$$C = 11.9\ (D^3/L) \quad ,$$

where D and L are expressed in cm and C has units of L/sec. The overall pumping speed, S, of a vacuum system is determined from:

$$1/S = 1/S_p + 1/C_1 + 1/C_2 + \cdots + 1/C_n \quad ,$$

where $S_p$ is the speed of the diffusion pump and the C's represent the conductances of each member of a series of n vacuum components.

A listing of the high vacuum system components and relevant dimensions, along with conductance or pumping speed values of each for air, is presented in Table C1. As noted in this table, net pumping speeds for the VHS-6 and M-4 vacuum systems were determined to be 820 and 400 L/s, respectively. The assistance provided by the M-4 stack in pumping the gas load of the main chamber was taken to be negligible because an approximate calculation indicated that the conductance through the nude ion source, to the flight tube pump was on the order of 20 L/s. From this, it was also predicted that the M-4 stack could maintain the flight tube at a pressure that was 20-fold lower than that of the main chamber (assuming the primary gas load was introduced into the main chamber). This prediction was verified experimentally, as a pressure drop of approximately 20-fold was noted.

Some assumptions were made in estimating the overall pumping speed of 820 L/s for the main vacuum system. First, the calculations were based on pumping speeds for air. Helium, the carrier gas used in this work, is normally pumped approximately 25 percent faster than air (219). Also, the CC/GC effluent was not introduced from the top of the chamber, as the calculations would imply, but from a position very close to the center of the chamber. From this standpoint, the effective vacuum chamber conductance should have been about twice the indicated value. However, the partial obstruction caused by the nude ion source structure was a factor that tended to reduce the effective chamber conductance. Thus, to conduct these approximate calculations it was assumed that these two

Table C1. High vacuum components: conductance and pumping speed

| Vacuum Component | Dimensions (cm) | Conductance/Pumping Speed for Air (L/s) |
|---|---|---|
| High Vacuum Chamber | D=31.5<br>L=28.7 | 13000 |
| Adapter Spool | D=19.8<br>L=11.2 | 8300 |
| 6-in. Aluminum Slide Valve | D=20.3<br>L=11.2 | 8900 |
| 6-in. Cryotrap | -----[a] | 2000 |
| VHS-6 Pump | -----[a] | 2400 |
| Net Pumping Speed Of Main Chamber Vacuum System: 820 L/s | | |
| 4-in. Aluminum Slide Valve | D=13.5<br>L=10.4 | 2800 |
| 4-in. Cryotrap | -----[a] | 1100 |
| M-4 Pump | -----[a] | 800 |
| Net Pumping Speed Of M-4 Diffusion Stack: 400 L/s | | |

[a]specified by Varian Industrial Products, Northbrook, IL.

effects canceled. A net pumping speed of 820 L/s likely represents a minimum value for a helium gas load.

The theoretical equilibrium pressure in the high vacuum chamber during operation of the chromatograph was calculated assuming a carrier flow rate of approximately 1 mL/min (at 760 torr) through the GC/MS interface. Thus, the net gas load entering the vacuum system was 0.013 torr-L/s. For a minimum pumping speed of 820 L/s, the equilibrium pressure in the main vacuum chamber was predicted to be no more than $1.6 \times 10^{-5}$ torr. Experimental high vacuum chamber pressures were, in fact, typically $6 \times 10^{-6}$ torr. Under these conditions the M-4 stack maintained a pressure of approximately $3 \times 10^{-7}$ torr in the flight tube. These equilibrium pressures are easily below the maximum allowed value for MEM operation (198).

An important criteria for efficient transmission of ions through the TOF/MS was that the mean free path of the ions ($\lambda_{cm}$) be greater than the length of the flight tube. The maximum allowable flight tube pressure ($P_M$) was, therefore, calculated from the following equation (219):

$$P_M = 4.85/\lambda_{cm} \quad ,$$

where $\lambda_{cm}$ and $P_M$ are expressed in units of cm and mtorr, repectively. Thus, for a flight tube length of 210 cm, the calculated maximum allowable flight tube pressure was $2.3 \times 10^{-5}$ torr. Again, the equilibrium flight tube pressure was well within this limitation.

Although the pumping speed of this vacuum system might be considered to be "over kill" for the applications presented in this dissertation, there are advantages in having this excess pumping capacity. Background signal from residual PAC may be a limitation in the current applications.

However, higher pumping speeds allow lower residual pressures to be maintained in the laser-analyte interaction region, which results in a reduction of background signal residual PAC. Also, these higher pumping speeds may be required in the future, upon implementation of a free-jet expansion sampling system for rotational cooling of the analyte. Other variations of this technique that will require these high pumping speeds are the incorporation of microbore liquid chromatography or supercritical fluid chromatography as a sample inlet system.